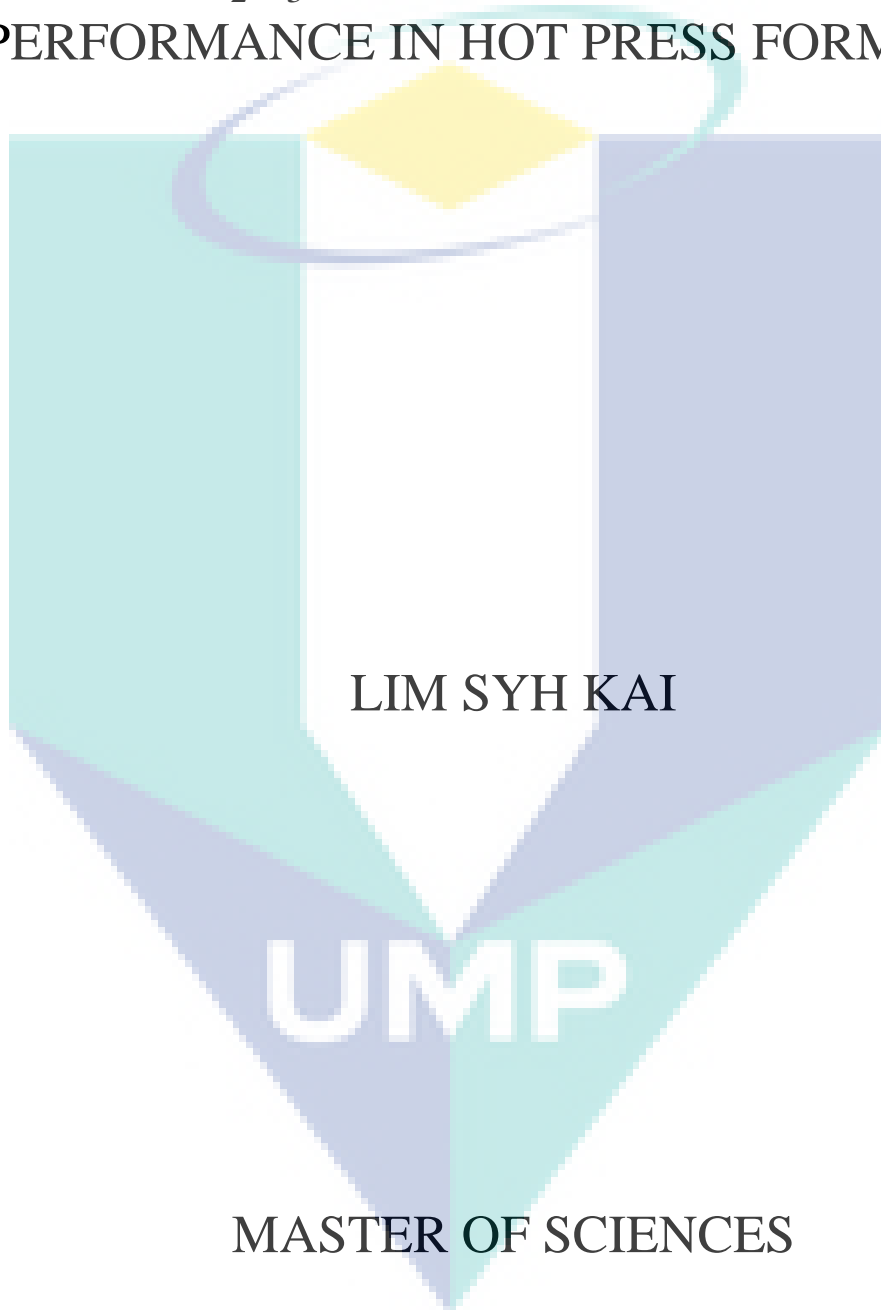


INVESTIGATIONS OF NANOCOOLANT
BASED Al_2O_3 FOR IMPROVING COOLING
PERFORMANCE IN HOT PRESS FORMING



LIM SYH KAI

UMP

MASTER OF SCIENCES

UNIVERSITI MALAYSIA PAHANG

UNIVERSITI MALAYSIA PAHANG

DECLARATION OF THESIS AND COPYRIGHT

Author's Full Name : LIM SYH KAI

Date of Birth : 06/02/1990

Title : INVESTIGATIONS OF NANOCOOLANT BASED Al_2O_3 FOR
IMPROVING COOLING PERFORMANCE IN HOT PRESS
FORMING

Academic Session : SEMESTER 2 2017/2018

I declare that this thesis is classified as:

- CONFIDENTIAL (Contains confidential information under the Official Secret Act 1997)*
- RESTRICTED (Contains restricted information as specified by the organization where research was done)*
- OPEN ACCESS I agree that my thesis to be published as online open access (Full Text)

I acknowledge that Universiti Malaysia Pahang reserves the following rights:

1. The Thesis is the Property of Universiti Malaysia Pahang
2. The Library of Universiti Malaysia Pahang has the right to make copies of the thesis for the purpose of research only.
3. The Library has the right to make copies of the thesis for academic exchange.

Certified by:

(Student's Signature)

(Supervisor's Signature)

900206-07-5467
New IC/Passport Number
Date: 23 MAY 2018

ASSOC. PROF. IR. DR. AHMAD
RAZLAN BIN YUSOFF
Name of Supervisor
Date: 23 MAY 2018

NOTE : * If the thesis is CONFIDENTIAL or RESTRICTED, please attach a thesis declaration letter.

SUPERVISOR'S DECLARATION

I hereby declare that I have checked this thesis and in my opinion, this thesis is adequate in terms of scope and quality for the award of the degree of Master of Science in Manufacturing Engineering.

(Supervisor's Signature)

Full Name : IR. DR. AHMAD RAZLAN BIN YUSOFF

Position : ASSOCIATE PROFESSOR

Date : 23 MAY 2018



UMP

STUDENT'S DECLARATION

I hereby declare that the work in this thesis is based on my original work except for quotations and citations which have been duly acknowledged. I also declare that it has not been previously or concurrently submitted for any other degree at Universiti Malaysia Pahang or any other institutions.

(Student's Signature)

Full Name : LIM SYH KAI

ID Number : MMF15007

Date : 23 MAY 2018



UMP

INVESTIGATIONS OF NANOCOOLANT BASED Al_2O_3 FOR IMPROVING
COOLING PERFORMANCE IN HOT PRESS FORMING



LIM SYH KAI

Thesis submitted in fulfillment of the requirements
for the award of the degree of
Master of Science

UMP

Faculty of Manufacturing Engineering
UNIVERSITI MALAYSIA PAHANG

MAY 2018

ACKNOWLEDGEMENTS

First and foremost, I would like to express my deepest appreciation to all those who provided me the possibility to complete this master degree research. This project would not have been possible generous assistance, cooperation and support of a number of people.

A special gratitude goes to my supervisor, Assoc. Prof. Ir. Dr. Ahmad Razlan bin Yusoff, who contributed significantly stimulating suggestions, continuous encouragement, valuable guidance and advices. His professional supervision and support truly help the progression and smoothness of my project in which his co-operation is highly appreciated.

My sincere appreciation goes to my lab mates, Ms. Norlida binti Jamil, Mr. Mohd Fawzi bin Zamri and Ms. Nik Nurul Husna binti Muhmed Razali for their continuous support. Besides, a million thanks to Assoc. Prof. Dr. Abdul Aziz bin Jaafar, Dr. Zamzuri bin Hamedon and Ms. Law Hoon Chit in hsaring knowledge and ideas generously and giving me helping hands to resolve my doubts in research jobs. Also, I would like to convey my gratefulness to laboratory assistants, Mr. Aidil Shafiza bin Safiee, Mr. Shahandzir bin Baharom and Mr. Mohd Nursyazwan bin MD Talip for the guidance in using the testing equipment.

Last but not least, I acknowledge my sincere indebtedness and gratitude to my lovely family for their continuous support, encouragement and sacrifice throughout my life. A special thanks to my parents who consistently encouraged me to pursue my studies to a higher education level as well as with their mental and physical support, their tolerance of my ignorance and naïve mistakes.



UMP

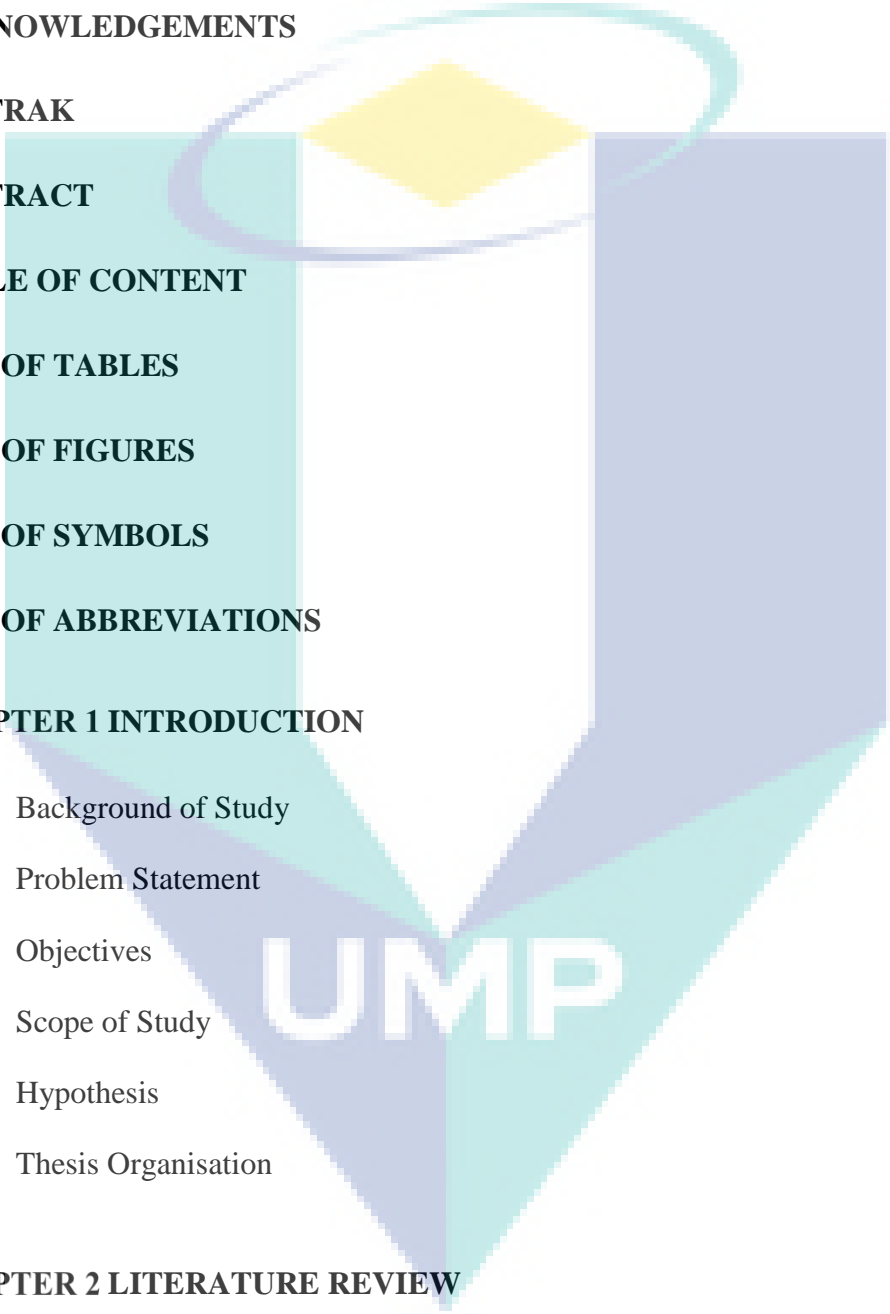
ABSTRAK

Pembentukan kepingan keluli panas (HPF) untuk membangunkan UHSS boron keluli untuk panel badan dalaman kenderaan menawarkan penggunaan bahan api yang efisien untuk mengurangkan pelepasan gas karbon dioksida oleh pengurangan berat badan dan meningkatkan keselamatan penumpang kerana sifat mekanikal yang tinggi. Boron keluli dipanaskan sehingga suhu austenitik dan kemudian disejutkan dengan cepat dalam sebuah acuan dalam masa pelindapkejutan tertentu untuk mempamerkan fasa transformasi martensit. Pada masa ini, air digunakan sebagai cecair penyejuk dalam proses HPF untuk menghilangkan keluli boron dalam sebuah acuan tertutup dengan saluran bendalir penyejukan. Walau bagaimanapun, untuk meningkatkan prestasi acuan HPF dan meningkatkan sifat mekanikal boron keluli ditekan panas, bendalir dengan sifat termal yang lebih baik akan digunakan dan bukannya air biasa. Semasa operasi pelindapkejutan, kadar cecair penyejukan optimum dan pengagihan suhu homogen pada kekosongan panas ke arah pencapaian transformasi mikrostruktur martensitic serta sifat mekanikal yang tinggi. Kajian ini menyebarkan nanopartikel Al_2O_3 dari kepekatan isipadu sebanyak 0.2 hingga 1.0% dengan purata diameter 13 nm ke dalam tiga peratusan air ke etilena glikol seperti 60%:40%, 50%:50%, dan 40%: 60% dengan menggunakan kaedah penyediaan dua langkah. Kedua-dua parameter utama dalam prestasi kadar cecair penyejukan adalah kekonduksian terma dan kelikatan dinamik. Pengedaran pemindahan haba pekali panas dengan nanocoolant dan air sejuk disimulasikan untuk analisis haba sementara dalam simulasi unsur terhingga melalui ANSYS untuk menilai peningkatan pekali pemindahan haba konveksi dan menentukan kadar cecair penyejukan optimum bendalir penyejukan sistem dalam acuan HPF. Data simulasi kemudian dibandingkan dengan penemuan eksperimen untuk tujuan pengesahan. Telah didapati bahawa peningkatan kekonduksian terma tertinggi adalah 10% lebih tinggi daripada bendalir asas untuk kepekatan volum 1,0% Al_2O_3 pada 55 °C dalam 60%:40% (W/EG). Walau bagaimanapun, peningkatan kelikatan dinamik yang paling tinggi diukur sebanyak 39% untuk kepekatan volum 1.0% Al_2O_3 dalam 40%:60% (W/EG) pada 25 °C. Koefisien pemindahan haba konveksi kepekatan 1.0% dalam 60%:40% (W/EG) pada 25 °C ditingkatkan dengan 25.4% lebih baik daripada 50%:50% dan 40%:60% (W/EG) cecair. Oleh itu, kajian ini memperakukan penggunaan Al_2O_3 dalam campuran 60%:40% (W/EG) dengan kepekatan volum Al_2O_3 kurang daripada 1.0% untuk aplikasi dalam saluran bendalir penyejukan acuan HPF. Itu juga terbukti bahawa corak pengedaran suhu model analisis unsur terhingga bersesuaian dengan hasil eksperimen. Kekuatan tegangan dan nilai kekerasan Vickers bahagian yang ditekan panas dinilai masing-masing kira-kira 1,550 MPa dan 588 HV. Sebagai kesimpulan, nanocoolant sebagai cecair penyejuk dengan pekali pemindahan haba konveksi yang lebih tinggi berbanding dengan air sejuk boleh mengurangkan masa pelindapkejutan dalam proses HPF.

ABSTRACT

Hot press forming (HPF) to develop UHSS of boron sheet metals for vehicle inner body panels offers efficient fuel consumption in order to reduce carbon dioxide gas emissions by weight reduction and improves passenger safety because of its high mechanical properties. The sheet metal is heated up to austenitic temperature and then rapidly quenched in an enclosure dies in a certain quenching time to exhibit martensitic transformation phase. Currently, water is used as coolant in the HPF process to quench boron steels in a closed die with a cooling channel. However, to enhance the performance of HPF dies and increase the mechanical properties of hot pressed boron steel, the fluid with better thermal properties will be used instead of normal water. During the quenching operation, an optimum cooling rate and homogeneous temperature distribution on hot blanks towards the achievement of the martensitic microstructure transformation as well as high mechanical properties. This study dispersed Al_2O_3 nanoparticles from the range of 0.2 to 1.0% volume concentration with an average diameter of 13 nm into three volume percentages of water to ethylene glycol such as 60%:40%, 50%:50%, and 40%:60% by using the two-step preparation method. The two main parameters in cooling rate performance are thermal conductivity and dynamic viscosity. The heat transfer distribution of the hot blanks with nanocoolant and chilled water are simulated for transient thermal analysis in finite element simulation via ANSYS to evaluate the enhancement of convection heat transfer coefficient and determine the optimum cooling rate of cooling system in HPF tool. The simulation data were then compared with experimental findings for validation purpose. It was found that the highest enhancement of thermal conductivity was observed to be 10% higher than base fluid for 1.0% volume concentration of Al_2O_3 at 55 °C in 60%:40% (W/EG). However, the highest enhancement of dynamic viscosity was measured to be 39% for 1.0% volume concentration of Al_2O_3 in 40%:60% (W/EG) at 25 °C. The convective heat transfer coefficient of 1.0% concentration in 60%:40% (W/EG) at 25 °C is enhanced by 25.4% better than that of 50%:50% and 40%:60% (W/EG) base fluid. Therefore, this study recommends the use of Al_2O_3 in 60%:40% (W/EG) mixture with volume concentration of Al_2O_3 less than 1.0% for application in cooling channel of HPF dies. It was also evident that the pattern of the temperature distribution of the finite element analysis model was in agreement with the experimental results. The tensile strength and Vickers hardness values of the hot pressed parts were evaluated to be approximately 1,550 MPa and 588 HV, respectively. In conclusion, nanocoolant as cooling fluid with higher convection heat transfer coefficient compared to the chilled water can reduce the quenching time of HPF process.

TABLE OF CONTENT



DECLARATION	
TITLE PAGE	
ACKNOWLEDGEMENTS	ii
ABSTRAK	iii
ABSTRACT	iv
TABLE OF CONTENT	v
LIST OF TABLES	ix
LIST OF FIGURES	x
LIST OF SYMBOLS	xiii
LIST OF ABBREVIATIONS	xiv
CHAPTER 1 INTRODUCTION	1
1.1 Background of Study	1
1.2 Problem Statement	4
1.3 Objectives	6
1.4 Scope of Study	6
1.5 Hypothesis	8
1.6 Thesis Organisation	8
CHAPTER 2 LITERATURE REVIEW	11
2.1 Introduction	11
2.2 Background of Nanofluids as Coolant	12
2.3 Properties of Water-Ethylene Glycol Based Nanocoolants	13

2.4	Nanoparticles as Suspended Material	15
2.4.1	Nanoparticle materials	17
2.4.2	Types of synthesized nanofluids	19
2.5	Nanofluids Preparation	20
2.6	Thermal Properties of Nanofluids	22
2.6.1	Dynamic viscosity	23
2.6.2	Thermal conductivity	25
2.7	Sheet Metal of Boron Steel	27
2.8	Hot Press Forming Process	30
2.8.1	Heating operation	32
2.8.2	Forming operation	36
2.8.3	Punching and loading force	38
2.9	Heat Transfer Mechanism	40
2.9.1	Tools temperature and contact pressure	41
2.9.2	Cooling Channel Design for Fluid Flow Types	44
2.10	Finite Element Thermal Analysis in Hot Press Forming	46
2.11	Summary	52
CHAPTER 3 METHODOLOGY		54
3.1	Introduction	54
3.2	Materials and Preparation of Nanocoolants	56
3.3	Thermal Conductivity Measurement	60
3.4	Dynamic Viscosity Measurement	62
3.5	Finite Element Analysis	64
3.5.1	Thermal analysis	66
3.5.2	Geometric modelling of hat-shaped tools	68

3.5.3	Boundary conditions and constraint parameters	69
3.5.4	Meshing	70
3.5.5	Numerical simulation	72
3.6	Experimental Approach of Hot Press Forming	74
3.6.1	Sample preparation	76
3.6.2	Location of thermocouples	77
3.6.3	Hot press forming of boron steel sheet metal	78
3.6.4	Experimental study of heat transfer distribution	80
3.6.5	Tensile test measurements	83
3.6.6	Micro-hardness measurements	85
3.6.7	Metallographic observation study	86
3.7	Summary	88
CHAPTER 4 RESULTS AND DISCUSSION		89
4.1	Introduction	89
4.2	Thermal Physical Properties	90
4.2.1	Thermal conductivity of nanocoolant	90
4.2.2	Dynamic viscosity of nanocoolant	94
4.2.3	Heat transfer coefficient of nanocoolant	98
4.3	Thermal Analysis Results and Validation with Hat-Shaped Tools	101
4.3.1	Comparison of nanocoolant with chilled water in simulation	104
4.3.2	Temperature validation of hot press forming with thermal analysis	106
4.4	Experimental Analysis of Hot Pressed Boron Steel	107
4.4.1	Microstructural transformation analysis	107
4.4.2	Tensile strength analysis	111

4.4.3	Hardness analysis of hot formed boron steel	114
4.5	Summary	116
CHAPTER 5 CONCLUSION		118
5.1	Conclusion	118
5.2	Contributions to Knowledge	120
5.3	Future Works	121
REFERENCES		123
APPENDIX A G-code for cutting tensile test specimen from hat-shaped part		140
APPENDIX B Heat transfer coefficient values of nanocoolant		141
APPENDIX B1 Sample of cooling rate for heated sheet metal blank		142
APPENDIX C Sedimentation observation of aluminium oxide/water-EG mixture after a month of preparation		143
APPENDIX D Sample of tensile strength and hardness measurement		145
List of publication		146



The logo for UMP (Universiti Malaysia Perlis) is a large, stylized letter 'V' shape. The left side of the 'V' is light blue, the right side is a darker blue, and the bottom point is a teal color. The letters 'UMP' are written in white, bold, sans-serif font across the center of the 'V'.

UMP

LIST OF TABLES

Table 2.1	Thermo-physical property of different types of metal and liquid	13
Table 2.2	Various types of nanoparticles and micrograph images	17
Table 2.3	Types of nanoparticles dispersed in nanofluids	20
Table 2.4	Dynamic viscosity investigations for different types of nanocoolants	24
Table 2.5	Thermal conductivity study for diverse types of nanofluids	26
Table 2.6	Chemical compositions of boron steel weight percentage and mechanical properties before and after quenching operation	28
Table 2.7	Thermal-physical properties of boron steel	29
Table 2.8	Stamping process in hot temperature conditions	39
Table 2.9	Results of contact pressure and standard deviation of HTC	42
Table 3.1	Properties of nanoparticles used in experiment	57
Table 3.2	Properties of Ethylene Glycol solution	58
Table 3.3	Thermal conductivity models for nanocoolant	62
Table 3.4	Dynamic viscosity models for nanocoolant	64
Table 3.5	Material properties of SKD 61 and 22MnB5 at room and hot temperature	67
Table 3.6	Boundary condition for thermal analysis simulation	69
Table 3.7	Results of three different meshing sizes for hat-shaped tool	72
Table 3.8	The features of mechanical press machine model OCP 80	79
Table 3.9	The features of hydraulic press machine	80
Table 3.10	Specifications of Universal Tensile Machine	84
Table 3.11	Specifications of Wilson Vickers 402 MVD machine	86
Table 3.12	Specification of LOM, Olympus BX51M machine	87
Table 4.1	Temperature distribution for HPF tools and heated blank	104
Table 4.2	Micrographs of boron steel blank with several quenching time periods	108
Table 4.3	Tensile strength value for several specimens of hot formed boron steel	111
Table 4.4	Hardness value for several specimens of hat-shaped boron steel	114

LIST OF FIGURES

Figure 1.1	Tensile strength between UHSS and typical sheet metal	1
Figure 1.2	Mechanical properties of boron steel before and after hot forming process	3
Figure 1.3	Thesis organisation	10
Figure 2.1	Freezing point and boiling point of water-EG mixture	14
Figure 2.2	One-step method technique	21
Figure 2.3	Two-step method technique	22
Figure 2.4	Graph of velocity pattern versus velocity	23
Figure 2.5	Temperature, time and transformation diagram of boron steel at various cooling rates	29
Figure 2.6	Direct hot forming process	30
Figure 2.7	Indirect hot press forming	31
Figure 2.8	Hat-shape profile bending operation	32
Figure 2.9	Various types of heating system (a) Roller hearth furnace, (b) Induction heating and (c) Electrical resistance heating	33
Figure 2.10	Induction heating operation (a) Schematics diagram of the customized induction furnace and (b) Variation of temperature curve as function of time for several feeding speed	34
Figure 2.11	Localize heating (a) Positioning two rectangular electrodes on the blank and the temperature distribution diagram; and (b) Result of punching load for different heating temperatures in shearing region	35
Figure 2.12	Forming Limit Diagram of B-pillar	36
Figure 2.13	Simulation of B-pillar in hot press forming process	37
Figure 2.14	Geometries of tools and steel sheet for hat-shape and V-shape	37
Figure 2.15	Degree of springback after V-shape bending with the relationship of temperature in (a) Bending region; and (b) Flange region	38
Figure 2.16	Hot forming process of UHSS sheet metal by using resistance heating	39
Figure 2.17	Relationship between the maximum stamping load and heating temperature of UHSS sheet metal	40
Figure 2.18	Experimental setup and instrument for heat transfer coefficient testing	42
Figure 2.19	Relation between HTC as function of contact pressure for different tool temperatures	43
Figure 2.20	Thermal contact resistance (a) Ideal thermal contact; (b) Actual thermal contact	43

Figure 2.21	Schematic diagram of hot press forming tool design	45
Figure 2.22	Schematic diagram of the quenching tool integrated with hot forming operation	45
Figure 2.23	Interactions between the effects of heat transfer, microstructural evolution and deformation	48
Figure 2.24	temperature changes in heat transfer analysis	49
Figure 2.25	Tool cooling performance between SKD 61 and HTCS 150 tool materials with same cooling channel parameter	50
Figure 2.26	Heat transfer distributions on the dies during quenching step took completely 20 s	51
Figure 2.27	Hot stamping with several holding times in dies	51
Figure 3.1	Flow chart of introducing nanocoolant as cooling medium for HPF process	56
Figure 3.2	FESEM result of dry Al ₂ O ₃ nanoparticles at X300,000 magnification	57
Figure 3.3	Al ₂ O ₃ nanocoolant immersed in ultrasonic bath heater	59
Figure 3.4	Nanocoolant samples of Al ₂ O ₃ /water-EG mixtures after a month of preparation	60
Figure 3.5	(a) Schematic diagram of thermal conductivity measurement; (b) Experiment setup for thermal conductivity measurement.	61
Figure 3.6	(a) Schematic diagram of dynamic viscosity measurement; (b) Experiment setup for dynamic viscosity measurement	63
Figure 3.7	Flow chart of thermal finite element analysis on HPF	66
Figure 3.8	Simulation starts from the steady-state and ends with the transient thermal analysis	67
Figure 3.9	Geometric modelling in ANSYS simulation software	68
Figure 3.10	Hat-shaped tool imported into ANSYS simulation software	69
Figure 3.11	Surface contact between sheet metal blank and dies	71
Figure 3.12	The grid distribution of Hat-shaped tool and blank	72
Figure 3.13	Temperature distribution of hot pressed blank by using nanocoolant from ANSYS simulation	74
Figure 3.14	The process sequences of HPF experimental analysis	75
Figure 3.15	Pre-forming process of hat-shaped samples	76
Figure 3.16	Thermocouples location in HPF tool (a) Schematic diagram (b) Three thermocouples in upper tool	78
Figure 3.17	Fabrication of hat-shape sample by using mechanical press machine, OCP 80	79
Figure 3.18	Hydraulic press machine used in hot forming operation	80
Figure 3.19	The experimental equipment setup for hot press forming tool	81

Figure 3.20	Hot press forming process flow of hat-shaped blank	82
Figure 3.21	Location of hot formed samples for tensile specimen, hardness test and microstructure analysis	84
Figure 3.22	Specimen for tensile strength test	84
Figure 3.23	Tensile strength measurement with Universal Tensile Machine	85
Figure 3.24	Hardness measurement with Vickers Micro-hardness Machine, Wilson Vickers 402 MVD	86
Figure 3.25	Microstructural analysis by using light optical microscopy machine	87
Figure 4.1	Variation of thermal conductivity enhancement as function of nanoparticles volume concentrations in W/EG mixture at 25 °C	91
Figure 4.2	Thermal conductivity of different nanoparticle concentrations for three different mixture of W/EG base fluids	94
Figure 4.3	Variation of viscosity ratio as fraction of nanoparticle volume concentrations in W/EG mixture at 25 °C	95
Figure 4.4	Viscosity of different nanoparticle concentrations for three different mixture of water-EG base fluids	98
Figure 4.5	Relationship between thermal conductivity as function of nanoparticles volume concentration for three different mixture base fluids	99
Figure 4.6	Distribution of heat transfer coefficient of 60%:40% water-EG mixture based Al ₂ O ₃ nanocoolant	101
Figure 4.7	Thermal analysis at steady state condition for HPF simulation	102
Figure 4.8	Transient thermal analysis for HPF simulation by introducing nanocoolant	103
Figure 4.9	Transient thermal analysis for HPF simulation by introducing chilled water	103
Figure 4.10	Heat transfer distribution between nanocoolant and chilled water for hat-shaped tool	105
Figure 4.11	Comparison of heat transfer distribution between FEA and experiments for hat-shaped tool	107
Figure 4.12	Ultimate tensile strength of blank samples at several cooling conditions	112
Figure 4.13	Vickers hardness reading HV1 with diamond shaped indent 50 μm	114
Figure 4.14	Hardness value of hot pressed samples at several cooling conditions	115

LIST OF SYMBOLS

A	Heat transfer area
B	Bending length
C_{bf}	Specific heat of base fluid
C_{nf}	Specific heat of nanocoolant
C_p	Specific heat of particle
D	Pipe length
dT	Temperature difference
dX	Differential length
E	Modulus elasticity
h	Heat transfer coefficient
k	Thermal conductivity
k_{bf}	Thermal conductivity of base fluid
k_{nf}	Thermal conductivity of nanocoolant
L	Length
Nu	Nusselt number
P	Loading force
Pr	Prandtl number
Pr	Prandtl number of nanocoolant
q	Heat transfer
Re	Reynolds number
s	Second
t	Thickness
T_1	Inlet temperature
T_2	Outlet temperature
T_b	Bulk temperature
T_f	Surrounding fluid temperature
T_s	Surface temperature
V	Velocity
μ	Dynamic viscosity
μ_{bf}	Dynamic viscosity of base fluid
μ_{nf}	Dynamic viscosity of nanocoolant
ω	Weight concentration
ϕ	Volume fraction
ρ	Density
ρ_{bf}	Density of base fluid
ρ_{nf}	Density of nanocoolant
ρ_p	Density of particle
ϕ	Volume concentration
ϕ_1	Initial volume concentration
ϕ_2	Final volume concentration

LIST OF ABBREVIATIONS



AHSS	Advanced High Strength Steel
Al ₂ O ₃	Aluminium Oxide
ASTM	American Society for Testing and Materials International
ASHRAE	American Society of Heating, Refrigerating and Air Conditioning Engineers
BR	Base Ratio
CuO	Copper Oxide
EG	Ethylene Glycol
FESEM	Field Emission Scanning Electron Microscopy
FEA	Finite Element Analysis
FLD	Forming Limit Diagram
FCNT	Functionalised Carbon Nanotube
DIN EN ISO	German Institute European Standard
HTC	Heat Transfer Coefficient
HSS	High Strength Steel
HTCS	High Thermal Conductivity Tool Steel
HPF	Hot Press Forming
SKD	Hot Work Tool Steel
IUPAC	International Union of Pure and Applied Chemistry
LOM	Light Optical Microscopy
MWCNT	Multi-walled Carbon Nanotube
SEM	Scanning Electron Microscopy
SiC	Silicon Carbide
SiO ₂	Silicon Oxide
TEM	Transmission Electron Microscopy
UHSS	Ultra-High Strength Steel
UTM	Universal Tensile Machine
W	Water

CHAPTER 1

INTRODUCTION

1.1 Background of Study

The increasing awareness of environmental pollution caused by vehicle emission has driven automotive manufacturers around the world to improve fuel efficiency by producing a lighter vehicle without compromising vehicle safety. Reducing the weight of the vehicle requires the component to have thinner material, but at the same time, it should not discredit the mechanical properties. This has resulted in the introduction of ultra-high strength steel (UHSS) materials. The development of UHSS material has paved the reduction in gas emission to the environment, energy saving and the production of safer vehicles. UHSS material has a higher tensile strength and lower weight ratio when compared to the mild steel (Atlan and Tekkaya, 2012). Most of the UHSS materials are having high mechanical properties as shown in Figure 1.1.

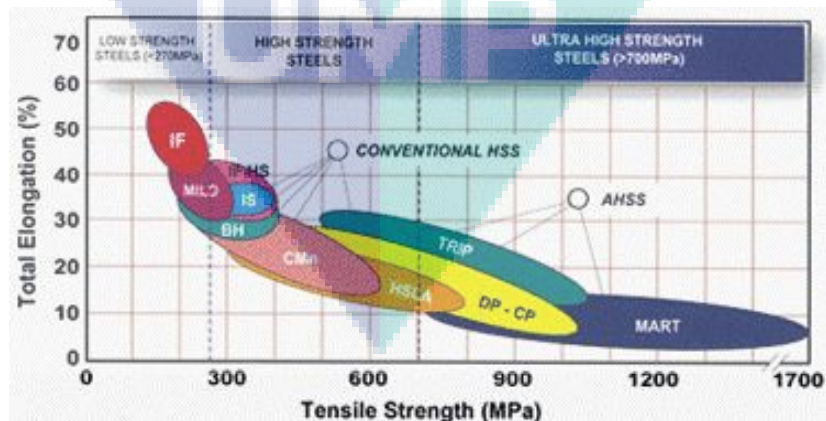


Figure 1.1 Tensile strength between UHSS and typical sheet metal

Source: Atlan and Tekkaya (2012)

In conventional cold forming process, the issues of poor formability, forming accuracy and greater springback have often occurred in high strength steel (HSS), advanced high strength steel (AHSS) and UHSS, respectively. Hence, to overcome these problems of high strength steel forming, researchers and industries are actively developing hot press forming (HPF) technologies (Karbasian and Tekkaya, 2010). HPF process is a new forming method that can significantly enhance the formability of UHSS. In addition to high strength and dimensional accuracy of steel sheet formed, it can further avoid the springback of UHSS from cold forming process and achieve the purpose of weight reduction (Sever et al., 2012; Thanadgarn et al., 2013). Furthermore, UHSS material such as boron steel gains its final strength through the HPF process as heat treatment, which can increase the hardness and mechanical strength of boron steel up to 1,400 MPa (Atlan and Tekkaya, 2012). The obtained strength is two-fold higher than the boron steel in annealed condition. As the capability of having an ultimate tensile strength of 1,400 MPa and the possibility of weight reduction. Automotive industry implements the hot pressed parts as vehicle components such as the chassis, A-pillar, B-pillar, tunnel, bumper, roof rail and many others being formed by boron steel.

Naderi (2007) reported that boron steel, 22MnB5 produced a fully martensitic microstructure after using HPF process. Figure 1.2 shows the boron steel has a tensile strength of approximately 600 MPa at the initial state. Higher ultimate tensile strength can be attained by a rapid cooling of the hot forming tool at the cooling rate of at least $27 \text{ K}\cdot\text{s}^{-1}$ (Merklein et al., 2014). Before HPF process, the boron steel consists of ferrite-pearlite microstructure must be austenitized in order to increase the elongation which is practical for the press forming operation. However, the yield strength of the boron steel is reduced during the austenite transformation phase. Finally, the martensitic transformation transpired if the austenite cools immediate during the HPF process (Karbasian and Tekkaya, 2010).

The HPF process also named as a press hardening process, which consists of three phases such as heating the sheet metal blank, press forming operation and part quenching (So et al., 2012). In the process, UHSS blank is cut into the rough dimension, and the blank is heated up to the required temperature of $900 \text{ }^\circ\text{C}$ for 5 minutes inside the furnace. Then, the heated blank is quickly transferred to the press to avoid the temperature of the blank cooled down in the atmosphere before forming operation. Subsequently, the part is

pressed and cooled simultaneously by the water-cooled die for roughly 10 s. Due to the contact between the cool HPF dies and heated blank, the blank is cooled in the enclosure tools (Karbasiyan and Tekkaya, 2010). Besides that, HPF process exists in two different methods that are the direct HPF and indirect HPF method. For direct HPF process, a blank is heated up in a furnace, transferred to the press and subsequently formed and quenched in the enclosure tool. While, for indirect HPF process, before the blank is austenitized inside the furnace, it has to perform the cold pre-forming operation. In this research project, the indirect HPF process was chosen due to the ability to install the heating element inside the hot forming tool.

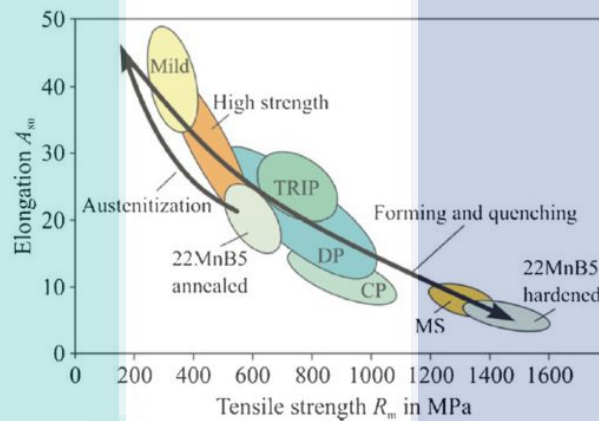


Figure 1.2 Mechanical properties of boron steel before and after hot forming process

Source: Karbasiyan and Tekkaya (2010)

The quenching operation during the HPF process does influence not only the cost effectiveness of the process, but also the final properties of the product. The purpose of the cooling channel system is to quench the hot specimen effectively and to achieve the cooling rate of at least $27 \text{ K}\cdot\text{s}^{-1}$ during the martensitic transformation. The HPF dies cooling system provides the fluid coolant that flows through the cooling channel around the contours of the part. The heat flow in the formed part depends on the heat transfer from the specimen to the HPF dies, the thermal conductivity within the dies, and the heat transfer from the dies to the coolant. The thermal conductivity and heat transfer within the tool and coolant can be considerably influenced by the types of cooling fluid and thermal cooling system.

Forced convection is the mechanism of heat transfer in most of the thermal cooling system or cooling system in engineering practice, and few such examples include automobile radiators and industrial power plant cooling system. Forced convection defines as to drive the fluid motion in the process of transferring the heat between mediums. The significant challenges involved in thermal engineering are to find approaches to reduce the heat transfer to a minimum or increase the heat to a maximum value. Pioneer researchers subjected to the nanocoolant field, such as Choi et al. (2004) has successfully encountered new superior fluid called nanocoolants that has the ability to transfer heat as good as conventional heat transfer fluids or even better. Thus, the development of nanocoolant technology has expanded considerably over the past several years after the pioneer research made by Choi et al. (2004) in the end 90's and is still growing until today.

The production of water base nanocoolants has been widely employed in many kinds of research over the past years. Several kinds of research have been reported on the experimental studies of nanocoolant in mixture (Lim et al., 2016; Bayat and Nikseresht, 2012). Lim et al. (2016) conducted an investigation on forced convection heat transfer for the base fluid mixture which composed of water and ethylene glycol in percentage of 60%:40%, where the enhancement was found to be 25.4%. Bayat and Nikseresht (2012) demonstrated that the enhancement of the average heat transfer coefficient was more significant in higher concentrations and higher Reynolds number by using 40%:60% water-EG mixture. The nanocoolant as a heat transfer fluid is essentially determined through the heat transfer coefficient. While, the efficiency of the nanocoolant is evaluated from the heat transfer parameters, such as the Prandtl number, Nusselt number, and heat transfer coefficient (Bhanvase et al., 2014).

1.2 Problem Statement

Hot press forming (HPF) process requires rapid cooling of the sheet metal blank inside the enclosure dies, and this includes the cooling system to be integrated with the hot forming tools to control the cooling rate. The cooling system must be designed to cool efficiently to achieve the maximum cooling rate and homogeneous temperature distribution over the hot formed products. In cooling channel development, the effect of

heat transfer, hot forming tool materials and blank materials must be considered. At the same time, it must fulfil the required process system regarding to the heating temperature to press forming operation, transmitting time and heating furnace. Thus, one of the significant factors to be considered during the process is the design of the cooling channel, including the size, location and distribution temperature (Zhong et al., 2010; Liu et al., 2013).

Current practice in a local industry (Miyazu (M) Sdn. Bhd.), the mean for holding time during quenching is 12 s, and it takes about 25 to 30 s to completely produce one single part with a predicted $27 \text{ K}\cdot\text{s}^{-1}$ of cooling rate. The cooling fluids that have been used in the HPF process are water or chilled water with the thermal conductivity of approximately $0.5 \text{ W}\cdot\text{m}^{-1}\cdot\text{K}^{-1}$ (Lin et al., 2014). The side beam hot forming die is segmented into 12 blocks due to the cooling channel drilling process capability, with a limitation of 400 mm in length (Hafizuddin, 2014). The diameter of the cooling channel is 8 to 12 mm, the distance to loading surface is 10 to 12 mm, and the pitch is 10 mm. Therefore, dealing with ultra-high strength steel (UHSS) properties in HPF process, it requires the tool to cool down the blank immediately, for that a cooling system must be integrated into the hot forming tools.

The thermal-physical properties in convection heat transfer in terms of thermal conductivity is vital for HPF process. Researchers are working to optimize the thermal conductivity with minimum cooling channel by implementing nanocoolants to replace water and chilled water as cooling fluids in HPF process. This research project intends to increase the efficiency of thermal conductivity in order to enhance the convection heat transfer values by utilizing the nanocoolants, and to report a comparative study between conventional coolants and nanocoolants. There are several studies reported on the introduction of nanocoolants in the automotive field. Sharma et al. (2013) proposed a nanocoolant as engine based coolant and showed the improvement of thermal physical properties over the conventional fluids. The mixture of nanocoolant is based on the synthesizing of Al_2O_3 with base fluids. The results indicated that the thermal conductivity and dynamic viscosity increases with the increase of volume concentration. Therefore, the fluids with better thermal physical properties will be used instead of normal water to enhance the cooling performance of the HPF dies, thereby providing the optimum cooling system. This cooling system must be capable of lowering the tool temperature to

accelerate the sheet metal blank cooling rate as well as sinking away the heat to the cooling fluid as fast as possible (Karbasiyan and Tekkaya, 2010; Altan and Tekkaya, 2012).

1.3 Objectives

The primary aim of this study would be to experimentally investigate the suitability and potential of nanocoolants to be introduced into the cooling channel of hot press forming (HPF) process. Thus, improving the mechanical properties of the hot pressed part and increasing the productivity of the automotive industry. The objectives of this research project are as follows:

- 1) To characterize the aluminium oxide, Al_2O_3 /water-EG mixture with optimum thermal physical properties in terms of thermal conductivity and dynamic viscosity.
- 2) To determine the temperature distribution of nanocoolants in the HPF tool by using finite element thermal analysis and validate with the experimental hat-shaped tools.
- 3) To analyse the mechanical properties of boron steel product in terms of tensile strength and hardness together with the microstructure transformation of the chilled water and nanocoolants.

1.4 Scope of Study

The scope of this research project is as follows:

- a) Nanocoolants with different volume concentrations of aluminium oxide, Al_2O_3 nanoparticles from 0 to 1.0% are prepared by using the dilution process in a water-EG mixture in this study due to the potential heat transfer rate in the engineering field and it is advanced fluids in the current trend.

- b) Several concentrations of nanoparticles are suspended in three different volume percentage of water-EG base fluids, which are 60%:40%, 50%:50% and 40%:60%, respectively. The mixture prevents the galvanic corrosion of the cooling channel system, and also prevent distilled water from boiling or freezing at extreme temperature.
- c) The thermal properties of nanocoolants are measured at a temperature range of 15 to 55 °C in a closed chamber. It is because the bulk temperature in the HPF process is 25 °C and the mean temperature of the hot formed tool is approximately 45 °C after the quenching operation.
- d) A geometry part of a hat-shaped tool is selected to evaluate the results in finite element simulation based on thermal analysis by using the convection heat transfer coefficient value between nanocoolant and chilled water. The heat transfer distribution data are collected and validated with the experimental results. This is important for cost effective commercial manufacturing of the final product and hot formed tools within a short time.
- e) Boron steels are chosen as the sheet metal blank materials while SKD 61 is selected as hot formed tools in this research. It is due to that the boron steel can achieve ultra-high strength steel grade after austenitization process. SKD 61 defined as a hot work tool with higher contact heat transfer coefficient value.
- f) The thickness of the boron steel blank is 1.8 mm at the austenite temperature of 900 °C in 5 minutes heating time. The experimentally measured heat distribution is attained via *k*-type thermocouples located inside the hot forming tool. The selection of these austenitization parameters is explained in detail in Section 2.8.1 and 4.3.3.
- g) The analyses on the mechanical properties of the hot formed parts are performed. The hardness and tensile strength test are conducted by using the Wilson Vickers 402 MVD machine and Universal Testing Machine model Instron 3369, respectively.

- h) Microstructure morphology evaluation cover from austenite transformation to martensite transformation phase for boron steel as delivered, chilled water formed boron steel and nanocoolants formed boron steel under the Light Optical Microscopy machine.

1.5 Hypothesis

Introduction of nanocoolants as cooling fluid in the HPF process is anticipated to be an effective method to enhance the heat transfer coefficient value and the cooling rate during quenching operation. The higher the volume concentration of nanoparticles, the thermal conductivity and heat transfer value would be positively affected. The heat transfer distribution analysis of the nanocoolants and chilled water are mapped based on the simulation and experimental performance. At the end of the research, it is anticipated that the microstructure transformation on the hot pressed part can be improved through the introduction of nanocoolants instead of chilled water. Thus, complementing of nanocoolants as an advanced heat transfer fluid to enhance the tensile strength and Vickers hardness value of hot pressed part.

1.6 Thesis Organisation

The organisation of the thesis is arranged and discussed as follows, and the structure is shown in Figure 1.3.

Chapter 2 presents the review of the kinds of literatures starting from the background of nanocoolants and a comprehensive review on the technology of high strength steel (HSS) materials as well as the most recent research for the hot press forming (HPF) process with the finite element simulation.

The information on the raw nanocoolant materials, the procedure of preparation, measurements, and investigations on the thermal physical properties of nanocoolants are covered in Chapter 3. This chapter demonstrates the experimental investigation of thermal conductivity and dynamic viscosity of aluminium oxides suspended in water-EG

mixture nanocoolant for the cooling channel of HPF tools application. Once the results from the characterization are obtained, the optimum convection heat transfer coefficient value is used to the finite element simulation to compare with chilled water.

Chapter 4 presents the finite element simulation for the hot forming tools and sheet metal blank which are analysed by means of thermal analysis. The temperature changes of the HPF tools and blank by using nanocoolant and chilled water are compared with several periods of quenching time. Once the results from the simulation are attained, the best parameter from HPF experiment will be validated against the heat transfer distribution of the simulation. This analysis is required for the improvement of HPF process in order to enhance the productivity and power consumption of HPF process. The mechanical properties like tensile strength and hardness and microstructure of the hot formed part will be examined.

Chapter 5 summarises the thesis by drawing conclusion and contributions of the present study to the body of knowledge as well as suggestions for the future works.

The logo for UIMP (University of Malakka) is a large, stylized letter 'V' shape. The left side of the 'V' is light blue, the right side is a darker blue, and the bottom point is a teal color. The letters 'UIMP' are written in white, bold, sans-serif font across the bottom of the 'V' shape.

UIMP

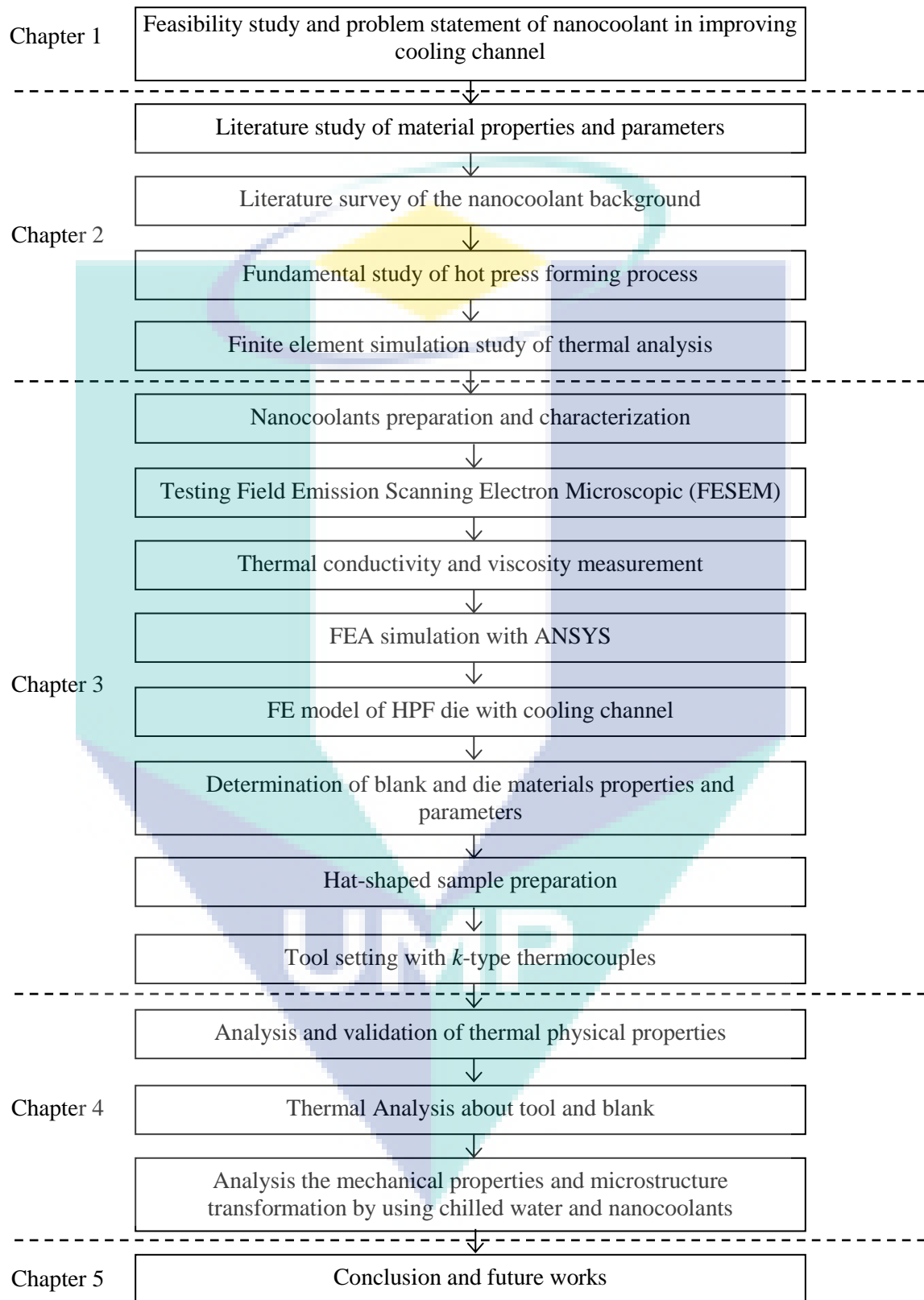


Figure 1.3 Thesis organisation

CHAPTER 2

LITERATURE REVIEW

2.1 Introduction

In this chapter the significance of the general field of nanocoolants study and hot press forming (HPF) process have been reviewed from various relevant studies, and the research gap has been identified. This chapter provides a comprehensive review on previous researches related to the boron steel materials, HPF process, finite element simulation and nanocoolants over the past decade. Topics such as the nanocoolants background, the preparation of nanocoolants, thermal properties, ethylene glycol as the fundamental in nanocoolants, boron steel and SKD 61 materials, heating method, transfer time, the heat transfer mechanism between tools and blank, and close up of previous studies on thermal analysis simulation were discussed. The significant findings in each study related to the dies and blank materials, heat transfer analysis and thermal physical properties such as thermal conductivity and dynamic viscosity are reviewed from various types of materials and base fluids. The review of nanocoolant studies that used ethylene glycol as the base fluid is provided to observe the current benchmark and research gap. Finally, the overview of the HPF process is simulated by finite element analysis is described. The review structured chronologically from the background to the detailed study related to the present research as to give a clear understanding on the direction of the study.

2.2 Background of Nanofluids as Coolant

Ultra-fine nanoparticles dispersed in a base fluid called nanofluid which is the new generation of heat transfer fluid and conventional cutting fluid. The base fluids can be engine oil, ethylene glycol, water or any lubricants. Krishna et al. (2013) stated that augmentation of heat transfer and tribological properties of the nanofluids could serve as better cooling and lubrication agent during machining, hence making the production more viable. Nanofluid was first introduced by Choi et al. (2004) in the Argonne National Laboratory. The research experiments proved that nanofluids are superior heat transfer properties compared to conventional heat transfer fluids such as water and oil.

Heat transfer fluids are mainly used in the industrial and manufacturing company for cooling purposes. However, the conventional cutting fluids as a cooling medium in the industry, mostly exhibit poor performance regarding to thermal conductivity compared to solids (Krajnik et al., 2011; Amrita et al., 2013). Utilizing nanofluids as a cooling agent in machining is one of the novel concepts to replace the conventional heat transfer fluid. Due to their heat transfer and tribological properties, nanoparticles prepared from different materials such as aluminium oxide, zinc oxide, copper oxide and titanium oxide have been used in the machining operations. The applicability of nanofluids as coolant is considered because of the improved heat transfer coefficient of the fluid due to the solid particle inclusion (Azmi et al., 2014).

In the manufacturing industry, advanced heat transfer fluids with higher thermal conductivity and greater heat transfer coefficient are intensely needed. In recent years, the advances in nanoparticles synthesis techniques evidenced that the nanoparticles suspended in the base fluids can effectively substitute the conventional cutting fluids. Due to the nanofluids with engineered colloidal suspensions of nano-meter sized particles which are uniformly and stably dispersed in the base fluids attained higher thermal properties. There have been a lot of studies on heat transfer and the improvement of cooling capabilities are still in the developing stages in recent years (Krishna et al., 2013). The value of thermal conductivity of different materials and conventional fluids has been summarized in Table 2.1. It can be seen that the thermal conductivity of solid particles is much higher than the liquids. It is predicted that the thermal conductivity of fluids

containing suspended solid particles could be significantly higher than that of the conventional fluids.

Table 2.1 Thermo-physical property of different types of metal and liquid

Types of Metal	Thermal Conductivity, k (W.m ⁻¹ .K ⁻¹)	Reference(s)
Al ₂ O ₃	36.0	Elias et al. (2014a)
ZnO	13.0	Bolz (2007)
TiO ₂	8.4	Azmi et al. (2014)
SiO ₂	1.4	Vajjha et al. (2010a)
Types of Liquid	Thermal Conductivity, k (W.m ⁻¹ .K ⁻¹)	Reference(s)
Ethylene Glycol	0.258	Cengel (2011)
Engine oil	0.145	Cengel (2011)

2.3 Properties of Water-Ethylene Glycol Based Nanocoolants

In manufacturing field, it is prevalent to use water or conventional oil as a coolant in machining. However, the problem of applying water as coolant is that the water may either freeze or boil at extreme temperature conditions. Thus, some additives are added into the water to decrease the freezing point and to increase the boiling point of the water. The additives could avoid the coolant to freeze when the temperature is too low, on the other hand to reduce the system overheat when it is too hot. Ethylene glycol was the most common additive mixed with water. Ethylene glycol has the molar mass of 62 g.mol⁻¹ and chemical formula of C₂H₂O₂. According to the International Union of Pure and Applied Chemistry (IUPAC), ethylene glycol also named as ethane-1,2-diol. The solution is colourless, clear and syrupy texture liquid at room temperature. It is also soluble in water to form transparent solutions. In thermal engineering systems, ethylene glycol consists of hydroxyl and ethylene where the hydroxyl part bonds with inorganic materials or water molecules. Hence, ethylene glycol can disperse well in the water (Kumaresan and Velraj, 2012).

The presence of ethylene glycol in extreme cold situation can avoid water to freeze at 0 °C temperature due to the lower freezing point of ethylene glycol which is -12 °C temperature. While, the boiling point of ethylene glycol is much higher than that of water, which attains around 198 °C temperature (Peyghambarzadeh et al., 2011a).

Figure 2.1 shows boiling point and freezing point of water and ethylene glycol mixture. It was shown that the mixture percentage of 60%:40% water-EG did not freeze up to -45 °C. Hence, the solution with a high boiling point is required for the high temperature operating system to prevent damage to the system due to overheating.

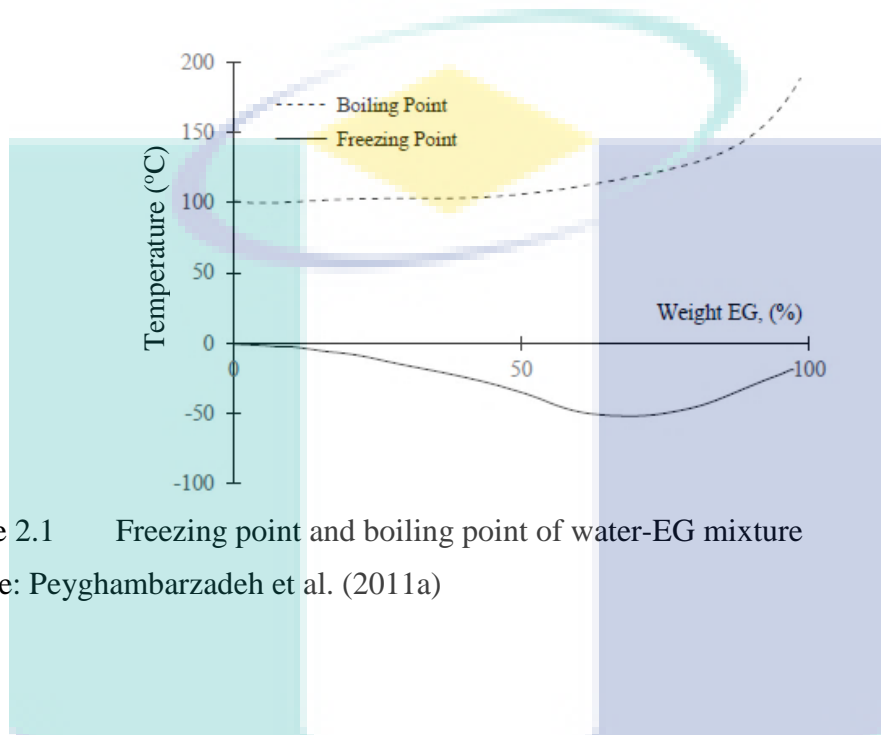


Figure 2.1 Freezing point and boiling point of water-EG mixture
Source: Peyghambarzadeh et al. (2011a)

Water and ethylene glycol mixture as a coolant for conventional thermal fluid is not a new concept in the thermal application. Coolant is used to cool down the system by flow through the instrument and prevent the instrument or system to be overheating. The coolant absorbed the heat produced by the device or system, and then transferred to the other places. A study from Denkena et al. (2014) stated that by controlling the volume flow rate of coolant can reduce the energy consumption of the machine in order to optimize the machine tools. These urged researchers in thermal fluids to use the mixture of ethylene glycol with high boiling temperature or low freezing point.

The most common choice of engine coolant has been a 50%:50% mixture of water and ethylene glycol in normal temperature and environment (Azmi et al., 2016). For extreme cold temperature, the higher percentage of ethylene glycol that greater than 70% in the coolant mixture lead breakdown of inhibitors towards corrosion effect. This high percentage of ethylene glycol decreased the anti-freeze protection and reduced the heat transfer performance (Azmi et al., 2016). In the year 2014, research on SiO₂ nanoparticles suspended in 40%:60% of water-EG mixture for three particle sizes of 20, 50 and 100

nm was reported (Azmi et al., 2014). Their experimental study on fluid dynamic characteristics and convective heat transfer enhancement with nanoparticle volume concentrations range from 2 to 10% with Reynolds number of 3,000 to 12,000. The research concluded that heat transfer coefficient increases as the increment of nanoparticle volume concentration and the effects are more significant for temperature around 0 °C. Bayat and Nikseresht (2012) conducted a research on forced convection heat transfer with water-EG based Al_2O_3 nanofluid at the temperature of 20 °C. The study was carried out with nanoparticles volume concentration of 1 to 10% and the Reynolds number from the range of 10,000 to 100,000. The thermal performance of nanofluids was measured by using $K-T$ model, a dimensionless quantity model. The study showed that the convective heat transfer performance was enhanced with the increased of nanoparticle volume concentrations at the same Reynolds number. On the other hand, a significant pressure drop and pumping power were measured by using nanofluids in the turbulence region.

2.4 Nanoparticles as Suspended Material

Nanoparticles defined as ultrafine particles with the size below 100 nm which can be denoted as ten to the power of minus nine. Therefore, nanotechnology manipulates particles of nano-meter sizes that are much smaller than objects that obey Newton's laws of motion. However, it is not small enough as atomic level or simple molecule that is governed by quantum mechanics (Estelrich et al., 2014). Due to the development of modern nanotechnology manufacturing capabilities, varies the type of nanoparticles that had been produced. These are evolving interests to the engineering research to explore the research area of nanoparticle for various potential applications, especially in microelectronic, automotive and medical fields.

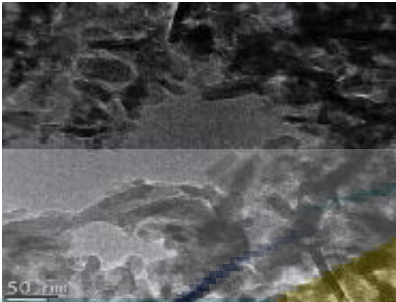
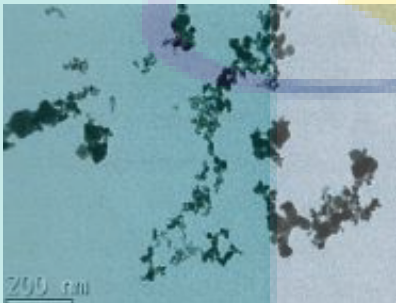
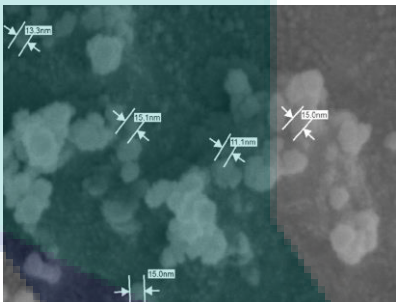
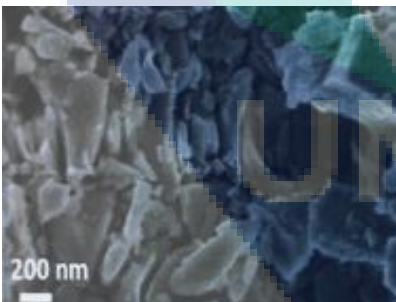
One of the novel approaches is utilizing the nanoparticle in a base fluid as a cooling agent in the hot press forming (HPF) process to replace the conventional fluid cooling. The size of nanoparticles has a large surface area-to-volume ratio that influences the dispersible and performance of heat transfer between the nanoparticles and their adjacent environment. For instance, a 1 nm spherical particle has a surface area-to-volume ratio 1000 times greater than a 1 μm particle (Esfe et al., 2015). Therefore, the

size of particles significantly affected the melting point and thermal properties. When the nanoparticles are in suspension form, the free mobility condition is significantly enhancing the heat transfer performance of the fluid. In an experiment, few types of nanoparticles in small amounts have been dispersed in a conventional solution, and the results showed the rise of thermal conductivity (Wu and Zhao, 2013).

Physical properties of nanoparticles included their shape, size and morphological sub-structure. The actual shape and size of nanoparticles are identified through high magnification microscopes such as the Transmission Electron Microscopy (TEM) for particles suspended in liquid and Field Emission Scanning Electron Microscopy (FESEM) for solid particles. Lee et al. (2012) obtained TEM for nanofluid based Al_2O_3 morphology determination. The Al_2O_3 nanoparticles in nanofluid were observed to have the cylindrical shape and less than 50 nm size. Mariano et al. (2013) used TEM techniques to observe the structure and size distribution of ethylene glycol based SnO_2 nanofluid in a study on rheological behaviour and thermal conductivity of nanofluids. The picture obtained from TEM showed that the composition of quasi-spherical shape and less than 100 nm size.

Abdolbaqi et al. (2016) had obtained the FESEM for water-bioglycol mixture based Al_2O_3 nanofluids. The images revealed that the shape of the nanoparticles was spherical and size of the nanoparticles in nanofluid was measured to have an average diameter of 13 nm. In a study on rheological behaviour and thermal physical properties of SiC nanofluids, Nikkam et al. (2014) used the SEM machine to determine the morphology of the nanofluids. The picture showed that the hexagonal crystal structure with an average nanoparticles size of approximately 115 nm. The summary of several types of nanoparticles and micrograph pictures are compiled in Table 2.2.

Table 2.2 Various types of nanoparticles and micrograph images

Micrograph Image	Types of Particles
	<p>Author(s) : Lee et al. (2012) Micrograph : TEM Nanoparticles : Al₂O₃ Shape : Cylindrical Size : 50 nm</p>
	<p>Author(s) : Mariano et al. (2013) Micrograph : TEM Nanoparticles : SnO₂ Shape : Quasi-spherical Size : <100 nm</p>
	<p>Author(s) : Abdolbaqi et al. (2016) Micrograph : FESEM Nanoparticles : Al₂O₃ Shape : Spherical Size : 13 nm</p>
	<p>Author(s) : Nikkam et al. (2014) Micrograph : SEM Nanoparticles : α-SiC Shape : Crystalline Size : 115 nm</p>

2.4.1 Nanoparticle materials

Several types of nanoparticles are produced by utilizing the advancements in the nanotechnology industry, but the selection of nanoparticles depends on the properties and application. Nanoparticles can be categorized into few types based on the material and

structure of the particles. Many research investigations with different types of nanoparticles have been reported to enhance the thermal properties.

Pure metallic nanoparticles are the materials that have single ions such as silver (Ag), aluminium (Al), iron (Fe), copper (Cu), and gold (Au) (Monosson, 2013). The metallic nanoparticles are preferable for thermal application as they share the similar properties. Several studies of metallic nanoparticles suspended in base fluids have been carried out than the oxide nanoparticles. Heris et al. (2013) investigated that thermal conductivity of nanofluid based copper is enhanced by 23.85% compared to water when nanoparticles volume concentration of 0.1%. However, authors found that the thermal conductivity considerably decreased with the elapsed time when no surfactant was introduced in the nanofluids. Their chemical reaction with base fluid required to be considered for the application purpose.

Polymer and carbon nanotubes are majority used in the fundamental studies of nanofluids. The behaviour of multi-walled carbon nanotubes (MWCNT) mixed with water showed a significant increment of heat transfer efficiency compared to the pure water. Nevertheless, in a study of heat transfer of carbon nanotubes based nanofluid, they concluded that the enhancement of heat transfer depends on the condition of the flow and the volume concentration of carbon nanotubes with minimum pH effect (Haddad et al., 2014).

Metal oxide nanoparticles such as carbide ceramics, oxide ceramics and nitride ceramics as ceramics nanoparticles are the first materials that are used to synthesize nanofluids (Hadadian et al., 2013). The reason behind the preferable is easy to prepare and its chemical stability. Each ceramics class developed distinctive material properties as they dispersed in the conventional heat transfer fluid. Among these kinds of ceramics, the most interested nanoparticles by the researchers are oxide ceramic nanoparticles. The pioneer of the new class fluid such as Pak and Cho (1998) choose Al_2O_3 nanoparticles with the unexpected finding of thermal conductivity enhancement to enhance heat transfer performance. This finding triggered interest for further development.

2.4.2 Types of synthesized nanofluids

Nanofluids consist of two elements which are nanoparticles and base fluids. A variety of materials such as metal oxide, carbon nanotube, carbide, metal and hybrid are used in preparing the nanofluids. The selection of nanoparticles material depends on many reasons, including the application and performance. Initially, metal oxide and metal were used since the access to the material was easier where many manufacturers abundantly produced the materials.

In 2010, a group of researchers used copper nanoparticles suspended in an ethylene glycol base fluid by using a novel one-step method to prepare the nanofluids (Yu et al., 2010). For thermal conductivity and heat transfer performance, Chun et al. (2011) used silicon carbide (SiC) with water base nanofluid to investigate the effect of nanofluid on a boiling thin platinum wire. Nikkam et al. (2014) used α -SiC for investigation of rheological behaviour and thermal-physical properties. For a new modification of carbon nanotube (CNT), researchers such as Gao et al. (2012) and Esfe et al. (2014) for the study of nanofluid thermal physical properties and heat transfer performance by using functionalized carbon nanotube (FCNT) and multi-walled carbon nanotube (MWCNT), respectively.

Another popular type of material used in the nanofluid field is the metal oxide such as copper oxide (CuO), silicon oxide (SiO₂) and aluminium oxide (Al₂O₃). Azmi et al (2013) investigated on the convective heat transfer enhancement with nanofluids consisting dispersion of SiO₂ in the water-EG mixture base fluid. For a study on the effective electrical conductivity of nanofluids, Zakaria et al (2015) used Al₂O₃ nanoparticles suspended in water-EG mixture. In 2014, researchers such as Azmi et al. (2014a), Said et al. (2014) and Hajjar et al. (2014) used several types of metal oxide nanoparticles in water dispersion such as SiO₂, TiO₂, Al₂O₃ and graphene oxide (GO). These studies were about the effects of temperature and nanoparticles volume concentration on the thermo-physical properties and convective heat transfer performance of nanofluids under turbulent regions.

Hybrid nanoparticles are the latest type of nanoparticles in nanofluids studies. More than two materials are combined to produce the hybrid material by using chemical

processes. In 2011, Suresh et al. (2011) demonstrated an experiment on thermal physical properties of nanofluids based Al₂O₃-Cu hybrid nanoparticles. Madhesh et al. (2014) used the hybrid nanoparticles of Cu-TiO₂ for investigation on rheological properties and heat transfer performance. The summary of several types of nanoparticles used in different studies is gathered in Table 2.3.

Table 2.3 Types of nanoparticles dispersed in nanofluids

Nanoparticles	Base fluid	Reference(s)
Metal		
Copper, Cu	EG	Yu et al. (2010)
Carbide		
Silicon carbide, SiC	De-ionized water	Chun et al. (2011)
α – type Silicon carbide, α -SiC	Water/EG (50:50)	Nikkam et al. (2014)
Carbon Nanotube		
Functionalized CNT, FCNT	Water	Gao et al. (2012)
Multi-walled CNT, MWCNT	Water	Esfe et al. (2014)
Metal Oxide		
Silicon oxide, SiO ₂	Water/EG (60:40)	Azmi et al. (2013)
Aluminium oxide, Al ₂ O ₃	Water/EG	Zakaria et al. (2015)
Silicon oxide, SiO ₂	Water	Azmi et al. (2014a)
Titanium oxide, TiO ₂	Water	Hajjar et al. (2014)
Graphene oxide, GO	Water	Hajjar et al. (2014)
Aluminium oxide, Al ₂ O ₃	Water	Said et al. (2014)
Titanium oxide, TiO ₂	Water	Said et al. (2014)
Hybrid Particle		
Al ₂ O ₃ -Cu	Water	Suresh et al. (2011)
Cu-TiO ₂	Water	Madhesh et al. (2014)

2.5 Nanofluids Preparation

Nanofluids can be defined as synthesizing nanoparticles with base fluid where the nanoparticles remain in suspension for a certain time period. Two ways of well-known methods for preparation of nanofluids are two-step method and one-step method. However, many studies used the two-step method in which nanoparticles are first produced as dry powders and then dispersed into the base fluid as the second processing step. The one-step method can be defined as a process of combining the nanofluid

synthesis and preparation of nanoparticles directly in the heat transfer fluid. Figure 2.2 illustrates the technique of the one-step method for nanofluids synthesis.

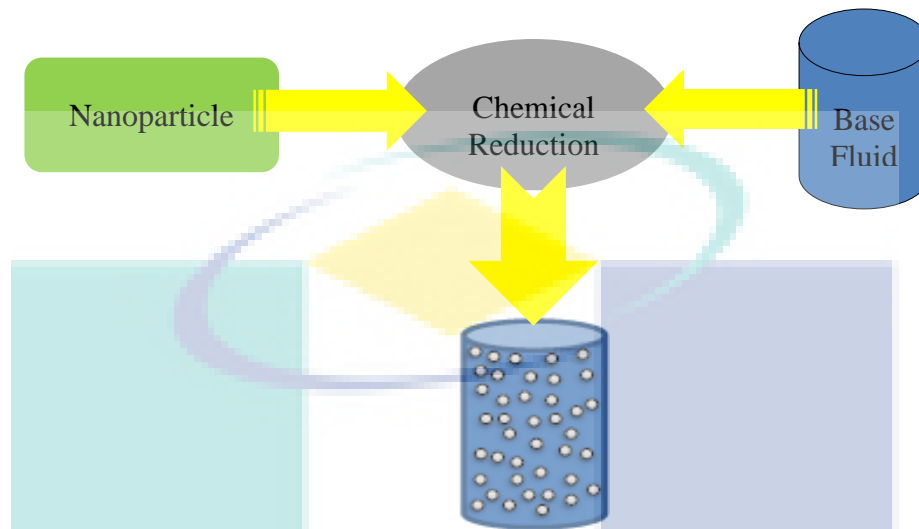


Figure 2.2 One-step method technique

Some researchers have used the one-step method to synthesize copper nanofluids (Zhu et al., 2009, Liu et al., 2006). In one-step method, copper nanoparticles are contacted with ethylene glycol, and then under the nitrogen atmosphere by chemical reduction method to produce Cu-water nanofluids (Liu et al., 2006). This method was found to be an efficient and fast method that Cu nanofluids obtained better stabilization and higher reaction rate (Zhu et al., 2009). However, the disadvantages of the one-step method are very costly and the nanofluids cannot be produced on a large scale for industrial implementation. Regarding Yu and Xie (2012), nanofluids might have contaminated or impurity due to incomplete chemical reaction and preparation process in the one-step method.

Two-step method requires dispersion process for better stabilization of nanoparticle into a base fluid and is illustrated in Figure 2.3. According to Sidik et al. (2014), nanofluids preparation was using the two-step method begins by directly synthesizing nanoparticles with the base fluid. This method is the most extensively used to process for preparing nanofluids (Suresh et al., 2011). Reddy et al. (2013) dispersed TiO_2 with an average diameter of 20 nm size into water-EG mixture as the base fluid. Lim et al. (2016) experimented Al_2O_3 /water-EG mixture nanofluid and found that nanofluid under ultra-sonication process for 1 hour has enhanced the stability of

nanofluids for one month. The two-step method is the most cost-effective method to produce a large amount of nanofluids due to nanoparticle synthesis techniques have already been scaled up to industrial production level (Yu and Xie, 2012). Furthermore, ultra-sonication using an ultrasonic bath was used for nanofluids preparation to achieve uniform nanoparticles dispersion.

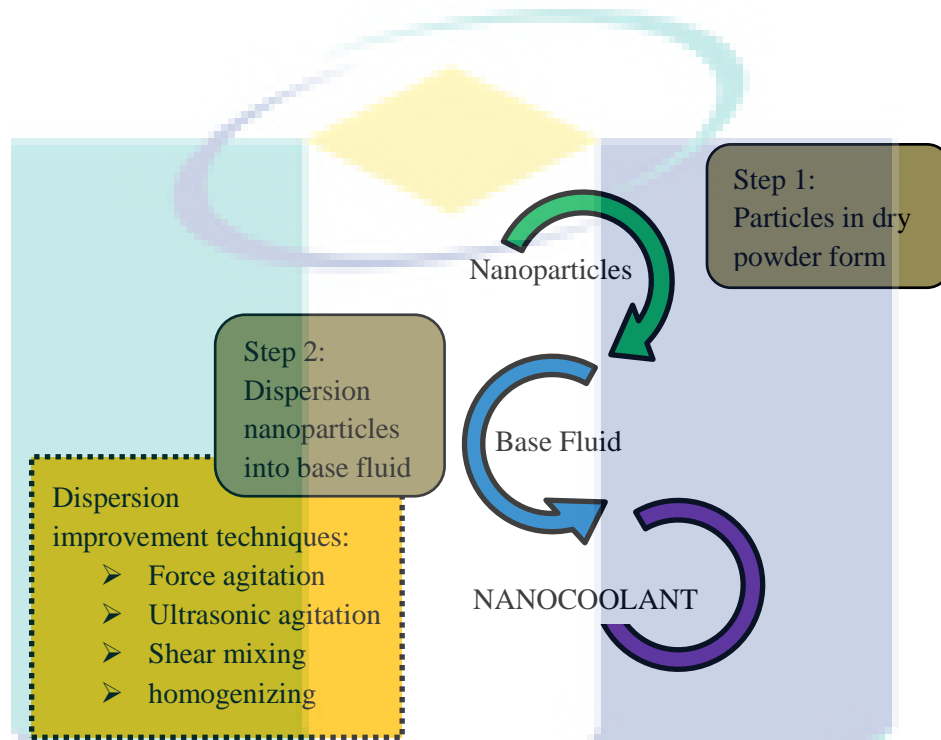


Figure 2.3 Two-step method technique

2.6 Thermal Properties of Nanofluids

Thermal physical properties of nanofluids include dynamic viscosity, thermal conductivity, density and specific heat. These thermal physical properties are related to the convection heat transfer coefficient, h and enhancement of heat transfer (Hussein et al., 2014). The researchers found that the trend of heat transfer coefficient increases with effective thermal conductivity, density and specific heat but decreases with dynamic viscosity.

2.6.1 Dynamic viscosity

Property of collisions between particles and subsequent particles in a fluid that is moving at different velocity is named as dynamic viscosity. The graph of velocity pattern versus velocity is shown in Figure 2.4. Regarding the graph, shear stress is related to the velocity gradient when the fluid flow in the straight channel. The constant of proportionality is called as dynamic viscosity, μ with the unit of $\text{kg}\cdot\text{m}^{-1}\cdot\text{s}^{-1}$, or $\text{N}\cdot\text{s}\cdot\text{m}^{-2}$, or Pa·s (Cengel, 2010). However, the majority of researches suggested that the nanocoolants have the best performance with high thermal conductivity and low viscosity (Azmi et al., 2014a; Lim et al., 2016). Therefore, nanocoolants as heat transfer fluids are expected to show the increased of thermal conductivity without increased of pressure drop. Nanoparticles with base fluid mixtures are suitable to replace water because of the disadvantages of water such as high vapour pressure, high corrosive and limited operating temperature range (Timofeeva et al., 2011).

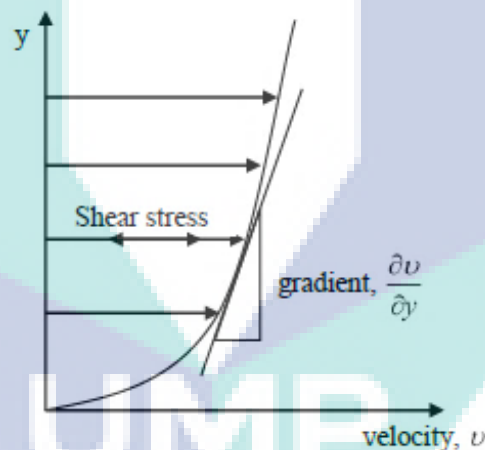


Figure 2.4 Graph of velocity pattern versus velocity

Source: Cengel (2010)

The dynamic viscosity of nanocoolants is not a constant variable which is affected by temperature difference and volume concentration (Yu et al., 2012; Vajravelu et al., 2013). The published research such as Samira et al. (2015) used CuO nanoparticles dispersed in 40%:60% water-EG mixture and a temperature range from 10 to 50 °C. Authors found that the dynamic viscosity of nanocoolants decreased with the increase of temperature. The dynamic viscosity of nanocoolant based CuO was enhanced about

73.21% compared with the base fluid. Another researcher, Sundar et al. (2012) observed that the dynamic viscosity of nanocoolants increased with the increment of volume concentration and decreased with the temperature range from 0 to 50 °C by dispersing Fe₃O₄ nanoparticles in 80%:20% water-EG mixture. The viscosity of Fe₃O₄ at 1.0% volume concentration in 80%:20% mixture was enhanced by 2.94 times compared with the base fluid.

In 2013, one of the researchers conducted an experiment with 40%:60% water-EG mixture based Al₂O₃. The results show that water-EG based Al₂O₃ nanocoolants present Newtonian behaviours for low concentration after the temperature below 40 °C (Said et al., 2013). Thus, nanocoolants viscosity not only depends on the temperature and volume concentration, but also the type of base fluid used to contribute to the nanocoolants viscosity. Moreover, Timofeeva et al. (2011) investigated the effect of base fluid and temperature to heat transfer performance. The experimental studies on SiC dispersed in water-EG mixture of ratio 50%:50% showed that the efficiency of nanocoolants was higher for mixture based fluids compared to water based fluids. Also, the heat transfer performance of nanocoolants is enhanced by increasing in temperature as viscosity decreased. Table 2.4 shows the summary of dynamic viscosity investigations made by several researchers for different types of nanocoolants and relevant findings.

Table 2.4 Dynamic viscosity investigations for different types of nanocoolants

Author(s)	Nanoparticles & Base Fluids	Temperature Range & Concentration Range	Findings
Samira et al. (2015)	CuO, W/EG (40:60)	T: -35 – 50 °C φ: 1.00 – 6.12%	Dynamic viscosity decreases with increasing temperature. ↓
Kole and Dey (2010)	Al ₂ O ₃ , W/PG (50:50)	T: 10 – 50 °C φ: 0.1 – 1.5%	Dynamic viscosity decreases with increasing temperature. ↓
Timofeeva et al. (2011)	SiC, W/EG (50:50)	T: 15 – 85 °C φ: 4.0%	Dynamic viscosity decreases with increasing temperature and mixture based fluids better than water based fluids. ↓
Kole and Dey (2011)	CuO, Gear oil	T: 10 – 80 °C φ: 0.5 – 2.5%	Non-Newtonian behaviour observed, as concentration increased.

Table 2.4 Continued

Author(s)	Nanoparticles & Base Fluids	Temperature Range & Concentration Range	Findings
Yu et al. (2012)	Al ₂ O ₃ , W/EG (55:45)	T: 10 – 70 °C ϕ : 1.0 – 3.0%	Newtonian behaviour after temperature below 45 °C.
Sundar et al. (2012)	Fe ₃ O ₄ , W/EG (80:20)	T: 0 – 50 °C ϕ : 0 – 1.0%	Dynamic viscosity enhanced by 2.94 times at 1.0% concentration. ↑
Said et al. (2013)	Al ₂ O ₃ , W/EG (40:60)	T: 25 – 80 °C ϕ : 0.05 – 1.0%	Newtonian behaviour in low concentration after temperature below 40 °C.
Jarahnejad et al. (2015)	TiO ₂ , Water	T: 20 – 50 °C ϕ : 3.0 – 14.0%	Dynamic viscosity increased with increasing concentration, while it decreased with increasing temperature. ↑
Serebryakova et al. (2015)	Al ₂ O ₃ , W/EG (10:90)	T: 20 – 80 °C ϕ : 0 – 1.5%	Dynamic viscosity increased with increasing concentration. ↑

2.6.2 Thermal conductivity

Thermal conductivity is the property of a substance to conduct heat. The thermal conductivity of substances is temperature dependent. Nanoparticles disperse in conventional base fluids such as engine oil, water and ethylene glycol has been found to enhance the thermal performance compared to pure traditional base fluids (Azmi et al., 2013; Abbasi et al., 2014). Nanometer sized particles with a diameter of 1-100 nm suspended in base fluids are better than those fluids containing milli- or macro- sized particle regarding to particles sedimentation issue and significant enhancement of the effective thermal conductivity (Lim et al., 2016). The study of the thermal conductivity of a fluid plays vital role in the improvement of energy-efficient heat transfer equipment. Several experimental and theoretical investigations on increasing the thermal conductivity of water base fluids by suspending nanoparticles such as TiO₂, Al₂O₃ and SiO₂ have been conducted. Currently, many researchers applied different types of nanoparticles to study the rheological behaviour of the nanofluids experimentally.

Sundar et al. (2013a) conducted a study on thermal properties using CuO with 27 nm sized particles suspended in 50%:50% mixture of water-EG base fluid. They found that there was a positive augmentation of thermal conductivity of CuO nanofluid as the nanoparticles volume fraction and temperature of nanofluids increased. Lim et al. (2016) conducted an experimental investigation of thermal properties by dispersing Al₂O₃ in a mixture of water-EG base fluid and observed that the enhancement of thermal conductivity is about 10% higher than the base fluid in 1.0% concentration at 55 °C temperature. Apart from these two outstanding factors, thermal conductivity enhancement also found to be influenced by the types of base fluids and type of nanoparticles as well as the stability of the nanofluids (Pastoriza-Gallego et al., 2011; Javadi et al., 2013).

Ethylene glycol based nanoparticles provided better heat transfer enhancement than water base nanofluids. It is proven by Esfe et al. (2015) in a study of heat transfer behaviour of water based γ -Al₂O₃ and ethylene glycol based γ -Al₂O₃. Another investigation of thermal conductivity found that thermal conductivity of nanofluids follows the behaviour of ethylene glycol as base fluid at the same temperature in a pure base fluid (Beck et al., 2010). Researchers conducted thermal conductivity measurement of different types of nanoparticles such as copper oxide (CuO), silicon oxide (SiO) and multiwall carbon nanotubes (MWCNT) suspended in ethylene glycol and water base fluid. Each measurement showed enhancement of thermal conductivity as the different ratio of ethylene glycol base fluid (Esfe et al., 2015). Table 2.5 concluded that the thermal conductivity study by several researchers using different types of nanofluids.

Table 2.5 Thermal conductivity study for diverse types of nanofluids

Author(s)	Nanoparticles & Base Fluids	Scope of Experiment	Enhancement of k (%)
Lee et al. (1999)	CuO (35 nm) Ethylene glycol	Concentration: 4.0%	20
Beck et al. (2010)	Al ₂ O ₃ (20 nm) Ethylene Glycol	Concentration: 0 – 4% Temperature: 25 – 138 °C	↑
Timofeeva et al. (2011)	Al ₂ O ₃ (40 nm) Water Ethylene Glycol	Concentration: 0.5-10% Temperature: 10 – 60 °C	10 13

Table 2.5 Continued

Author(s)	Nanoparticles & Base Fluids	Scope of Experiment	Enhancement of k (%)
Suganthi et al. (2014)	ZnO (29 nm) Ethylene glycol	Concentration: 5.0%	26.5
Yu et al. (2012)	Al ₂ O ₃ (20 nm) CuO (29 nm) R113	Concentration: 0.1 – 1.2%	3-7
Vajjha and Das (2010)	CuO (29 nm) ZnO (29 nm)	Concentration: 0 – 7% Temperature: 25 – 90 °C	18 21.4
Parekh and Lee (2010)	Fe ₃ O ₄ (9.9 nm) Ethanol	Concentration: 4.7% Temperature: 25 – 65 °C	30
Pang et al. (2012)	Al ₂ O ₃ (40 nm) SiO ₂ (20 nm) Methanol	Concentration: 0.005 - 0.5% Temperature: 20 °C	10.74 14.29
Sundar et al. (2013a)	CuO (27 nm) Al ₂ O ₃ (36.5 nm) EG:W/50:50	Concentration: 0.2 – 0.8% Temperature: 20 – 60 °C	↑

Notation: ↑ - increased pattern

2.7 Sheet Metal of Boron Steel

Boron steel is one of the low carbon martensitic steel. Srithananan et al. (2016) stated that after the austenitization process, boron steel sheet metal only could achieve ultra-high strength steel (UHSS) grade. The strength of boron steel is around 600 MPa as delivered form and the final formation of boron steel to obtain 1,400 MPa strength after hot press forming (HPF) process (Naderi, 2007). The capability of boron steel to obtain complex geometry with good hot formability and optimum performance of mechanical properties are the primary purposes of using this material. Moreover, it is desirable owing to its exceptional fatigue strength and the absence of springback effect as hot formed boron steel.

Boron steel is categorised as low alloyed steel, and it is well-known for its ability to be strengthened through heat treatment to increase mechanical properties in terms of tensile strength and hardness. Boron steel contains several alloying elements such as Manganese (*Mn*), Silicon (*S*), Carbon (*C*), Titanium (*Ti*), Phosphorus (*P*), Aluminium

(Al), Sulphur (S) and Boron (B) as shown in Table 2.6. Typically, boron is the most significant element that greatly improves the hardenability of boron steel sheet metal among the overall elements, while the existence of carbon determined the hardness of boron steel (KarbAsian and Tekkaya, 2010).

Table 2.6 Chemical compositions of boron steel weight percentage and mechanical properties before and after quenching operation

	Alloy Element							
	<i>Mn</i>	<i>Si</i>	<i>C</i>	<i>Ti</i>	<i>P</i>	<i>Al</i>	<i>S</i>	<i>B</i>
22MnB5	1.100 - 1.400	0.150 - 0.350	0.200 - 0.250	0.020 - 0.050	≤0.025	≥0.015	≤0.008	0.002 - 0.005
Mechanical Properties								
	<i>Yield Strength (MPa)</i>		<i>Ultimate Strength (MPa)</i>		<i>Elongation (%)</i>			
As delivered	400		600		25			
After quenching	1200		1400		5			

Source: KarbAsian and Tekkaya (2010)

Annealed boron steel has a mixture of ferrite and pearlite phase microstructure with an ultimate strength of 600 MPa. The microstructure of boron steel gradually transformed into austenitic phase by heating about 830 °C and it is fully transformed at the temperature range of 900 to 950 °C (KarbAsian and Tekkaya, 2010). When the austenitic phase of boron steel is quenched or immediately cooled down, its phase is transformed to martensite or bainite phase or a mixture of both phases depending on its cooling rate as presented in Figure 2.5. In order to obtain the high strength of the final part with 1,400 MPa, the austenitic phase must be fully transformed to the martensitic phase where it must be cool down at a rate of at least 27 K·s⁻¹ (Zhang et al., 2014).

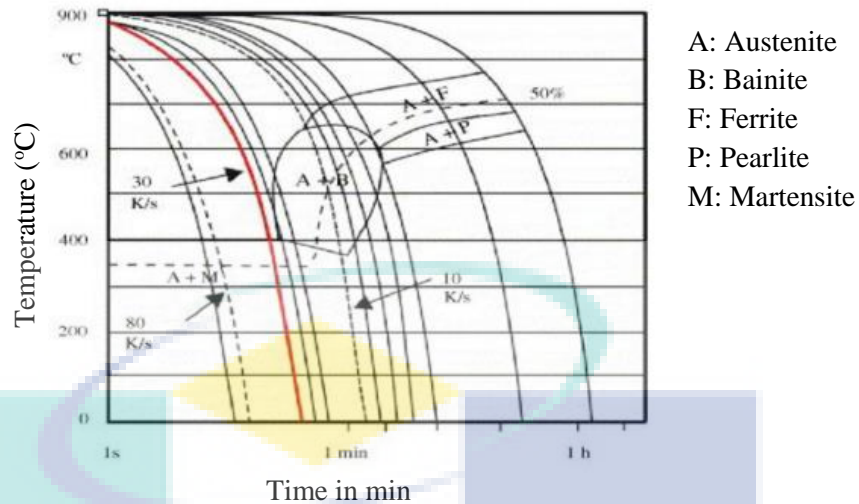


Figure 2.5 Temperature, time and transformation diagram of boron steel at various cooling rates

Source: Abdul-Hay et al. (2010)

The graph shows that the austenitic phase is continuously transformed into martensitic phase, which starts at the temperature of approximately 400 °C during quenching operation and it is fully martensitic transformation at a temperature range of 200 to 250 °C. In 2012, a researcher investigated metallurgical transformation of boron steel and found that HPF process significantly improves the mechanical properties of boron steel in terms of strength and hardness but reduces the percentage of elongation (Jiang et al., 2012). It is because thermal properties of boron steel such as thermal conductivity, k , specific heat, C_p and elastic modulus, E are likely to vary with the change of material microstructure from the austenitic phase to martensitic phase. Table 2.7 concludes the summary of boron steel with different microstructure phases in temperature range from 20 to 1,000 °C during processing.

Table 2.7 Thermal-physical properties of boron steel

	Temperature, T (°C)										
	20	100	200	300	400	500	600	700	800	900	1000
k ($\text{W}\cdot\text{m}^{-1}\cdot\text{K}^{-1}$)	30.7	31.	30	27.5	21.7		23.6		25.6		27.6
C_p ($\text{J}\cdot\text{kg}^{-1}\cdot\text{K}^{-1}$)	444	487	520	544	561	573	581	586	590	596	603
E (GPa)	212	207	199	193	166	158	150	142	134	126	118

Source: Bardelcik et al. (2014)

2.8 Hot Press Forming Process

In 1984, hot press forming (HPF) process was implemented in vehicle manufacturing to produce ultra-high strength steel (UHSS) boron steel. Currently, the HPF process exists in two different methods, namely direct and indirect process. The direct HPF process consists of a blank which is heated and fully austenite in a furnace for a certain period of time at temperature 900 °C. Then, the heated blank is transferred to an enclosure forming tool by a transfer unit. However, the lower punch force also can produce any complex shape of parts due to sheet metal exhibits excellent ductility properties at high temperature. (Liu et al., 2013). Finally, the heated blank is formed and quenched in a forming tool enclosure with coolant to produce the fully martensitic transformation part. Figure 2.6 shows the direct HPF process using a robotic arm to transfer the heated blank from the furnace to forming die. Figure 2.7 shows another HPF method namely as indirect HPF process which includes the conventional cold forming operation prior to the austenitization process. Indirect HPF process start from a part to be pre-formed, and drawn to approximately 90% of the final shaped in a cold die, then followed by a partial trimming operation (Hu et al., 2013). After that, it is heated in a furnace and quenched in the enclosure die. The reason for the additional step is to extend the forming limit for complex shapes by hot forming and quenching the pre-formed parts.

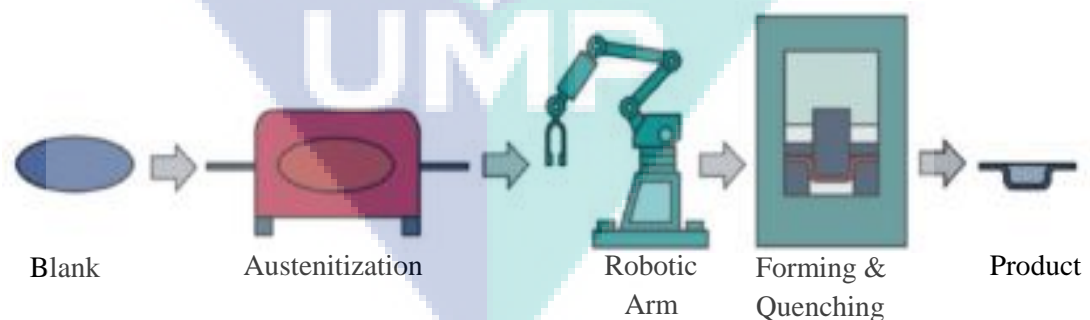


Figure 2.6 Direct hot forming process

Source: Karbasian and Tekkaya (2010)

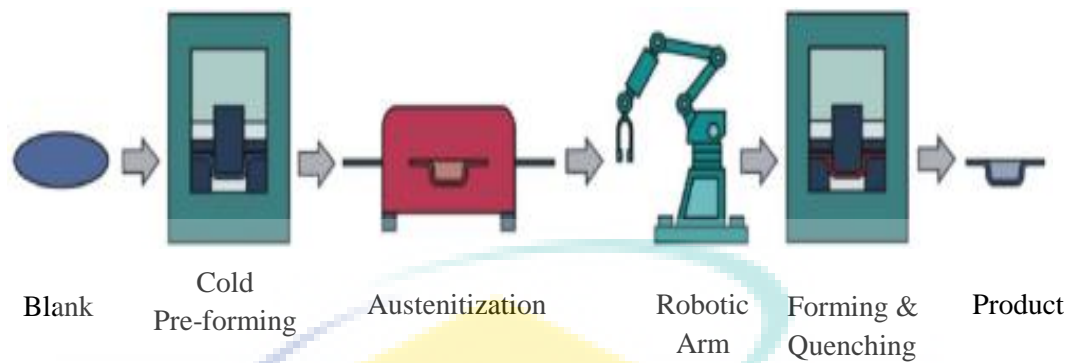


Figure 2.7 Indirect hot press forming

Source: Karbasian and Tekkaya (2010)

In 2014, the researchers stated that indirect HPF focused on quenching and calibration in the press after austenitization operation for complete cold pre-forming part (Merklein et al., 2014). The difference between indirect hot press forming and the direct process is the pre-formed part is heated in the continuous furnace and quenched in the tools. Naganathan reported that pre-forming operation is added to extend the forming limit for the complex shapes by hot stamping and quenching of the cold pre-formed products (Naganathan, 2010). Product designs of indirect HPF begin with cold pre-forming dies design before heating up the blank in the furnace and HPF process. Lastly, the hot formed parts are applied in the automotive industry for chassis components such as bumper, A-pillar, B-pillar and roof rail (Hu et al., 2013).

Sheet metal forming is crucial for cold pre-forming operation. The most general process is sheet metal bending which is used to form pieces such as hat-shape profile. It is also to enhance the stiffness of sheet metal by increasing its moment of inertia (Hu et al., 2017). Sheet metal with the hat-shaped profile is obtained when two parallel bending axes are produced in the same bending process and then a backing pad is used to force the sheet contacting with the punch bottom (Boljanovic and Paquin, 2006). Figure 2.8 shows the bending process to produce hat-shaped workpiece. In a hat-shaped bending process, the bending line (B) is present at two locations and the bending force with the double value of bending line length is applied to sheet metal (Misumi, 2015). In this project, hat-shaped profile bending as a sheet metal blank in HPF process for introducing nanocoolants of improvement cooling channel performance.

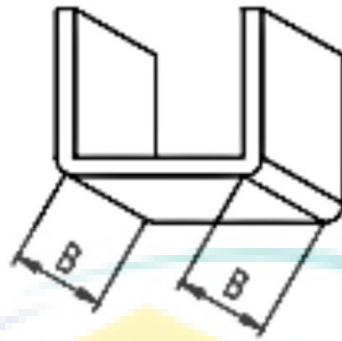


Figure 2.8 Hat-shape profile bending operation

Source: Misumi (2015)

2.8.1 Heating operation

The hot press forming (HPF) process starts with heating of the blank up to the austenitization temperature. In 2014, Maeno and his team demonstrated the annealing test by considering austenitization temperature and the time period for the determination of a homogeneous austenitization of the quenchable sheet metal 22MnB5 during HPF as a pre-condition for the desired fully martensitic transformation. In the experiment, the blanks were quenched through a full metallic contact pressure of 40 MPa on both sides (Maeno et al., 2014). To evaluate the occurring phase transformation, the hardness of the quenched blanks was measured according to the standard of Vickers HV 10. The fully martensitic microstructure and maximum hardness of approximately 470 HV of the quenchable sheet metal 22MnB5 were achieved with the austenitization duration time of 3 to 5 min from 900 to 950 °C austenitization temperatures (Karbasiyan and Tekkaya, 2010). The austenitization duration time increases with decreasing of furnace austenitization temperature.

In the HPF process, the blank can be heated using three different thermal phenomena: induction heating, electrical resistance heating and radiation in a furnace as presented in Figure 2.9. The heating method would be different depending on the purposes either research or production. Radiation inside the furnace is usually practiced in the mass production industry and it is proven that capable of heating the sheet metal blank. While in the research area, the three heating methods could be applied depending

on the adaptability and suitability of the operation to the experimental instruments (Karbasian and Tekkaya, 2010).

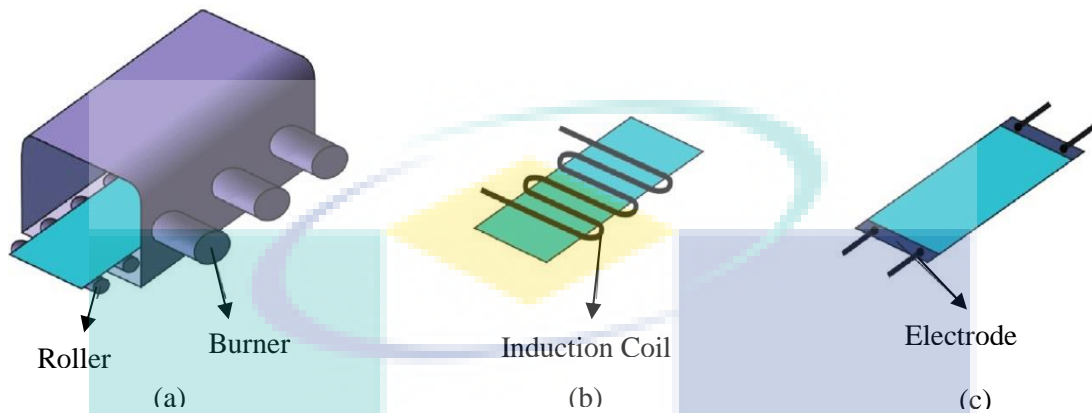


Figure 2.9 Various types of heating system (a) Roller hearth furnace, (b) Induction heating and (c) Electrical resistance heating

Source: Karbasian and Tekkaya (2010)

In the inductive heating operation, all electrically conducting or semiconducting materials can be heated by induction, and the resulting area of application is correspondingly large for this technology such as bulk forming, melting of metals and tempering. The geometry of the inductor determines the position of the magnetic field relative to the sheet metal blank, which causes different degrees of efficiency. The distance between blank and inductor also influences on the efficiency of the heating system. However, the electrical insulation between inductor and blank must be guaranteed, while shaped blanks tend to go out of shape when being heated (Karbasian and Tekkaya, 2010). An experiment conducted by Naderi et al. (2011) examined the capability of induction heating to heat up a blank to the austenitization temperature which was done by a special induction furnace. Figure 2.10a shows the two-step induction heating elements and a conveyor system of the induction furnace. Figure 2.10b presents the result of induction heating with different heating power and conveyor speed. The energy efficiency of induction heating is up to two times higher compared to the roller heating furnaces or radiation inside furnaces, because of the higher losses of the roller heating furnace by exhaust gases and rollers.

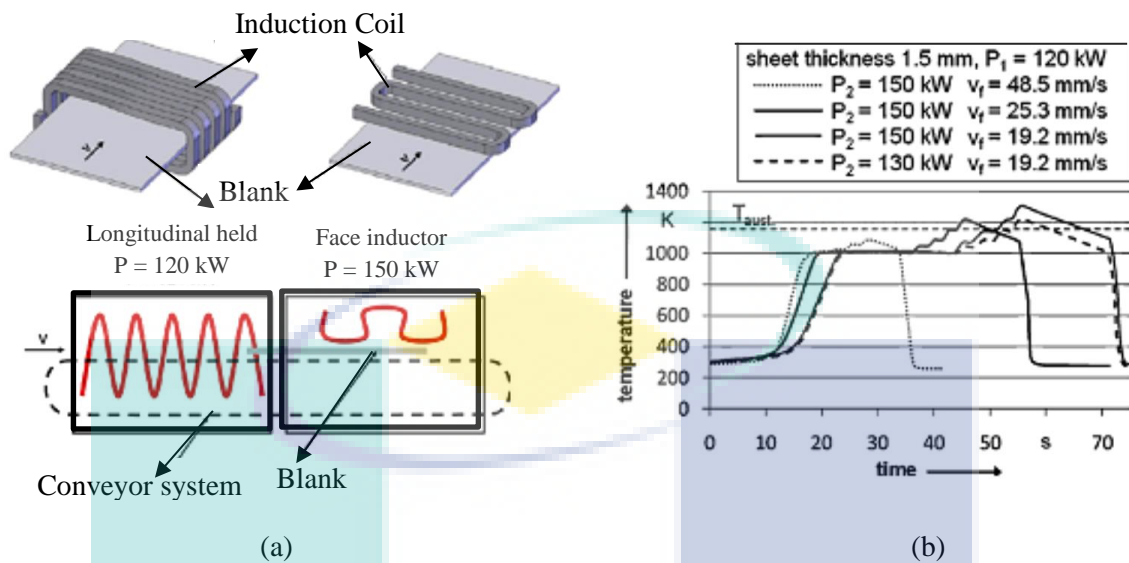


Figure 2.10 Induction heating operation (a) Schematics diagram of the customized induction furnace and (b) Variation of temperature curve as function of time for several feeding speed

Source: Naderi et al. (2011)

The most ordinary type of furnace used in the radiation inside furnace method is the roller hearth furnace. The connected load and size of the furnace depends on the throughput and material to be heated. Then, the pre-sized blank is continuously moved into the furnace by a conveyor passing through the austenitization chamber where the radiation from the combustion of petroleum gas increases the temperature of blank (Karbasiyan and Tekkaya, 2010). The cycle time for the form-hardened part is mainly dependent on the dies closing time and the furnace residence time required to heat up the blank. However, the furnace with approximately 30 to 40 m length in hot press forming production line caused high space requirement. Compared with the method of radiation inside the furnace, electrical energy used to austenite the blank could reduce furnace residence time in order to decrease the cycle time.

The principle of resistance heating is a blank clamped between the two pairs of electrodes as resistance for current passed through it (Mori et al., 2015). The resistance sheet metal caused the temperature of the part to heat up based on Joule's Law, which is due to that the heat generated in an electric circuit is proportional to the power of the electric circuit. Mori et al. (2015) investigated heat transfer distribution on the sheet metal

blank, and they discovered that a homogenous temperature distribution on blank with symmetrical shape could be achieved by properly arranging the position of the electrodes. Unfortunately, homogenous temperature or heat transfer distribution is very difficult for irregular and complex geometries blank shape due to the inconsistent distance between the negative and positive terminals. Mori et al. (2012) conducted a study of resistance heating was suitable for localizing heating and spot heating, although this heating method has limitations on heating the wide surface area and irregular blank shape. An experiment was demonstrated to punch a small hole on a hardened boron steel sheet metal part, and the cutting operation was done at several temperatures ranging from room temperature to 800 °C.

Figure 2.11 shows a small area of the hardened boron steel part was heated up by using a pair of rectangular electrode integrated inside the cutting tools. According to the experimental results indicated that proper selection of input electrical energy is vital for a resistance heating method to increase the temperature of sheet metal blank up to 800 °C in approximately 3 s. For this research project, the common heating furnace was used to austenite the sheet metal part inside the furnace. Then, the part was manually transferred to the HPF tools for quenching operation.

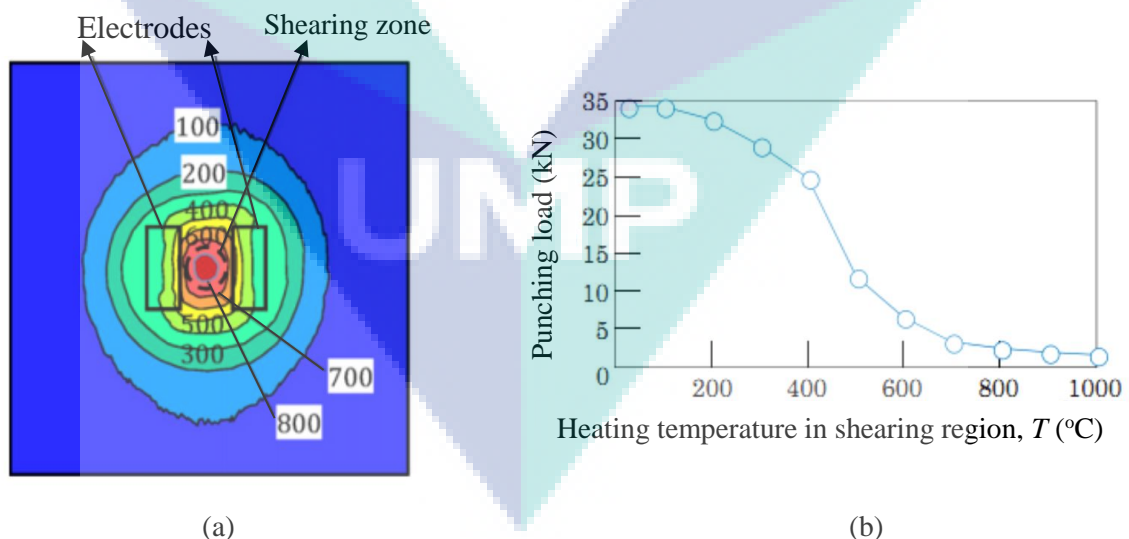


Figure 2.11 Localize heating (a) Positioning two rectangular electrodes on the blank and the temperature distribution diagram; and (b) Result of punching load for different heating temperatures in shearing region

Source: Mori et al. (2012)

2.8.2 Forming operation

Forming operation is a process where a sheet metal blank is drawn or plastically deformed into a specific shape of die and tool to produce the desired part (Banabic, 2010). Previously, the conventional cold forming operation was used to form sheet metal, but it was slowly replaced by hot press forming (HPF) process recently. Zhang et al. (2010) experimentally studied between hot press forming process and cold forming process, they found that the high dimensional accuracy can be obtained due to the low value of springback in HPF; and the thickness and weight of sheet metal can be reduced but the high strength part can be produced. Furthermore, the major parameter in a forming operation that needs to be considered are the behaviour of the materials and springback. The behaviour of material can be predicted by using the forming limit diagram (FLD) to simulate the result of material failure tests. Springback is when metal tends to return to its original shape or contour after undergoing a forming operation (Kim et al., 2015).

The forming limit diagram is used for forming the sheet metal to predict the forming behaviour of the blank (Cui et al., 2015). The diagram demonstrated graphical description of the material failure tests in order to determine the failure zone and the mechanical test is performed as shown in Figure 2.12. According to the simulation of B-pillar for geometry and tools, the initial temperature of sheet metal blank is 800 °C and tool surface temperature is approximately 200 °C. Figure 2.13 attempts to provide a simulated graphical description of the sheet metal part failure if it was formed at room temperature.

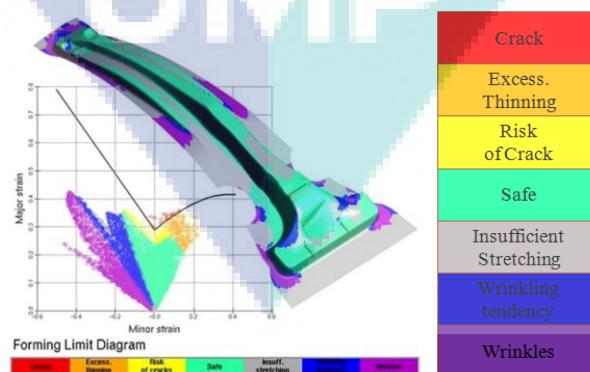


Figure 2.12 Forming Limit Diagram of B-pillar

Source: Skrikerud et al. (2010)

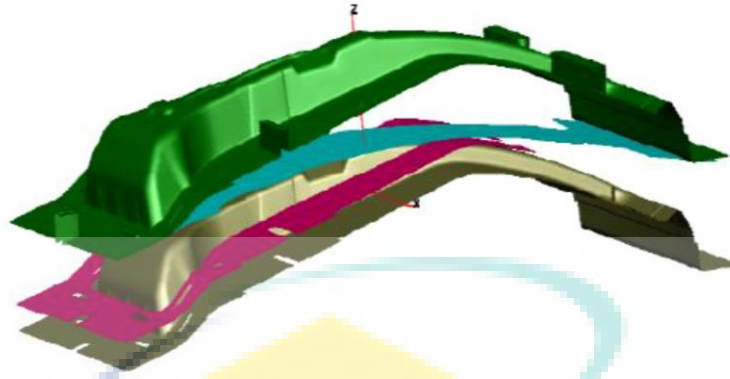


Figure 2.13 Simulation of B-pillar in hot press forming process
Source: Skrikerud et al. (2010)

The experimental investigation on the springback of high strength steel (HSS) after warm and hot sheet metal forming was performed by Thanadngarn and his crews (2013). They concluded that the springback of the hot steel sheet is reduced when the temperature of the steel sheet is beyond the recrystallisation temperature of austenite. They also cautiously changed the temperature of steel sheet for further investigation. Figure 2.14 shows the two different positions of A and B are selected for the plastically deforming region and flange zone, respectively.

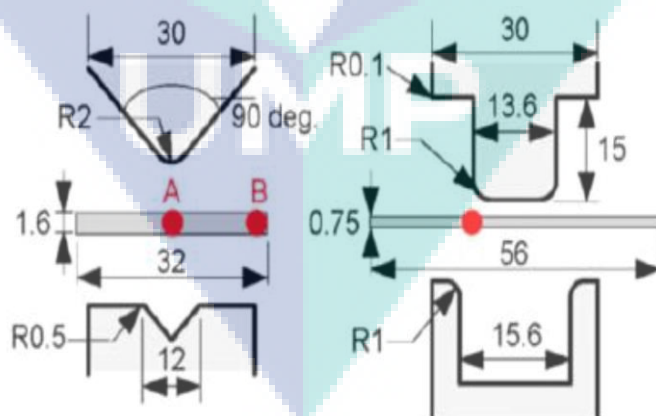


Figure 2.14 Geometries of tools and steel sheet for hat-shape and V-shape
Source: Thanadngarn et al. (2013)

Regarding to the experimental study of Sever et al. (2012), springback effect may be reduced when the temperature of a plastically deformation region is less than the recrystallisation temperature of austenite. Figure 2.15 presents the results of springback decreases with the temperature at bending zone higher than 750 K but the temperature in flange zone is higher than 1,000 K. Therefore, springback can be significantly reduced when the temperature of the bending area was at least in the warm forming range of 750 K and above.

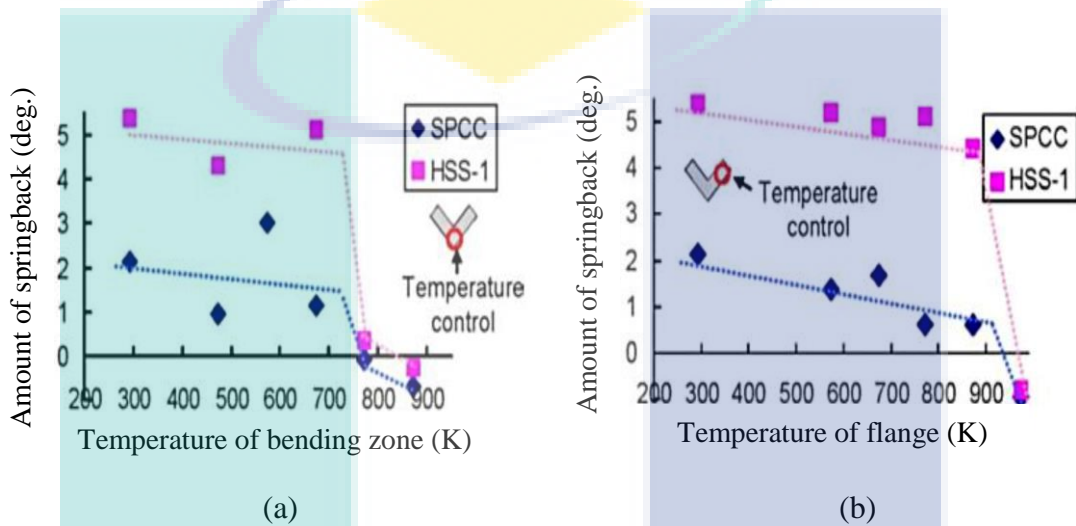


Figure 2.15 Degree of springback after V-shape bending with the relationship of temperature in (a) Bending region; and (b) Flange region

Source: Sever et al. (2012)

2.8.3 Punching and loading force

Ultra-high strength steel (UHSS) sheets have excellent strength, a hot forming operation with resistance heating was developed to reduce the punching force of UHSS sheet metal (Mori et al., 2012). The punching force or shearing load of UHSS sheet was decreased to improve the tool and dies life by heating the sheet. Mori et al. (2012) conducted a research of SPFC 980 sheet (UHSS) with a thickness of 2.0 mm was formed at elevated temperatures. Resistance heating was implemented in this research investigation which prevented oxidation and temperature decrement of the blank during warm and hot forming. The dimension of SPFC980 sheet metal is 130 mm length and 50 mm width, only 5 mm of each edge of the length is in contact with the electrodes as shown in Figure 2.16. The punch die with 10 mm in diameter was made of SKH 51 and

coated with TiCN. A stamping force of 8 MPa was applied with the sheet metal holder to acquire sufficient contact between the blank and electrodes for electrifying, which the current flow through the blank as resistance. Table 2.8 shows the different temperature conditions of hot forming operation.

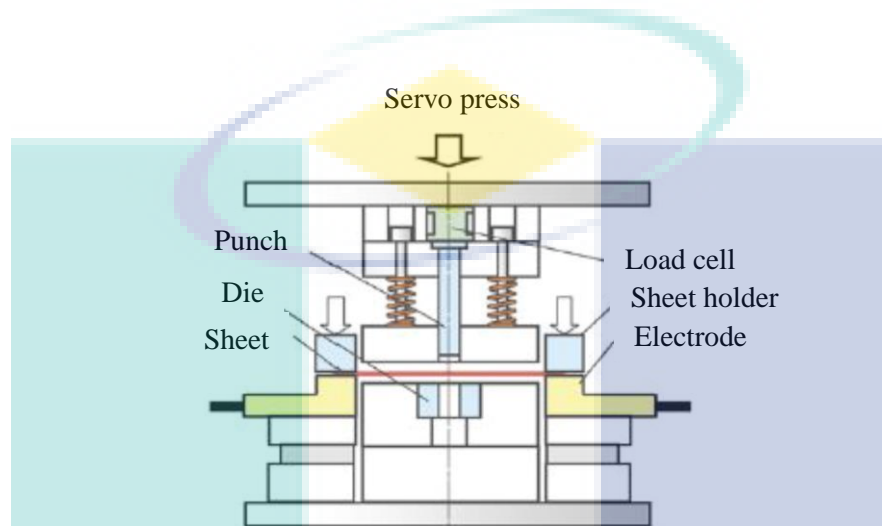


Figure 2.16 Hot forming process of UHSS sheet metal by using resistance heating
Source: Mori et al. (2012)

Table 2.8 Stamping process in hot temperature conditions

Parameters	Number
Austenite Temperature, T (°C)	650, 700, 830, 970, 1070
Stamping Velocity (mm·s ⁻¹)	150
Clearance Ratio, c (%)	5, 10, 15

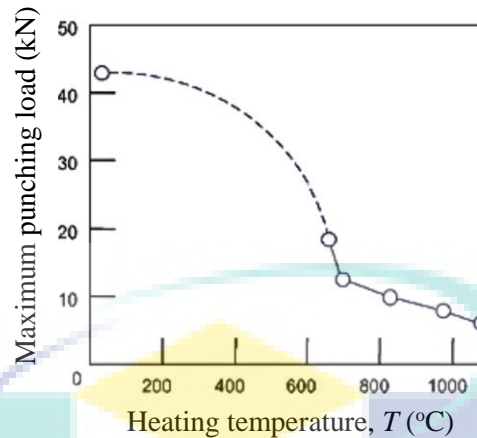


Figure 2.17 Relationship between the maximum stamping load and heating temperature of UHSS sheet metal

Source: Mori et al. (2015)

According to the experimental results of Mori et al. (2015), the increment of sheet metal austenite temperature, the smaller the stamping force to be given in the UHSS sheet. Figure 2.17 displays the relationship between the punching load and heating temperature of UHSS sheet. Based on the graph, the stamping force increased when the heating temperature was below 650 °C. Therefore, the forming operation of UHSS sheet metal is effective for warm and hot temperature conditions. Besides that, the advantages of austenite temperature are the decrease in shearing or punching load and also the improvement in the sheared edge quality (Mori et al., 2015).

2.9 Heat Transfer Mechanism

Heat is defined as a form of energy that can be transferred from one system to another as a result of temperature difference (Abdul-Hay et al., 2010). A thermodynamic analysis is concerned with the amount of heat transfer as the system experiences a process from one equilibrium to another. Heat transfer is the determination of the rate of energy transfer. Hence, the transfer of energy as heat is always from the higher temperature medium to the lower temperature medium, and heat transfer equilibrium when the two mediums attain the same temperature (Cengel and Ghajar, 2011).

The thermal contact resistance is an interface which provides some resistance to heat transfer and it is per unit interface area. When two such surfaces are through against each other, the peaks form good material contact but the valleys form voids filled with air. Thus, an interface contains numerous air gaps of varying sizes which act as insulation because of the low thermal conductivity of air (Cengel, 2010). There are several factors that lead to the factor dependency of heat transfer which are the surface condition, fluid flow types, tools temperature and contact pressure.

2.9.1 Tools temperature and contact pressure

Heat transfer coefficient (HTC) at the blank-dies interface has been studied and investigated under a certain value of pressure by Bosetti et al. (2010). He and his crews demonstrated an experiment to identify HTC in hot stamping of boron steel sheets under the condition which was very close to the industry. In the experiment, the process involved the compression of the sheet metal blank between two flat tools in imposing value of applied pressure without large scale sheet deformation. The quenching tools consisted of two 10 mm thick exchangeable water cooled contact plates and thermocouple equipped specimen as shown in Figure 2.18. The specimen was undergoing a previous homogeneous austenitization at a temperature of 900 °C in a furnace and manually transferred on four springs seated pins under atmospheric conditions. Similar experiments were also conducted by Merklein et al. (2014) by using a testing software to measure the specimen loaded during quenching with a defined nominal contact pressure up to 40 MPa. The temperature values of both contact plates and sheet metal blank were gathered by using integrated Ni/Cr-Ni-thermocouples during the experiment.

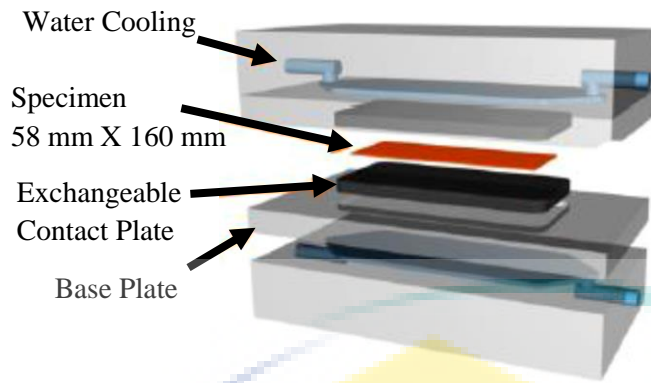


Figure 2.18 Experimental setup and instrument for heat transfer coefficient testing

Source: Bosetti et al. (2010)

Table 2.9 presents that the value of heat transfer coefficient increases with an increment of contact pressure and at the same time the standard deviation was also increased. Contact pressure is directly proportional to the heat transfer coefficient. Merklein et al. (2014) stated that the tool temperature is also directly proportional to the heat transfer coefficient. Figure 2.19 shows that the heat transfer coefficient increases as the temperature of tools increases.

Table 2.9 Results of contact pressure and standard deviation of HTC

Contact Pressure (MPa)	HTC ($\text{W}\cdot\text{m}^{-2}\cdot\text{K}^{-1}$)	Standard Deviation ($\text{W}\cdot\text{m}^{-2}\cdot\text{K}^{-1}$)
0	1231	82
5	1484	27
10	2025	37
20	2395	69
30	3065	117
40	3308	159

Source: Bosetti et al. (2010)

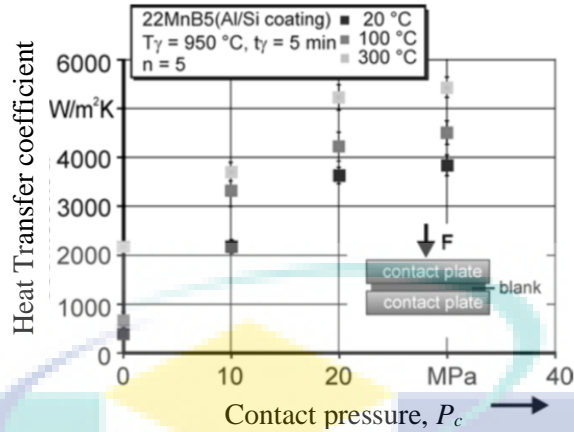


Figure 2.19 Relation between HTC as function of contact pressure for different tool temperatures

Source: Merklein et al. (2014)

The standard deviation of heat transfer coefficient happened due to the surface condition of the blank and tools. Surface condition can be identified as the perfect contact exists at the interface of two layers and no temperature drop occurs at the interface zone from the analysis of heat conduction through multilayer solids. This would be the case when the surfaces are perfectly smooth, and a perfect contact at each point is obtained (Cengel and Ghajar, 2011). Figure 2.20 illustrates the temperature distribution and heat flow lines along the two solid plates pressed against each other in the case of perfect and imperfect thermal contact.

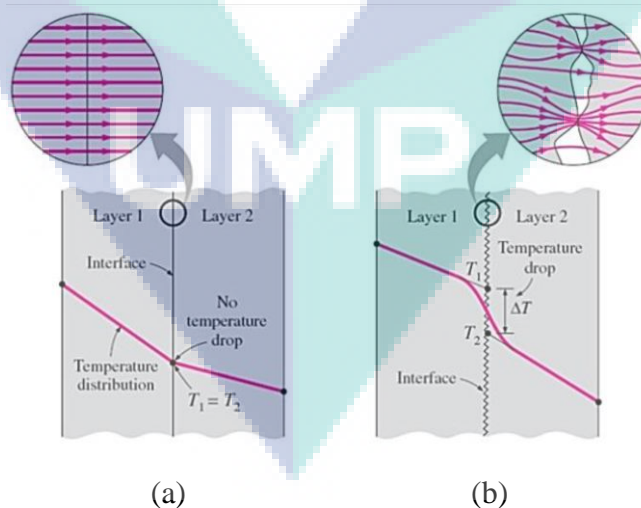


Figure 2.20 Thermal contact resistance (a) Ideal thermal contact; (b) Actual thermal contact

Source: Cengel and Ghajar (2011)

2.9.2 Cooling Channel Design for Fluid Flow Types

One of the vital equipment in hot press forming (HPF) production is the hot forming die. The crucial factors that need to be considered in the die design are the manufacturing cost of hot forming, productivity and quality (Hu et al., 2013). Moreover, die material, die clearance, cooling channel design and effect of heat transfer must also be considered in the die design concept development (Hoffmann et al., 2007). Besides that, it must also achieve the HPF process system requirement in terms of austenitization temperature transmitting time and the rate controlling for hot forming. However, some issues such as wrinkling, cracking, no uniform thickness distribution and failure to complete quenching were faced in dealing with ultra-high strength steel (UHSS) blank in HPF (Naganathan and Penter, 2012).

Hot forming tools used in HPF process are similar to typical stamping process except for the additional cooling system that is machined inside the tool. The objective of the cooling channel design is to quench or rapidly cooling down the hot formed part effectively and to achieve a cooling rate of at least $27 \text{ K}\cdot\text{s}^{-1}$ to attain martensitic transformation (Karbasian and Tekkaya, 2010). The main part of the overall tools for dies and instance punch are required to be designed to cool down sufficiently to ensure the excellent characteristics of the formed part (Merklein et al., 2014). These main tools are connected to a chiller, which is a medium to cool and recycling the coolant. Figure 2.21 shows the HPF tool for forming process. It consists of an upper die and lower die that are used to form the sheet metal blank. The punch acts as a metal block that is used for forming the sheet metal blank. While, the blank holder is a part of the HPF die that holds the blank against the die to control the metal flow. Hoffmann et al. (2007) employed a similar experimental setup to determine the heat transfer coefficient from the HPF process as shown in Figure 2.22. In this project, the cooling channel design was preliminary studied and manufactured in the HPF dies for forming the hat-shaped part.

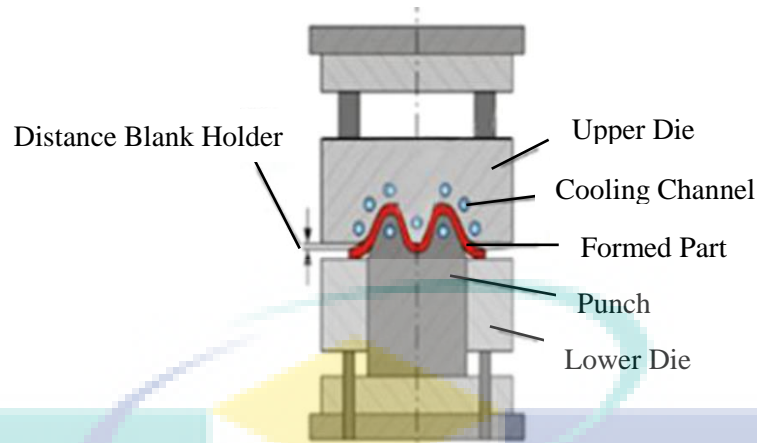


Figure 2.21 Schematic diagram of hot press forming tool design
Source: Karbasian and Tekkaya (2010)

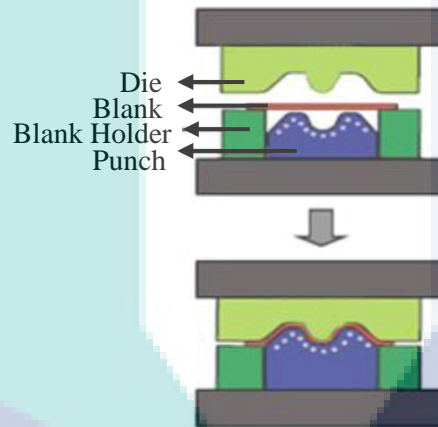


Figure 2.22 Schematic diagram of the quenching tool integrated with hot forming operation
Source: Hoffmann et al. (2007)

In the convection heat transfer, fluid flow could affect the heat transfer by different values of Reynolds number. Fluid flow can be classified as either laminar flow for Reynolds number not more than 2,000 or turbulent flow for Reynolds number is beyond 4,000 values. Reynolds number, Re is expressed by the Equation 2.1 (Cengel, 2010).

$$Re = \frac{\rho v D}{\mu} \quad 2.1$$

where, ρ is the density of the fluid; v is the fluid velocity; the characteristic length D is the diameter of the tube; and μ is the viscosity of the fluid. Typically, viscous stresses within a fluid tend to stabilize and organize the flow, whereas excessive fluid inertia tends to disrupt the organized fluid flow and lead to disordered turbulent behaviour (Cengel, 2010).

Azmi et al. (2014) conducted a study on forced convection heat transfer of water based nanofluids in a plain tube. The concentration of nanofluids used was up to 3% nanofluids concentration and the Reynolds number ranged from 5,000 to 25,000. The properties enhancement ratio was used to estimate the maximum heat transfer enhancement of the nanofluids as 17.6% for 1.0% concentration. In the same year, Reddy and Rao (2014) investigated TiO₂ nanofluids in a water/EG base for very low concentrations range from 0.0004 to 0.02%. The test section was a double pipe heat exchanger with copper tubes of 8.13 mm inner diameter. The experiment was undertaken for Reynolds number of 4,000 to 15,000 values. There was an enhancement of heat transfer in the range of 7.9% to 10% for TiO₂ nanofluids with 0.02% concentration. Azmi et al. (2014) and Reddy and Rao (2014) proved that the use of the mixture of water/EG can also provide heat transfer enhancements.

2.10 Finite Element Thermal Analysis in Hot Press Forming

Finite element simulation of the hot press forming (HPF) process provides several advantages to the automotive industry to predict the properties of the final part such as stress distribution, heat distribution and hardness distribution. The primary purpose of using hot press forming is to increase the tensile strength and to reduce the weight of the final product. Thus, obtaining the heat distribution and stress distribution through simulation can be very useful for the manufacturers. Finite element simulation can determine the effect of the various parameters involved in the HPF process. Bardelcik et al. (2014) conducted a simulation study to analyse the forming and temperature distribution of boron steel components. They found that the effect of variation in coefficient of friction and heat transfer coefficient can be accurately predicted by using finite element simulation.

Estimation of the HPF process quantitative and qualitative within a short time is essential for the commercial manufacturing of the hot formed part and hot forming tools. However, the simulation of HPF process is different from cold forming or warm forming processes. For cold forming, heat transfer is negligible and there are no microstructural variations. The numerical simulation can be conducted under the isothermal condition and without accounting for changes in the microstructure thus simplifying the simulation process (Ravindran, 2011).

In HPF process, the sheet metal blank is heated up to a temperature of 900 °C and then immediately cooled down to approximately 200 °C. Therefore, the simulation has to be non-isothermal in nature. Also, the microstructure of the final product changed from predominantly austenite to martensite during quenching operation. Bardelcik et al. (2014) concluded that the mechanical properties of the hot formed boron steel increases in terms of the tensile strength and hardness. Thus the evolution of microstructure should be considered for accurate simulation of the HPF process. Figure 2.23 presents the interrelationships between the effects of deformation, heat transfer and microstructural evolution. Therefore, an accurate finite element model of the process should be considered for the interaction between the thermal, microstructure and mechanical effects. Owing to the complexity involved in the numerical simulation of HPF process, researchers have experimented using several commercial codes such as LS-Dyna, AUTOFORM, ABAQUS, COSMOS and ANSYS (Hoffmann et al., 2007; Ravindran, 2011; Taha et al., 2014; Namklang et al., 2016).

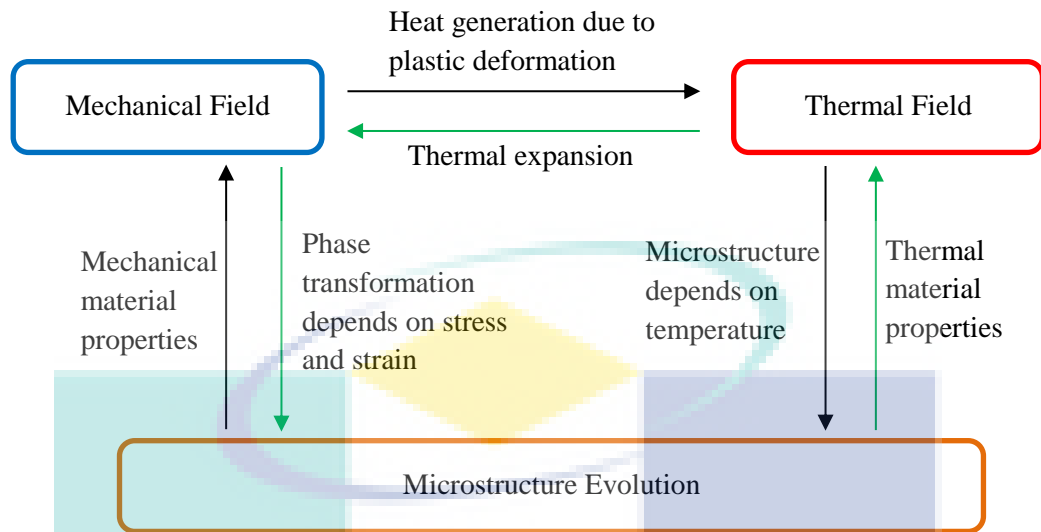


Figure 2.23 Interactions between the effects of heat transfer, microstructural evolution and deformation

Source: Ravindran et al. (2011)

Hoffmann et al. (2007) used finite element analysis to simulate two transient thermal analysis by using ABAQUS software, which uses an implicit method for this purpose. The simulation model consists of four tool components such as punch, counter punch, die and blank holder with two variants cooling channel of V1 and V2 for small cooling duct diameters and large cooling duct diameters, respectively. In thermal analysis, HPF process is simulated in the closed tools. The sheet metal blank has an initial homogeneous temperature of 850 °C due to free cooling from 950 °C during the transfer in the environment. The initial tool of SKD 61 temperature was assumed as 20 °C and the contact heat transfer coefficient was $5,000 \text{ W}\cdot\text{m}^{-2}\cdot\text{C}^{-1}$ at zero distance between blank and dies, named as a gap. Figure 2.24 shows the temperature changes in the tool components for 10 cycles at tool combination V1 and V2. The researchers found that the cooling rate obtained from the blank at the hottest point of 850 °C to 170 °C is $40 \text{ }^\circ\text{C}\cdot\text{s}^{-1}$ with the tool combination of V1 and $33 \text{ }^\circ\text{C}\cdot\text{s}^{-1}$ with the tool combination of V2. However, the values were greater than the minimum required rate of cooling of $27 \text{ }^\circ\text{C}\cdot\text{s}^{-1}$.

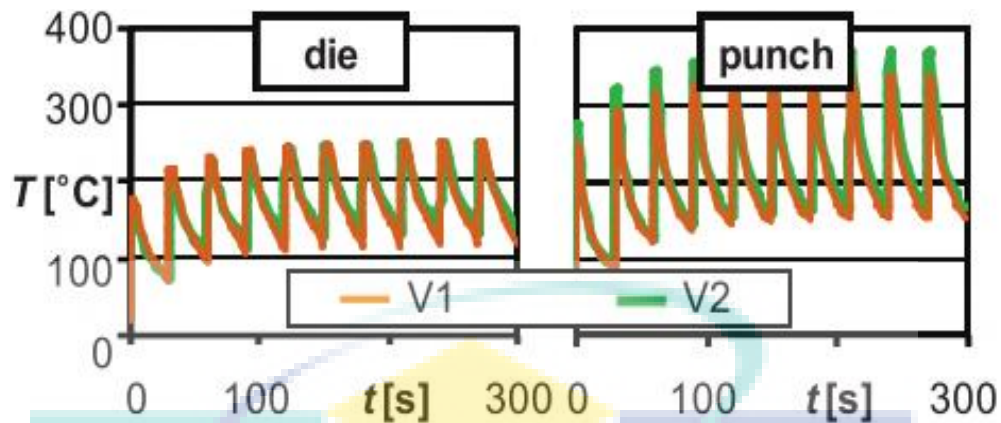


Figure 2.24 temperature changes in heat transfer analysis

Source: Hoffmann et al. (2007)

Taha et al. (2014) used finite element analysis to simulate thermal analysis by using COSMOS software. The simulation model is consisting of 3 components such as the upper tool, lower tool and blank with different hot forming tool materials named as high thermal conductivity tool steel (HTCS 150) and hot work tool steel (SKD 61). The purpose of the thermal analysis is to study the cooling characteristics of the tool by analysing the blank which comes in contact with the tool surface. The initial tool temperature is set at 20 °C temperature, while the heat convection coefficient of cooling channel surface is constant at $4,877.4 \text{ W}\cdot\text{m}^{-2}\cdot\text{K}^{-1}$ which is based on the calculated minimum flow rate to achieve turbulent flow behaviour inside the cooling channel. According to their findings in thermal analysis, the SKD 61 has a higher cooling rate compared to HTCS 150. This is due to the higher maximum tool surface temperature reached by SKD 61. Figure 2.25 shows the tool cooling performance between SKD 61 and HTCS 150 in thermal analysis simulation.

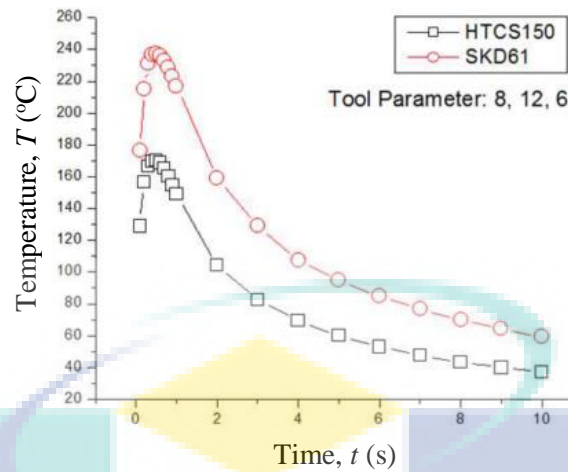


Figure 2.25 Tool cooling performance between SKD 61 and HTCS 150 tool materials with same cooling channel parameter

Source: Taha et al. (2014)

Manufacturing approach for predicting local mechanical properties of a hot stamped sample under consideration of temperature, cooling rate and correspondingly occurred phase transformations were introduced by Namklang et al. (2016). In this work, they conducted thermo-mechanical FE simulations of the investigated hot forming experiments. Further, local distributions of temperature, hardness and microstructure of formed hat-shaped part were predicted and verified with the experimental results. The FE simulations comprised three successive steps. The first step was transferring heated blank from furnace to hydraulic press. The second step concerned forming and quenching. And the last step was holding formed blank in dies for further cooling. In the simulations, occurred heat transfer from blank to dies with the cooling channels could be observed clearly. The temperatures of blank and dies continuously decreased with increasing holding time. Figure 2.26 illustrates the calculated temperature distributions on the blank and dies at different time step after forming. In 2016, researchers studied the influences of the holding time in dies with the quenching operation. The FE simulations of the hot stamping with different holding times in dies of 4, 5, 6 and 8 s were examined (Namklang et al., 2016). Figure 2.27 presents the resulted temperature developments of the blank and dies from each case.

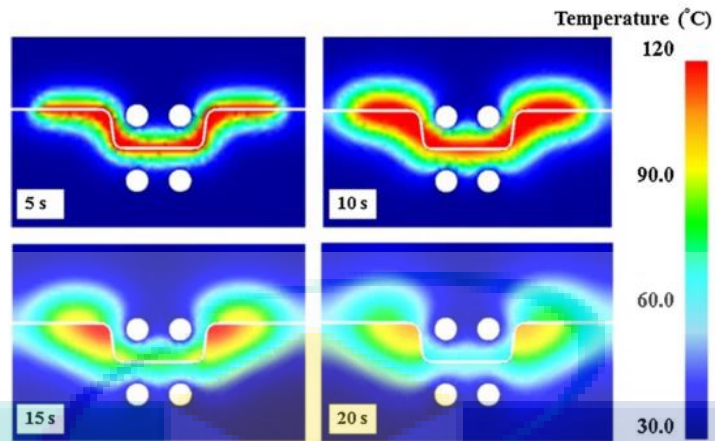


Figure 2.26 Heat transfer distributions on the dies during quenching step took completely 20 s

Source: Namklang et al. (2016)

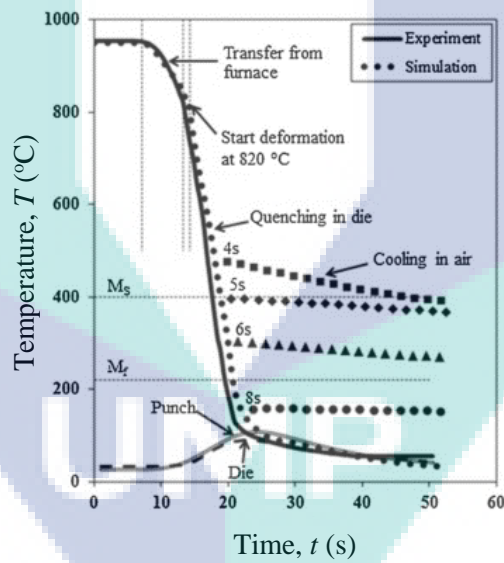


Figure 2.27 Hot stamping with several holding times in dies

Source: Namklang et al. (2016)

2.11 Summary

The studies of nanocoolants and hot press forming (HPF) process in this chapter have covered the thermal physical properties and experimental investigation on nanocoolant as the cooling medium for HPF tool application. Thermal conductivity and dynamic viscosity of nanocoolants behaved according to the particle size, temperature condition, volume concentration, types of materials and base fluids. The studies on dynamic viscosity and thermal conductivity of nanocoolants in a mixture of water-EG are very limited. Only Sundar et al. (2012), Azmi et al. (2014) and Said et al. (2014) conducted the experimental studies of Fe_3O_4 , SiO_2 and TiO_2 nanoparticles.

Following that the related previous studies using the nanocoolants base mixture are presented in this chapter. Most of the researchers found that the nanocoolants base mixture are stable for the convective heat transfer investigation and found that the significant enhancement in heat transfer performance. The enhancement of thermal conductivity using Al_2O_3 base mixture nanocoolants is observed initially by Sundar et al. (2014). However, limited discussion on the influence of different ratio base fluids on the performance of nanocoolants are stated. Thus, the evaluation of thermal conductivity and dynamic viscosity for Al_2O_3 nanocoolants were determined through experimental measurement and characterization in Chapter 3 before obtaining the application in HPF process data.

In order to achieve a tool with high cooling efficiency as well as having homogeneous temperature distribution throughout the tool, the heat transfer of the tool must be in a perfect condition where, no temperature drops at the interface. HPF dies with the cooling channel can dissipate heat from the tool as well as to control the tool temperature. Cooling fluid is introduced inside the tool as the medium for cooling the tool. In addition, heat transfer coefficient can be determined by obtaining the equations involved Reynolds number and Prandtl number to produce the Nusselt number as reported by Lim et al. (2016). Due to the above parameters, the heat transfer experiment needs to be arranged to obtain the tool with high cooling efficiency as well as having homogeneous temperature distribution throughout the HPF dies. George et al. (2012) and Lin et al. (2015) evaluated the heat transfer distribution of the tool by placing the thermocouples approximately 4 to 5 mm away from the loading counter. The experiment

results obtained from the present study would be compared with the finite element analysis (FEA) simulation for validation purposes. Namklang et al. (2016) validated their study by this method and acceptable agreement was found between FEA simulation and experimental results.

However, the influence of the nanocoolant, water-EG mixture based Al_2O_3 as a cooling medium in HPF process of heat transfer performance in forced convection heat transfer is still undiscovered. Hence the determination of heat transfer coefficient and cooling rate for the hot formed part is shown in the subsequence Chapter 4. In Chapter 4, the microstructure transformation phase and the mechanical properties such ultimate tensile strength and hardness of the final product from the HPF process are examined. Naderi et al. (2011) and Löbbe et al. (2016) investigated the effect of different cooling rates and quenching time periods towards the tensile strength and hardness of the hot pressed part.



UMP

CHAPTER 3

METHODOLOGY

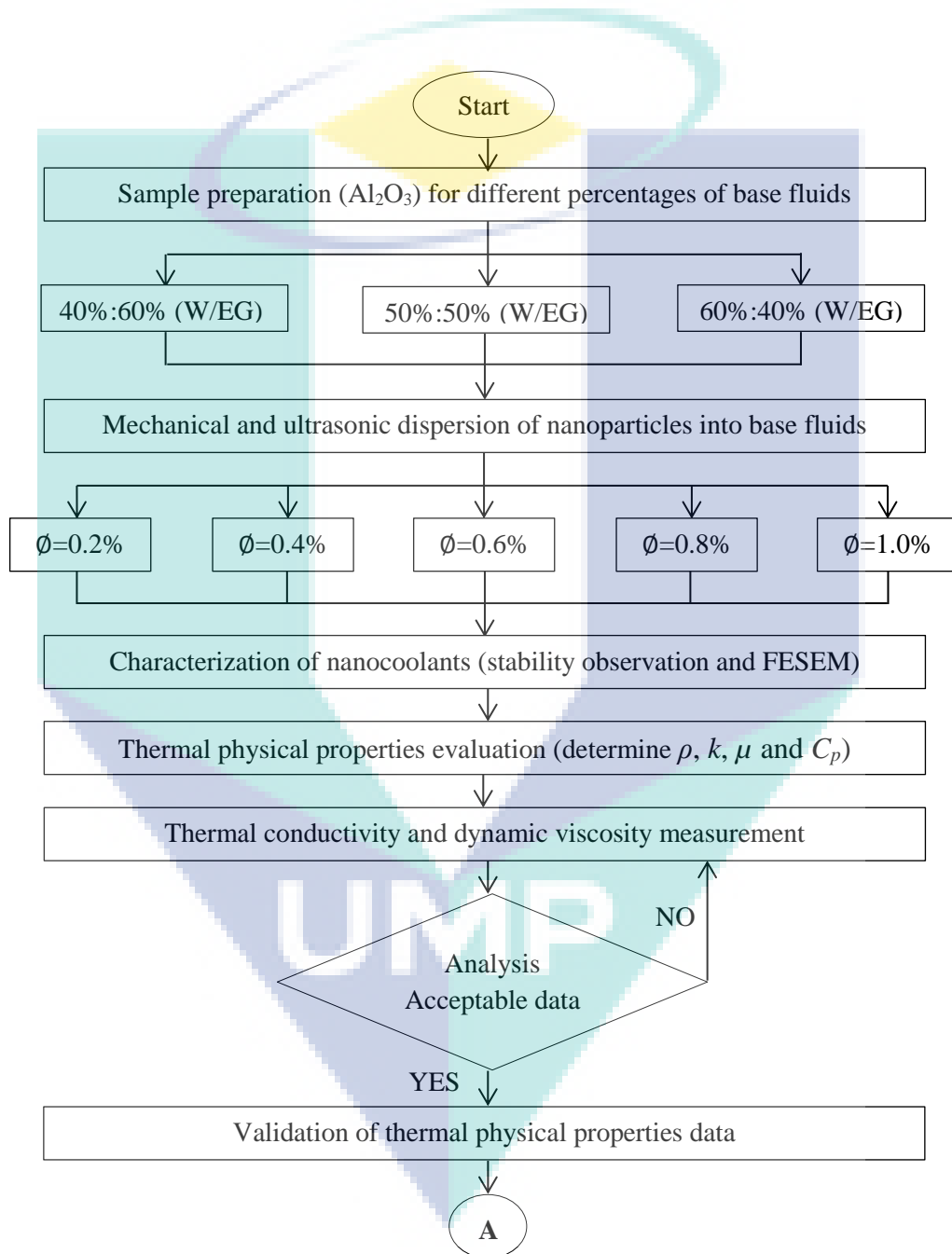
3.1 Introduction

In this chapter, the materials, solution and experimental procedures used in preparing the nanocoolants based aluminium oxide were briefly described. All the devices used to measure the thermal physical properties such as thermal conductivity and dynamic viscosity were explained item wise. The data were collected from the stability of nanoparticles observation, thermal physical properties of thermal conductivity measurement and dynamic viscosity measurement; and convective heat transfer analysis in relation to this research objective. This research project initially studied a detailed stability evaluation through several observations such as scanning micrograph evaluations and sedimentation observation.

Finite element analysis (FEA) was conducted as to analyse the best heat transfer distribution between the hot press forming (HPF) tools and heated sheet metal blank by introducing two different cooling agents such as chilled water and nanocoolant. Then, HPF process experiment was conducted in ambient temperature atmosphere to obtain the temperature distribution of the sheet metal blank and tools by validating with the FEA heat transfer distribution. Two factors such as quenching time, t_q and convection heat transfer coefficient (HTC) were used as input variables.

Finally, the mechanical properties of hot pressed products were measured based on American Society for Testing and Material International (ASTM) standard. The tensile strength test of the specimens were conducted with Universal Tensile Machine (UTM) and the hardness measurement was performed by using Vickers Micro-hardness

Machine. Light Optical Microscopy (LOM) was used to perform the metallographic study of the martensitic microstructure. All experiments were conducted in the Al-Jazari Laboratory and Material Laboratory, FKP, UMP. The methods of completing the experimental investigations on this project were presented briefly in Figure 3.1.



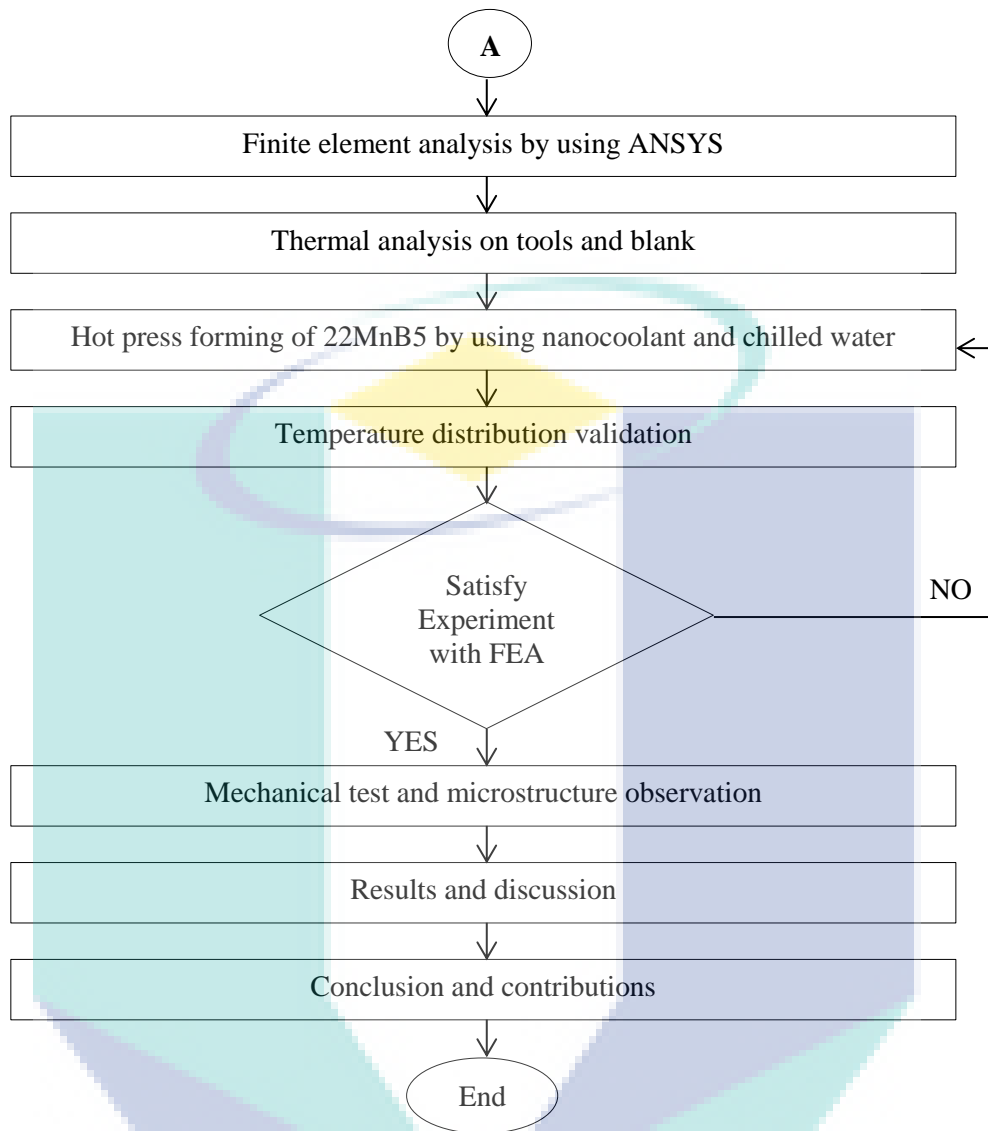


Figure 3.1 Flow chart of introducing nanocoolant as cooling medium for HPF process

3.2 Materials and Preparation of Nanocoolants

Preparation of stable nanocoolants is the critical stage in engineering convection heat transfer experiment (Haddad et al., 2014). Sidik et al. (2014) conducted a review of the nanocoolant preparation and noted that the preparation of nanocoolant influenced their thermal conductivity. As described in Section 2.5, the nanocoolants were prepared by dispersing the nanoparticles in different percentages of base fluid through proper mixing. After meticulous consideration, the selected nanoparticles was aluminium oxide,

Al₂O₃ with an average size of 13 nm and prepared by using the two step technique which was commonly used method for nanocoolant preparation (Azmi et al., 2013).

Nanocoolant was prepared in two volumes which were 100 mL and 20 L by dispersing the nanoparticles in three different percentages of water to ethylene glycol base fluids, which were 60%:40%, 50%:50%, and 40%:60% respectively. The Al₂O₃ nanoparticles in the powder form was used and procured from Sigma-Aldrich, USA. The fine particles of Al₂O₃ have an average particle diameter of 13 nm with 99.8% purity. The characterization of the Al₂O₃ nanoparticle was obtained by Field Emission Scanning Electron Microscopy (FESEM) imaging technique. Figure 3.2 shows the image from FESEM model JSM-7800F with the magnification of X300,000. Al₂O₃ nanoparticle shape is observed as spherical and the sizes are approximately 13 nm as shown in the FESEM image. The properties of Al₂O₃ nanoparticles are shown in Table 3.1 (Sundar et al., 2014; Azmi et al., 2013; Lim et al., 2016).

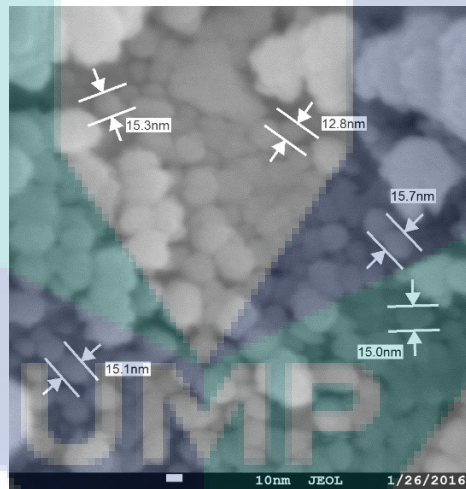


Figure 3.2 FESEM result of dry Al₂O₃ nanoparticles at X300,000 magnification

Table 3.1 Properties of nanoparticles used in experiment

Property	Al ₂ O ₃
Average nanoparticle size, nm	13
Molar mass, g·mol ⁻¹	101.96
Density, kg·m ⁻³	4,000
Thermal conductivity, W·m ⁻¹ ·K ⁻¹	36
Specific heat capacity, J·kg ⁻¹ ·K ⁻¹	880

Source: Sundar et al. (2014); Azmi et al. (2013); Lim et al. (2016)

Mixture of water-EG as base fluid was used to prevent the galvanic corrosion of the cooling channel system and to prevent distilled water from freezing or boiling at extreme temperature. Peyghambarzadeh et al. (2011) stated that the mixture percentage of water and ethylene glycol in 40%:60% does not freeze at $-45\text{ }^{\circ}\text{C}$ because ethylene glycol has lower volatility compared to water. Table 3.2 shows the properties of pure ethylene glycol in the liquid state (Peyghambarzadeh et al., 2011; Yu et al., 2012).

Table 3.2 Properties of Ethylene Glycol solution

Property	Ethylene Glycol
Vapor pressure, mmHg at $20\text{ }^{\circ}\text{C}$	0.08
Boiling point, $^{\circ}\text{C}$	195–198
Melting point, $^{\circ}\text{C}$	-13
Density, $\text{g}\cdot\text{ml}^{-1}$ at $25\text{ }^{\circ}\text{C}$	1.113

Source: Peyghambarzadeh et al. (2011); Yu et al. (2012)

Pre-calculated mass of Al_2O_3 nanoparticles by Equation 3.1 was dispersed in the base fluids with a two-step method proposed by Yu et al. (2012) and Reddy et al. (2013). The solution is diluted by Equation 3.2 from high to low concentration to prepare the nanocoolant of five volume concentrations with 0.2%, 0.4%, 0.6%, 0.8%, and 1.0%.

$$\phi = \frac{m_p / \rho_p}{V_p + V_{bf}} \times 100 \quad 3.1$$

$$\Delta V = (V_2 - V_1) = V_1 \left(\frac{\phi_1}{\phi_2} - 1 \right) \quad 3.2$$

where ϕ is the volume concentration of nanocoolant; V_{bf} is the volume of base fluids; and m_p , ρ_p and V_p are the mass of nanoparticles in SI unit of kg, the density of nanoparticles and volume of nanoparticles, respectively. The mixture of Al_2O_3 nanocoolant is prepared using a magnetic stirrer. The dispersion stability of the nanocoolant improved after immersion in ultrasonic homogenizer model Fisherbrand FB15051 for one hour. Figure 3.3 shows the process flow of preparation of nanocoolants based Al_2O_3 for investigation of heat transfer distribution in HPF process. There were no surfactants mixed in the preparation of nanocoolant as Serebryakova et al. (2015) and Zakaria et al. (2015) also

synthesized their nanocoolants without adding surfactants and they found that nanocoolant were in a stable condition. The stability of the nanocoolant is checked and confirmed after a month of preparation, as shown in Figure 3.4. A complete set of the nanocoolants sedimentation test with different volume concentrations of nanoparticles and three different ethylene glycol percentages could be viewed from Appendix C.

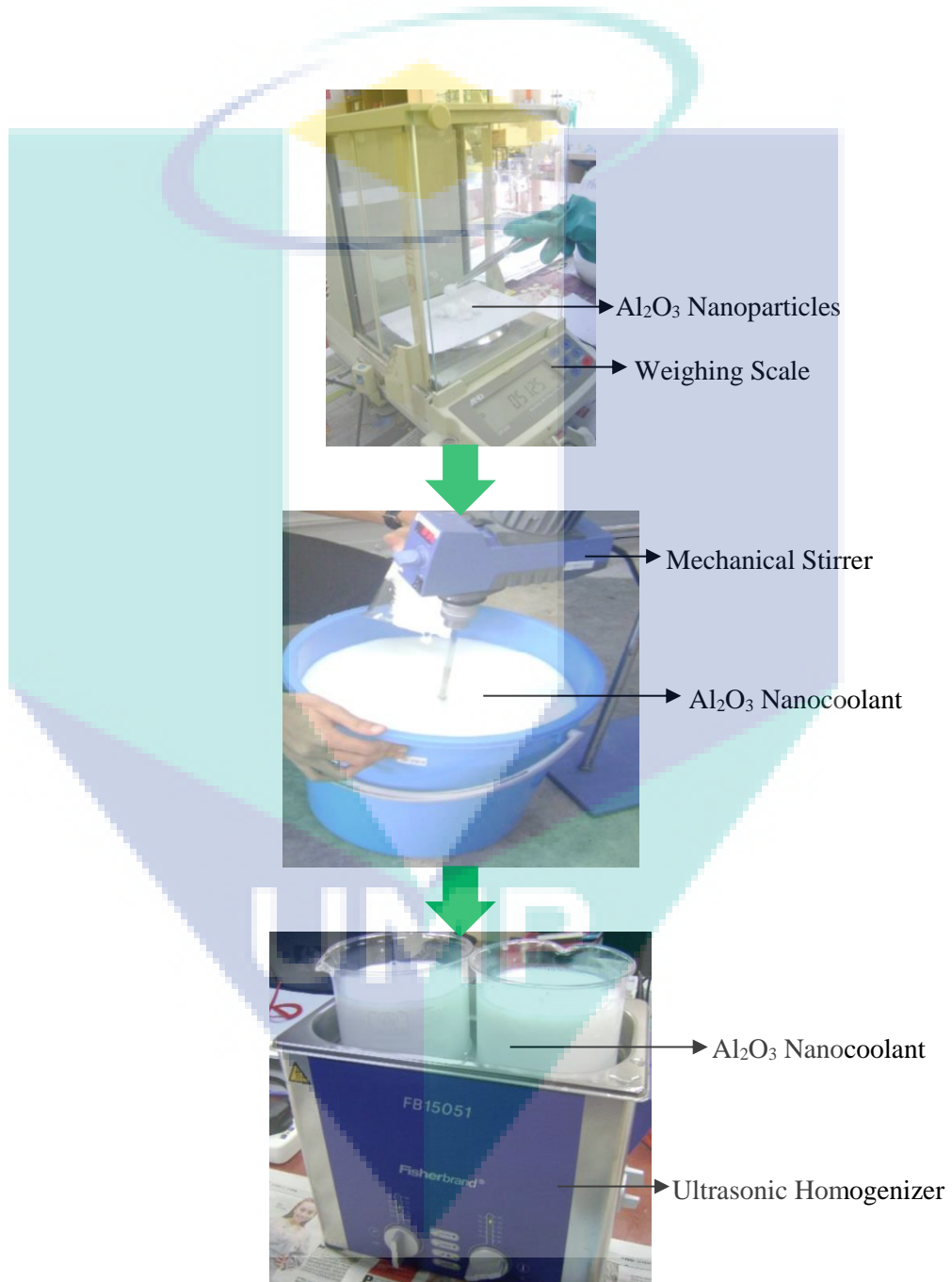


Figure 3.3 Al₂O₃ nanocoolant immersed in ultrasonic bath heater

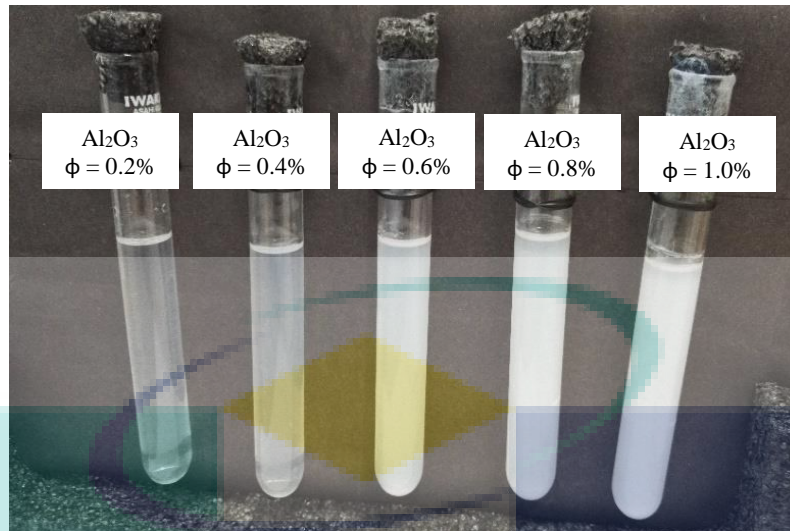


Figure 3.4 Nanocoolant samples of Al₂O₃/water-EG mixtures after a month of preparation

3.3 Thermal Conductivity Measurement

KD2 Pro thermal property analyser made from Decagon Devices, USA was used to measure the thermal conductivity of the nanocoolant, as illustrated in Figure 3.5. The thermal physical properties of liquids and solids were determined by the device using the transient line heat source. The device meets the standards of both IEEE 442-1981 and ASTM D5334.

A single needle sensor named as KS-1 in the range of 0.002 to 2.00 W·m⁻¹·K⁻¹ was used, and the sensor was validated by measuring the thermal conductivity of the verification liquid such as Glycerine, that was provided by the supplier. The measured value of Glycerine at 25 °C was 0.286 W·m⁻¹·K⁻¹, which agreed with the calibrated data of 0.285 W·m⁻¹·K⁻¹ and within ± 0.4% accuracy (Zakaria et al., 2015). The validation process of the sensor was checked before each measurement of thermal conductivity. A water bath of WNB7L1 model by Memmert was used to maintain a constant temperature of the sample with an accuracy of 0.1 °C (Azmi et al., 2013). The thermal conductivity of 0.2 to 1.0% volume concentrations of nanocoolant based Al₂O₃ and the nanocoolant was measured within the temperature range of 15 to 55 °C. The consistency of data measurement was ensured by taking a minimum of three values for every concentration at a specific temperature, and the average of the three values was analysed. The thermal

conductivity models (Hamilton and Crosser, 1962; Timofeeva et al., 2011; Wasp et al., 1977; Yu and Choi 2003) are shown in Table 3.3 and used to verify the experimental results of the thermal conductivity of nanocoolant.

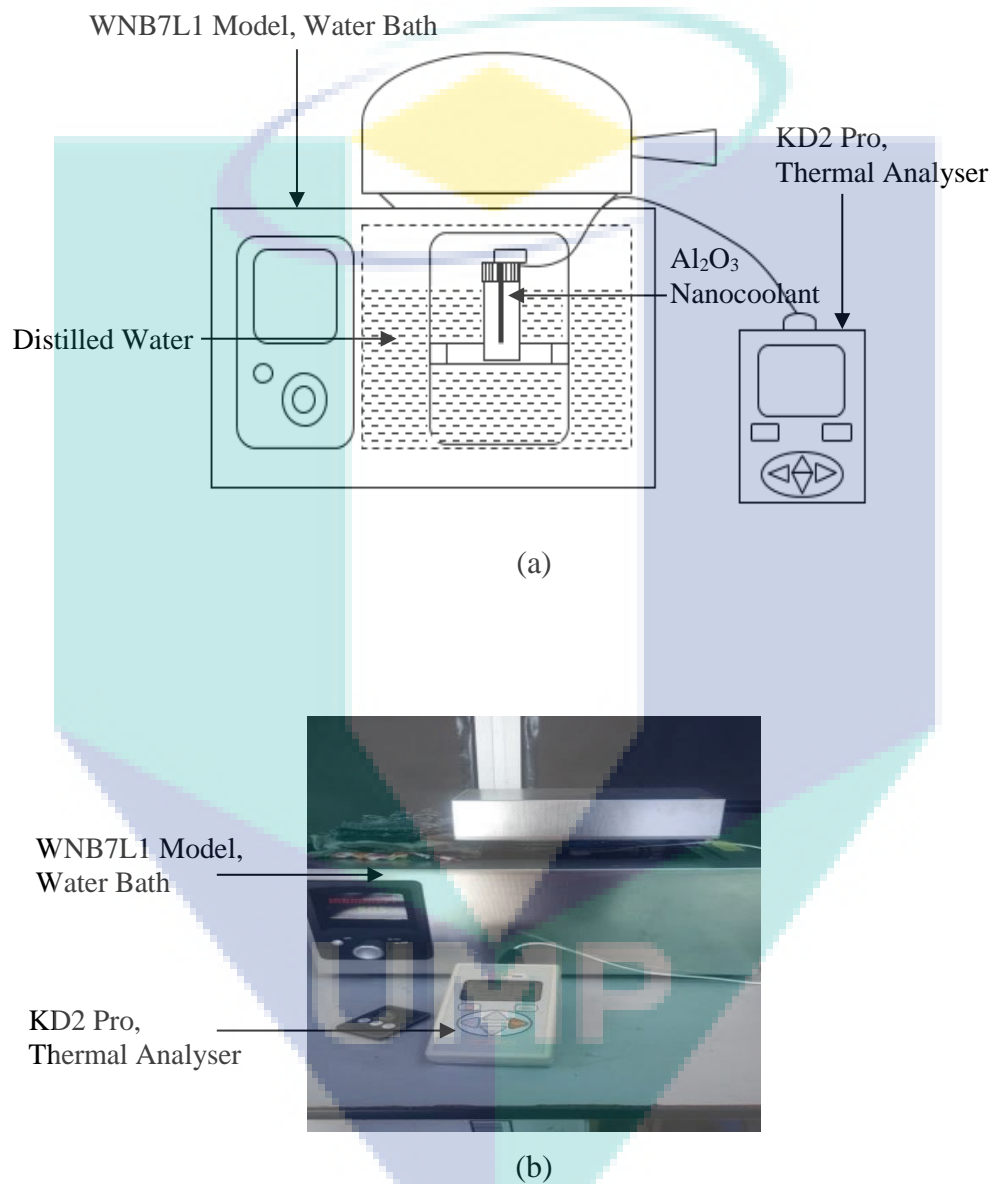


Figure 3.5 (a) Schematic diagram of thermal conductivity measurement; (b) Experiment setup for thermal conductivity measurement.

Table 3.3 Thermal conductivity models for nanocoolant

Model	Thermal Conductivity
Hamilton and Crosser (1962)	$k_r = \frac{k_{eff}}{k_{bf}} = \left[\frac{k_p + (n-1)k_{bf} - (n-1)(k_{bf} - k_p)\varphi}{k_p + (n-1)k_{bf} + (k_{bf} - k_p)\varphi} \right],$ <p style="text-align: center;">$n = 3 \Rightarrow$ spherical shape</p>
Timofeeva et al. (2011)	$k_r = \frac{k_{eff}}{k_{bf}} = (1 + 3\varphi)$
Wasp et al. (1977)	$k_r = \frac{k_{eff}}{k_{bf}} = \left[\frac{k_p + 2k_{bf} - 2(k_{bf} - k_p)\varphi}{k_p + 2k_{bf} + (k_{bf} - k_p)\varphi} \right]$
Yu and Choi (2003)	$k_r = \frac{k_{eff}}{k_{bf}} = \left[\frac{k_p + 2k_{bf} + 2(k_p - k_{bf})(1 + \beta)^3 \times \varphi}{k_p + 2k_{bf} - (k_p - k_{bf})(1 + \beta)^3 \times \varphi} \right], \beta = 0.1$

3.4 Dynamic Viscosity Measurement

Dynamic viscosity of 0.2 to 1.0% volume concentrations of aluminium oxide, Al₂O₃ in three different percentages of base fluids was measured by Brookfield which is a low viscosity digital viscometer with LVDV-III Ultra Programmable Rheometer, as depicted in Figure 3.6. The device is equipped with a personal computer for data collection and storage. The viscometer measures the dynamic viscosity of aqueous solutions that range from 1 to 6,000,000 mPa.s by utilizing an ultra-low adapter. The spindle connected to the viscometer was used to measure nanocoolants dynamic viscosity (Azmi et al., 2014).

The viscometer drives a spindle that was immersed in nanocoolants. Spindle rotation created a viscous drag of the fluid opposite to the spindle, which was measured by the deflection of the calibrated spring. The adapter in this experiment had a provision for temperature circulation of bath fluid. The dynamic viscosity of different volume concentrations of the Al₂O₃ nanocoolant started from 15 to 55 °C at an interval of 5 °C. Each measurement was conducted three times to generate a reliable data, and the average value of the three values was considered for analysis. The dynamic viscosity models (Pak and Cho, 1998; Wang et al., 1999; Sundar et al., 2013; Batchelor, 1977) are listed in Table 3.4 and used to compare the measured values of dynamic viscosity at different volume concentrations.

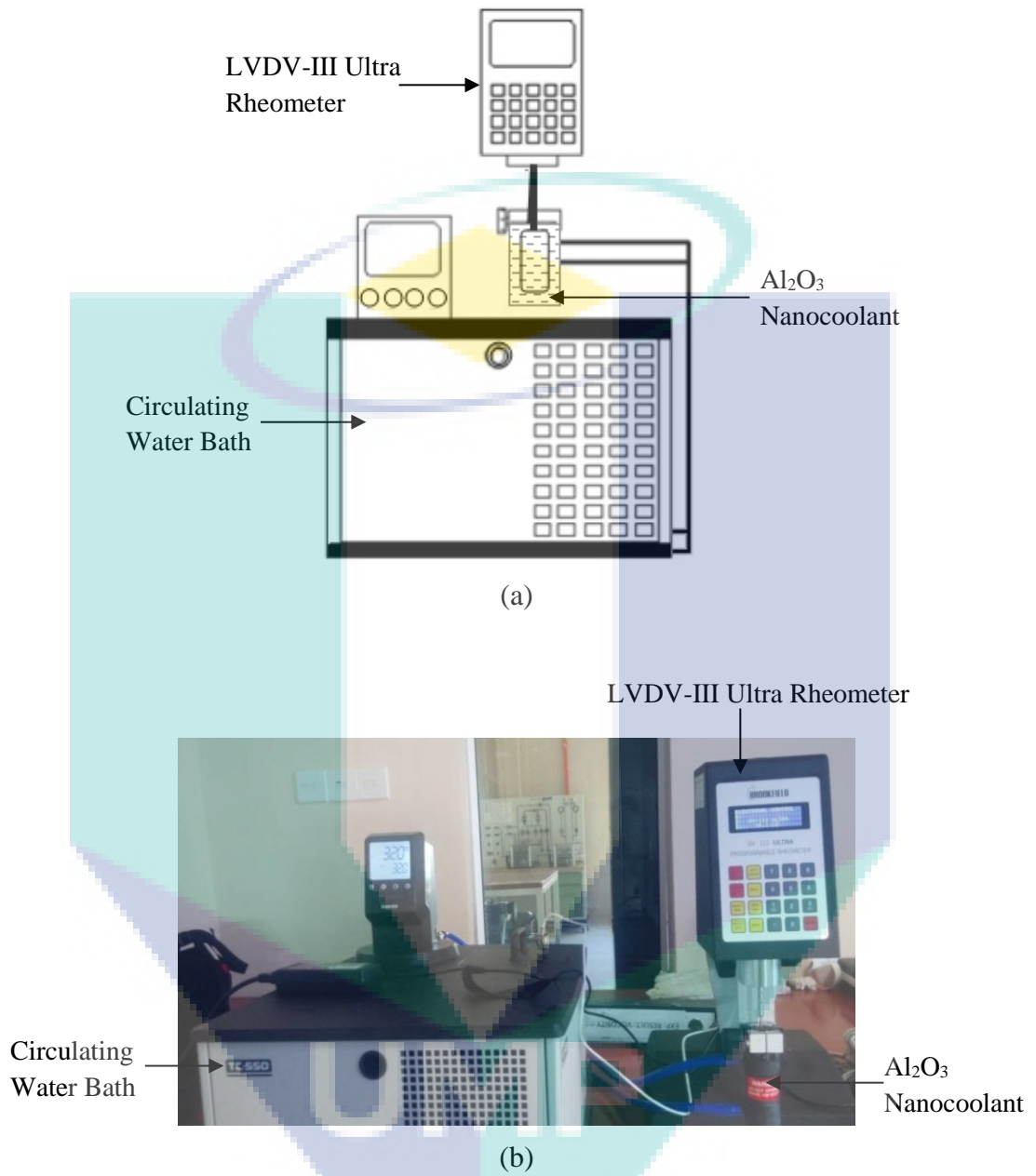


Figure 3.6 (a) Schematic diagram of dynamic viscosity measurement;
(b) Experiment setup for dynamic viscosity measurement

Table 3.4 Dynamic viscosity models for nanocoolant

Model	Dynamic Viscosity
Pak and Cho (1998)	$\mu_r = \frac{\mu_{eff}}{\mu_{bf}} = 533.9\varphi^2 + 39.11\varphi + 1$
Wang et al. (1999)	$\mu_r = \frac{\mu_{eff}}{\mu_{bf}} = 1 + 7.3\varphi + 123\varphi^2$
Sundar et al. (2013)	$\mu_r = \frac{\mu_{eff}}{\mu_{bf}} = Ae^{B\varphi}, A = 0.9299 \& B = 67.43 \Rightarrow 60:40\% (W/EG)$
Batchelor (1977)	$\mu_r = \frac{\mu_{eff}}{\mu_{bf}} = 1 + 2.5\varphi + 6.5\varphi^2$

3.5 Finite Element Analysis

Finite element analysis (FEA) is a powerful tool for determining the structural such as vehicle chassis, where the domain changes during a solid state reaction with a heat flux or moving boundary. When the desired precision varied over the entire domain or when the solution lacked of smoothness (Lin et al., 2014). Figure 3.7 presents numerical experiment of the hot press forming (HPF) tool and sheet metal blank. The simulation started by inserting the material data, namely as 22MnB5 boron steel and SKD 61 steel for blank and hot forming dies, respectively. Next, the geometry model from CATIA software was transferred into ANSYS simulation software and the constrained were identified. The most suitable meshing technique was defined to reduce the percentage error of absolute results. The surface contact between dies and sheet metal blank must be ensured (Tondini et al., 2011). FEA was began after all necessary parameters were imported into simulation. The accuracy of the FEA depended on the input parameters. Therefore, all the material properties such as thermal physical properties (thermal conductivity and specific heat capacity), density and surrounding temperature obtained from the literature (Kumar et al., 2011; Wu et al., 2014; Xiao et al., 2016) were taken into account in the thermal analysis. The meshing parameters such as coarse, medium and fine were done in order to select the best meshing type for FEA simulation. After the best result parameters are attained for meshing, the thermal analysis was just conducted.

Regarding to thermal analysis, the 3D geometry model of the upper die, lower die and blank were assembled to simulate and measure the heat transfer distribution among tools and part. As the next step of the analysis, the time taken was set to be 10 s to complete the full set of analysis. The thermal load was applied to the 3D geometry model as the temperature of the blank was set to 900 °C and 25 °C for the dies (Karbasiyan and Tekkaya, 2010). The convection heat transfer has been chosen as the heat transfer mechanism with the value of $4,700 \text{ W}\cdot\text{m}^{-2}\cdot\text{K}^{-1}$ for chilled water (Hoffmann et al., 2007) and $7,813 \text{ W}\cdot\text{m}^{-2}\cdot\text{K}^{-1}$ for nanocoolant (Lim et al., 2016). Contact set was chosen and defined between the tools and blank after selecting of connections advisor. As for the heat transfer from hot blank to tools, the input value was given as $5,000 \text{ W}\cdot\text{m}^{-2}\cdot\text{K}^{-1}$ (Wu et al., 2014). The meshing was done after setting all simulation parameters and the results of the transient thermal analysis were collected. The reason for this analysis was to ensure that the tools obtained high cooling efficiency with homogeneous heat transfer distribution. A different cooling agent such as nanocoolant and chilled water were introduced for improving cooling channel performance in HPF die. The range of time taken for meshing in this analysis was 3 to 10 s as the maximum time period. The reason was real industries only took 8 to 12 s to press the small part by using chilled water. Most of the articles journal studied chilled water as the cooling agent to produce martensite material in 10 s of quenching period (Hoffmann et al., 2007; Mori et al., 2015; Hu et al., 2013; Cui et al., 2015).

The logo for UMP (Universitas Muhammadiyah Purwokerto) is a large, stylized letter 'V' shape. The left side of the 'V' is light blue, the right side is light green, and the bottom point is a darker blue. The letters 'UMP' are written in white, bold, sans-serif font across the center of the 'V'.

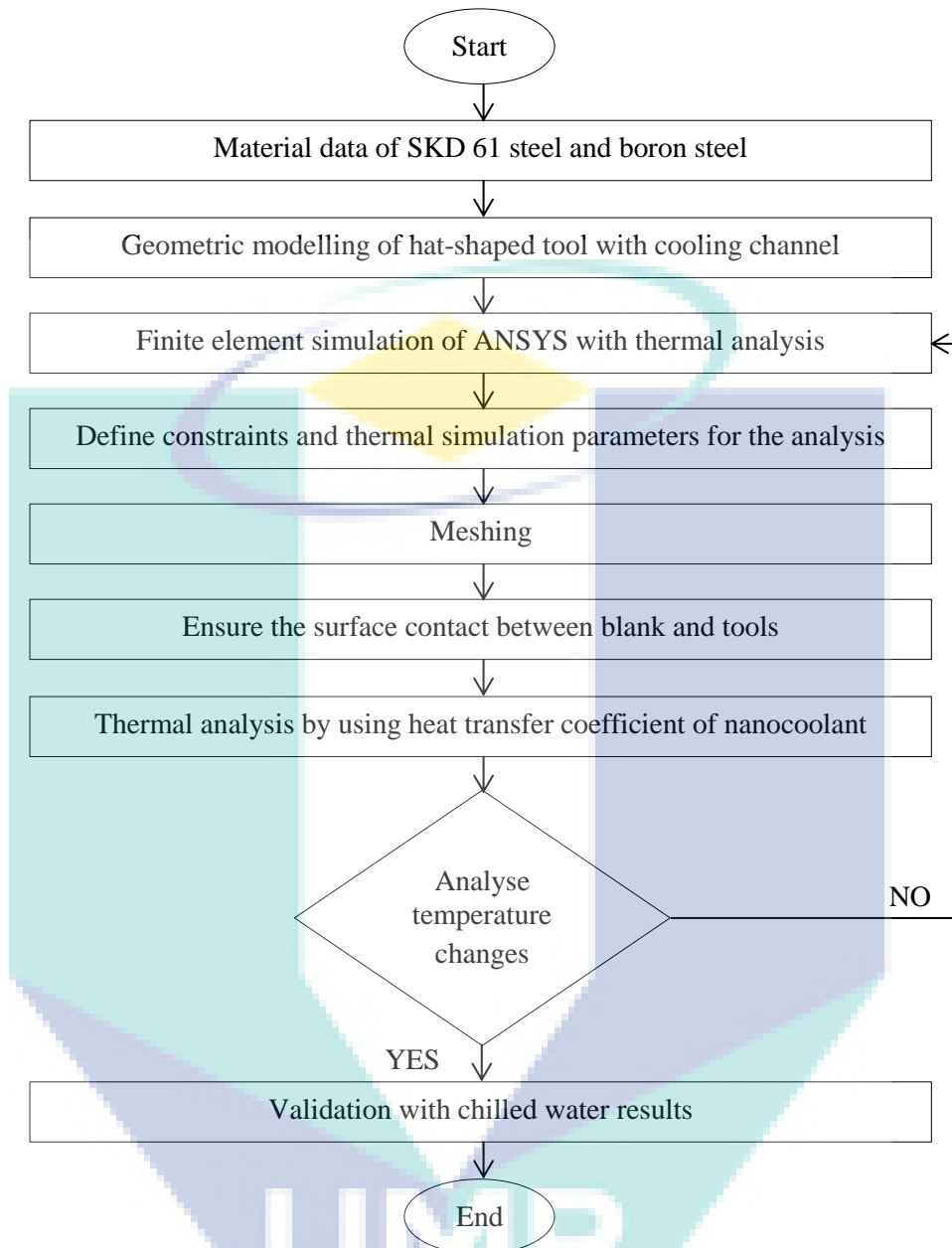


Figure 3.7 Flow chart of thermal finite element analysis on HPF

3.5.1 Thermal analysis

Thermal analysis was done to ensure that the hot press forming (HPF) tool obtained higher cooling rate and high cooling efficiency with the homogeneous temperature distribution (Hoffmann et al., 2007). In this research project, the combination of steady-state thermal analysis and transient thermal analysis were performed as shown

in Figure 3.8. The collected results were then verified with the experimental data to ensure the validity of the results.

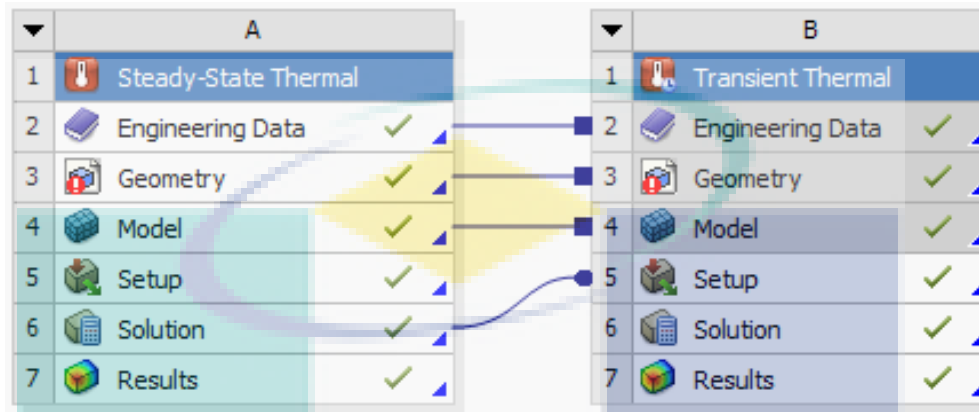


Figure 3.8 Simulation starts from the steady-state and ends with the transient thermal analysis

The type of materials used in this research project was boron steel as sheet metal blank and SKD 61 steel for tool components. The relevant engineering data with respect to thermal analysis were set as material input data. According to thermal analysis, the data of mass density and thermal conductivity of sheet metal blank and tools were needed as they were vital parameters for the simulation. Table 3.5 summaries the thermal and mechanical properties of SKD 61 steel and 22MnB5 boron steel in hot and ambient temperature conditions. The data was given as input into the menu of engineering in the ANSYS software because the SKD 61 steel and boron sheet metal were not available in the software standard libraries. These data were non-trivial as inaccurate data may cause an error in the output of the simulation.

Table 3.5 Material properties of SKD 61 and 22MnB5 at room and hot temperature

Property	SKD 61		22MnB5	
Temperature ($^{\circ}C$)	25	25	25	900
Mass Density, ρ ($kg\cdot m^{-3}$)	7700	7700	817	-
Yield Strength, σ (MPa)	550	550	505	126
Thermal Conductivity, k ($W\cdot m^{-1}\cdot K^{-1}$)	25	25	30.7	25.6
Heat Capacity, C_p ($J\cdot kg^{-1}\cdot K^{-1}$)	460	460	444	596

Source: Kumar et al. (2011) and Taha et al. (2014)

3.5.2 Geometric modelling of hat-shaped tools

The hat-shaped model was designed in CATIA design software. The finite element analysis (FEA) was performed through ANSYS simulation software. The drawing format for CATIA software was saved in the CATIA work format while FEA runs on .igs format. Thus, the model designed via CATIA software was saved as .igs format to allow the model to be imported into ANSYS software before FEA simulation began as shown in Figure 3.9. The materials used for the hat-shaped die model were discussed before in Section 3.5.1. Figure 3.10 shows the model of the hat-shaped die with the cooling channel which was imported into ANSYS software. The effect of the thermal structural field on the tool was completed by using ANSYS simulation thermal analysis.

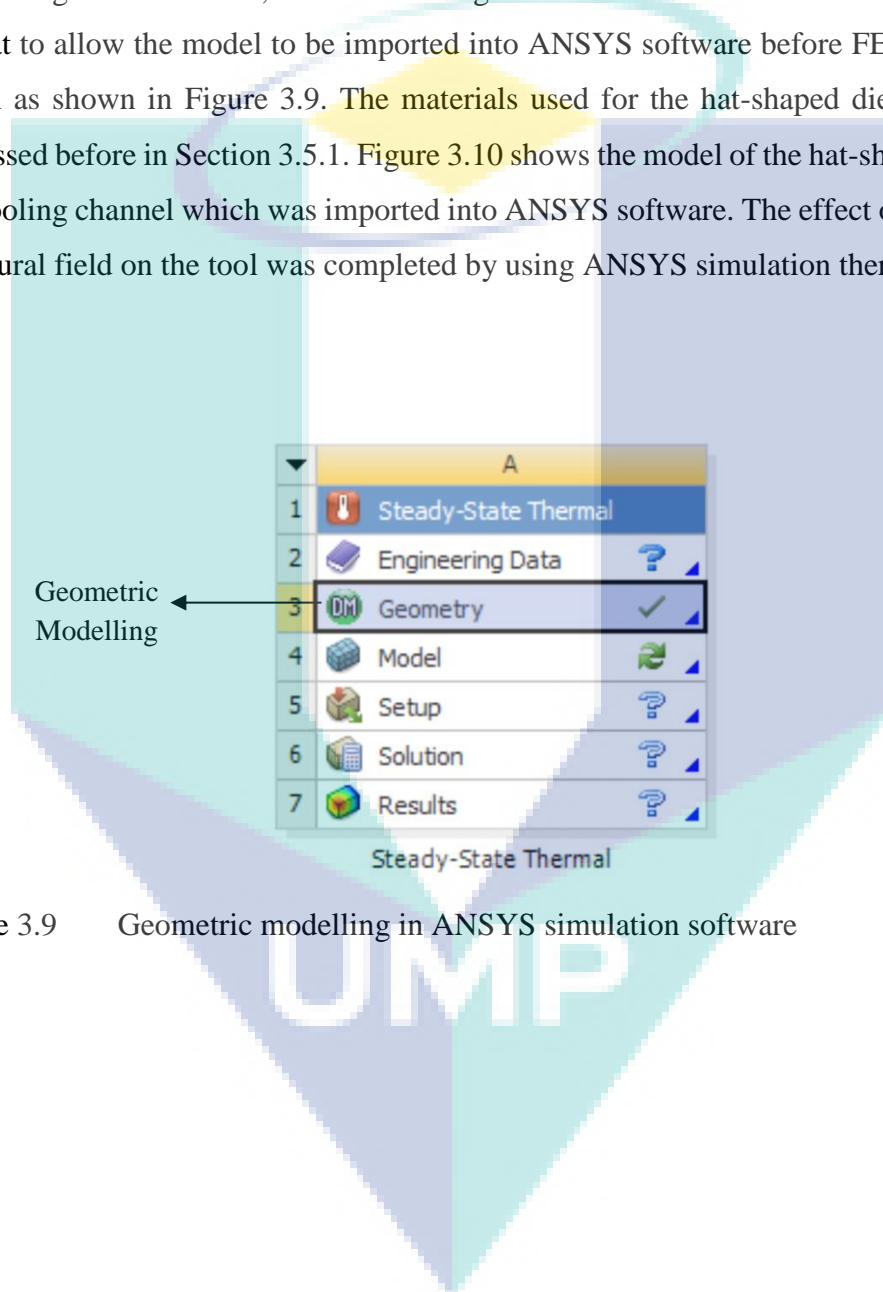


Figure 3.9 Geometric modelling in ANSYS simulation software

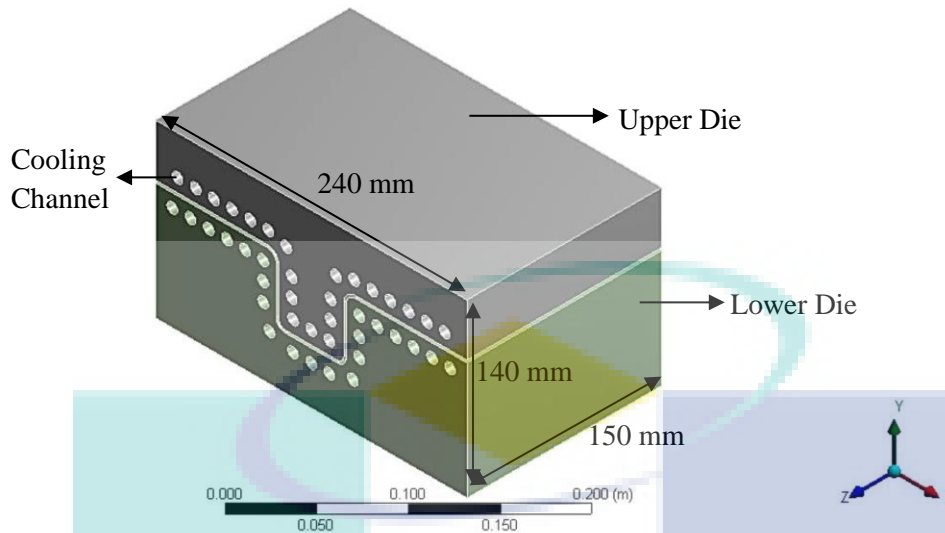


Figure 3.10 Hat-shaped tool imported into ANSYS simulation software

3.5.3 Boundary conditions and constraint parameters

The data of boundary conditions which was given as input to the simulation were taken from the analysis of Hoffmann et al. (2007); Wu and Zhao (2013) and Lim et al. (2016) at summarized in Table 3.6. The tool motion and sheet metal blank deformation were not considered as this simulation was intended to measure the heat transfer distribution or temperature changed between the blank and dies during the quenching operation. The sheet metal blank was estimated to be in its initial homogeneous temperature (Maeno et al., 2014; Hoffmann et al., 2007).

Table 3.6 Boundary condition for thermal analysis simulation

Parameters	Values
Initial Temperature of Blank, $T_{b,0}$ (°C)	900
Initial Temperature of Tool, $T_{t,0}$ (°C)	25
Thermal Contact Conductance, α_c ($\text{W}\cdot\text{m}^{-2}\cdot\text{K}^{-1}$)	5,000
Convection of Chilled Water Cooling Channel, h_{cw} ($\text{W}\cdot\text{m}^{-2}\cdot\text{K}^{-1}$)	4,700
Convection of Nanocoolant Cooling Channel, h_{nc} ($\text{W}\cdot\text{m}^{-2}\cdot\text{K}^{-1}$)	7,813
Convection of Environment, h_e ($\text{W}\cdot\text{m}^{-2}\cdot\text{K}^{-1}$)	3.6
Duration of Quenching Operation, t (s)	3, 5, 8, 10

Source: Hoffmann et al. (2007); Wu and Zhao (2013) and Lim et al. (2016)

3.5.4 Meshing

The meshing feature in ANSYS simulation software is a general purpose and automated high performance product. It produced the most appropriate mesh for precise, accurate and efficient multi-physics solutions. The well mesh for the specific analysis could be generated with a single click for all the components in a model. Fully controls over the options used to generate mesh were available for the professional user to fine-tune it. The power of parallel processing was automatically used to reduce the time taken for meshing generation (ANSYS Handbook, 2016). Meshing could be controlled by three substances such as fine, medium and coarse, which might vary the post-processing results. The ANSYS program can automatically mesh the model without specifying any mesh controls based on its default mesh.

Local meshing controls were focussed on the cooling channel inside the hot press forming (HPF) tools. Namklang et al. (2016) conducted hot forming experimental investigation for local distributions of temperature and local mechanical properties of a hot pressed part by using FE simulation. It was required a fine mesh as the cooling channel function was to control the cooling rate of the tool as well as to control the process. A better analysis with lower time consumption is required. There were several types of local meshing controls such as match control, method control, pinch control, sizing control, contact sizing control, inflation control, refinement control, and mapped face meshing.

Surface contact happened when the austenite sheet metal blank contacted the HPF tool (Wu et al., 2014). The contact between sheet metal blank with the upper die and the contact between sheet metal blank with the lower die were set as bonded in the analysis. Regarding to the literature review of thermal contact conductance (TCC), the closest value to the experimental condition of boron steel in contact with SKD 61 tool steel was $5,000 \text{ W}\cdot\text{m}^{-2}\cdot\text{K}^{-1}$ (Hoffmann et al., 2007; Wu et al., 2014; Taha et al., 2014). Figure 3.11 shows the TCC between HPF tool and the sheet metal blank in position.

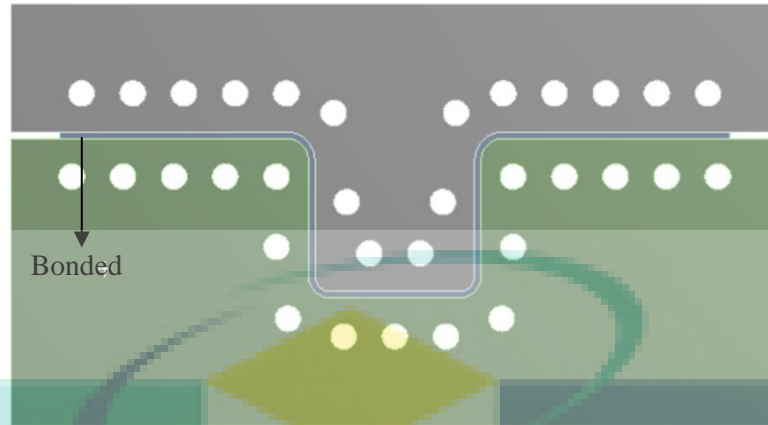


Figure 3.11 Surface contact between sheet metal blank and dies

The mapped face meshing and refinement control were used to compare the quality of meshing element in the simulation. This is because the suitability of the criteria in optimising the meshing quality of the cooling channel in HPF dies. The meshing quality criterion was evaluated by mesh skewness as it was one of the vital feature that determined the quality of mesh. The meshing smoothness and aspect ratio were applied to determine the meshing quality too. Skewness was basically defined as the geometrical orientation of a mesh. It was not defined with respect to nearby meshes, while it was measured as how much the generated mesh varies from the ideal mesh cell (Kumar and Visavale, 2013).

In order to have a fair comparison between the meshes of different relevance centre as to maintain the simulation parameters, the number of elements, nodes, solution time and meshing time for three different meshes were summarized in Table 3.7. According to the table below, the meshing time and solution time varies significantly between the medium sized and fine sized of mesh. Figure 3.12 shows the sample of the hat-shaped tool used in the simulation study with medium sized of mesh. It was applied to the sheet metal blank and tool body for the HPF simulation. The refine mesh was chosen as it yielded a convergence toward zero. Therefore, the medium sized of mesh and refinement control mesh were utilised in this research project. The medium sized of mesh provided reasonable accuracy with a bearable computational burden and the refinement control mesh quality was acceptable (ANSYS handbook, 2016).

Table 3.7 Results of three different meshing sizes for hat-shaped tool

Sizing Control	Course	Medium	Fine
Node	86977	134436	340786
Element	45732	71533	223431
Meshing Time (s)	16	22	120
Solution Time (s)	180	429	2400

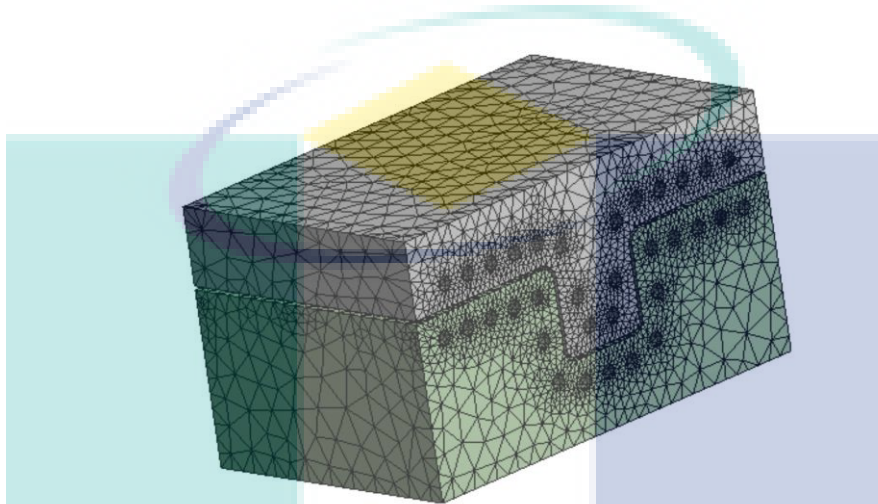


Figure 3.12 The grid distribution of Hat-shaped tool and blank

These results were then compared by introducing the different heat transfer coefficient value of cooling agents such as nanocoolant and chilled water into the cooling system of the hat-shaped geometrical model. The investigation of temperature distribution for the hat-shaped model based on the thermal parameters was examined. The thermal analysis of finite element simulation was validated with the actual experimental results. If the results were not acceptable, it must be reverted to the stage where the parameters were modified to satisfy the thermal analysis for quenching operation of the HPF.

3.5.5 Numerical simulation

The simulation analysis began with steady-state thermal analysis, in which tools were set to room temperature condition while the temperature of sheet metal blank was set to 900 °C, austenitization temperature condition. The analysis time was set to 0.1 s, assuming that the HPF process was not started yet. Several analysis time periods for

transient thermal analysis simulation were set as 3 s, 5 s, 8 s and 10 s, which was considered similar as the actual time of HPF process, and the punch motion was neglected. This resulted in the cooling rate of the HPF tool. According to the study of Cengel and Ghajar (2011), the heat transfer given by Fourier's Law of conduction was calculated from Equation 3.3 and Newton's Law of cooling was obtained as Equation 3.4 (Cengel, 2010).

$$\dot{Q}_{conduction} = -kA \frac{dT}{dX} \quad 3.3$$

$$\dot{Q}_{convection} = hA(T_f - T_s) \quad 3.4$$

where A is the contact area, k is thermal conductivity and $\frac{dT}{dX}$ is the temperature gradient; h is heat transfer coefficient, T_f is surface temperature and T_s represents the temperature of moving fluid. The heat transfer coefficient, h has the units of $W \cdot m^{-2} \cdot K^{-1}$; and A is the area of substances. It is typically named as a flow property but the heat transfer coefficient is not a thermodynamic property (Cengel and Ghajar, 2011). As for the thermal analysis, the heat transfer results of austenite sheet metal and dies were attained from finite element analysis (FEA) software. The heat transfer formulas of Equation 3.5 - 3.6 were used to calculate the cooling rate for the tool and heated blank (Merklein et al., 2014; Bosetti et al., 2010). Typically, the rate of heat transfer changes during the process with respect to time. The cooling rate for blank and tool can be resolved by dividing the amount of heat transfer with a time interval (Cengel and Ghajar, 2011).

$$Q = \Delta U = mc_p(T_2 - T_1) \quad 3.5$$

$$\dot{Q} = \frac{Q}{\Delta t} \quad 3.6$$

where c_p is specific heat at the bulk temperature, T_1 is the inlet temperature, T_2 is the outlet temperature and Δt differential of time. Figure 3.13 presents the zone of the computed cooling rate as the gradient of temperature-time graph. The method and sample of calculation for heated sheet metal blank are as shown in the Appendix B1. The time

interval between 1 to 7 s was chosen as it resulted in the best gradient compared to other time periods. The interval of time indicated where the mechanical properties of material changed from austenite to martensite transformation. In HPF process, heated sheet metal blank was needed to be fully martensite as to attain ultra-high strength steel (UHSS) behaviour (Karbasiyan and Tekkaya, 2010).

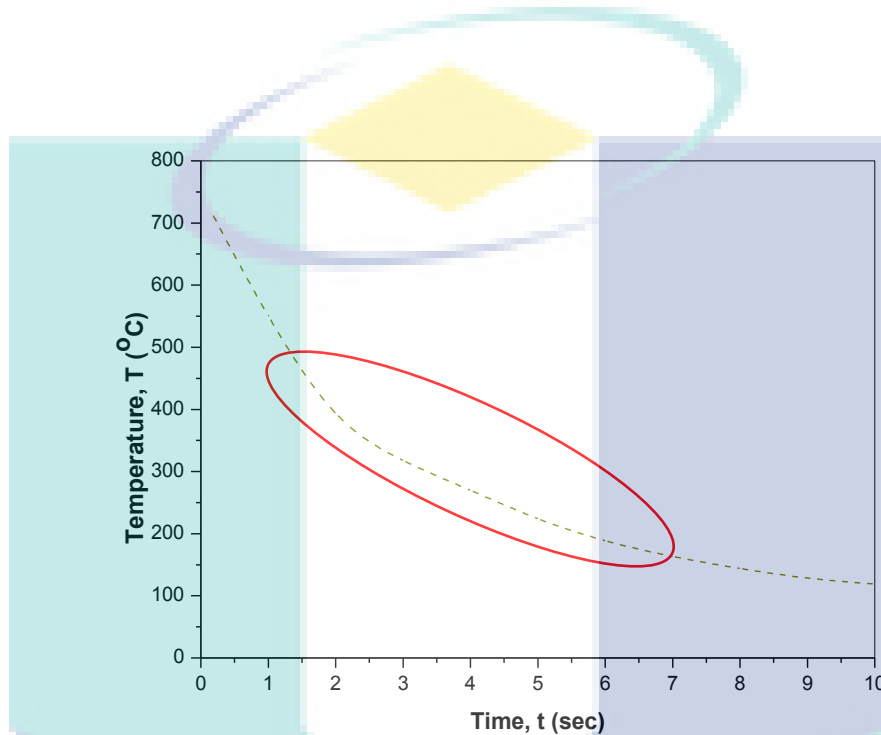


Figure 3.13 Temperature distribution of hot pressed blank by using nanocoolant from ANSYS simulation

3.6 Experimental Approach of Hot Press Forming

There are two major operations involved in hot press forming (HPF) process such as forming and cutting. Forming is a process of shaping the material into the desired shape (Banabic, 2010). While, cutting is a process of separating a piece of sheet metal by applying a sufficient force to cause the material to fail. In the cutting of the ultra-high strength steel (UHSS) material, the increase in shearing load brings about the reduction in tool life (Mori et al., 2012). Figure 3.14 illustrates the sequences of experimental measurement for heat transfer distribution on HPF process. The material used for the blank product was boron steel with the grade of 22MnB5. The experiment of HPF process started from the preparation of the hat-shaped boron steel blank by using cold forming die as pre-forming operation. The *k*-type thermocouples were installed to the HPF dies to

collect the temperature data during the HPF process (Kim et al., 2015). The two types of experiments such as nanocoolant and chilled water with constant flow rate and heat transfer experiment were conducted in this experimental study for investigating the heat transfer distribution of the HPF process. Lastly, the tensile tests were conducted according to American Society for Testing and Material International (ASTM) standard by using the Universal Tensile Machine (UTM) to find the ultimate tensile strength of the hot pressed part (Merklein et al., 2014; Mori et al., 2015). Once the tensile test had been performed, the hardness measurement was conducted for the sample by using Vickers Micro-hardness Machine according to DIN EN ISO 6507-1 standard at room temperature (Bardelcik et al., 2012; Wang and Lee, 2013; Maeno et al., 2015, L bbe et al., 2016). The microstructure transformation of boron steel blanks were evaluated by using Light Optical Microscopy (LOM) (Naderi et al., 2011; L bbe et al., 2016).

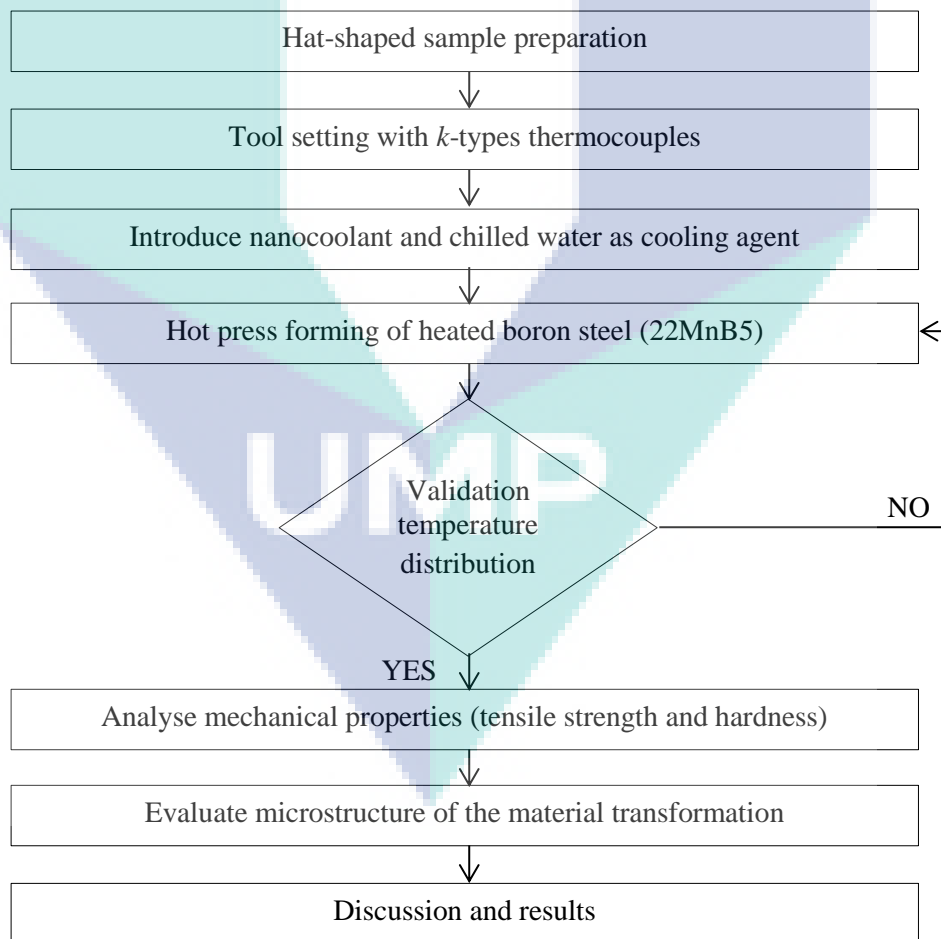


Figure 3.14 The process sequences of HPF experimental analysis

3.6.1 Sample preparation

Hat-shaped sample with tensile shape specification was used because the instrumentations in laboratory limited to hot press forming the real automotive parts. The hat-shaped part was formed by using cold forming tool. The material used for the sheet metal blank product was boron steel with the grade of 22MnB5. The SKD 61 was used as the hot press forming (HPF) tool material which can cover heat transfer distribution of the austenite sheet metal blank. Hat-shaped sample was chosen as the specimen of the experiment from Thanadngan et al. (2013) with the blank size dimension of 280 mm × 100 mm × 1.8 mm. Figure 3.15 concludes the process flow for hat-shaped samples fabrication by using cold dies as pre-forming operation with a mechanical press machine model OCP 80.

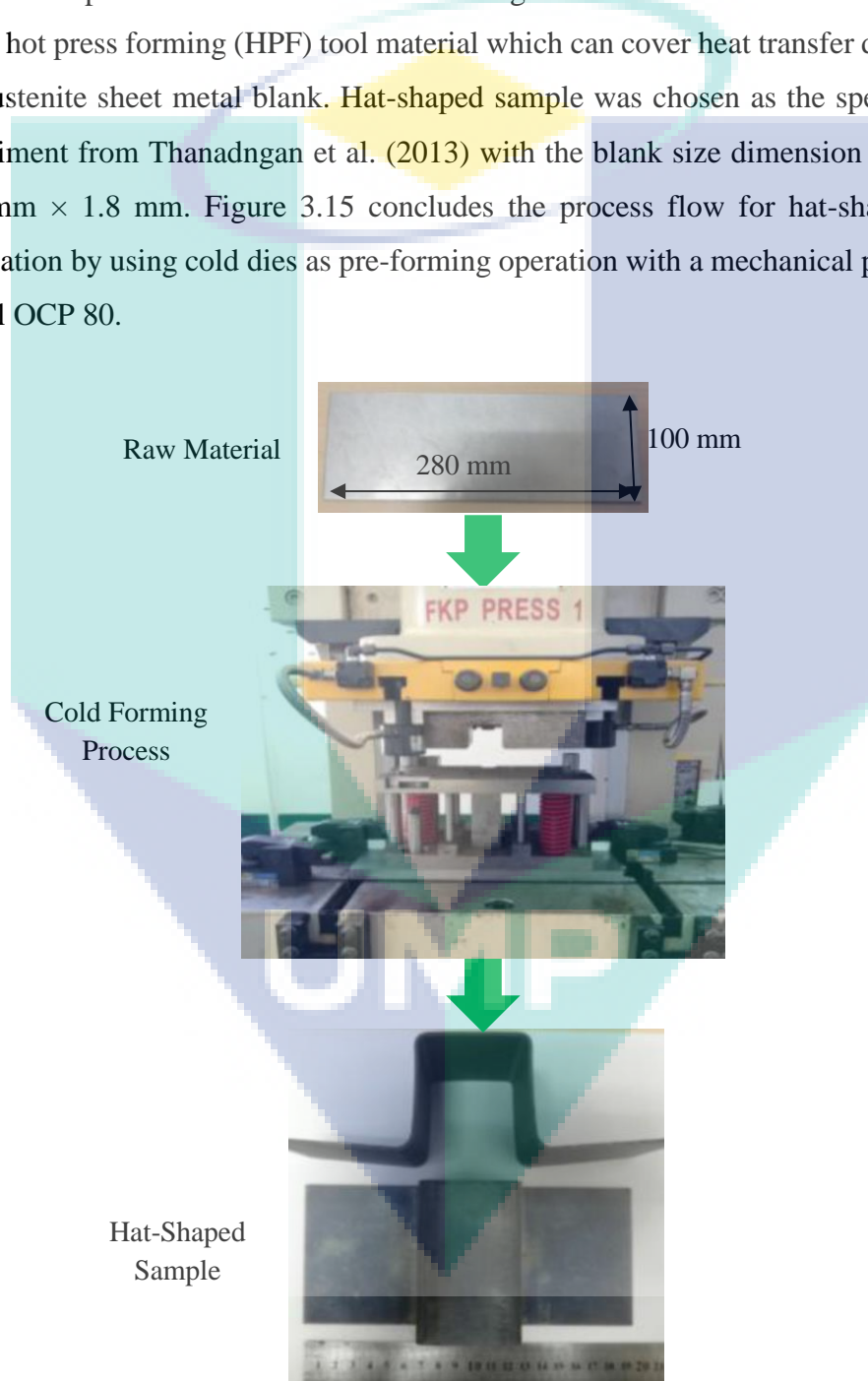
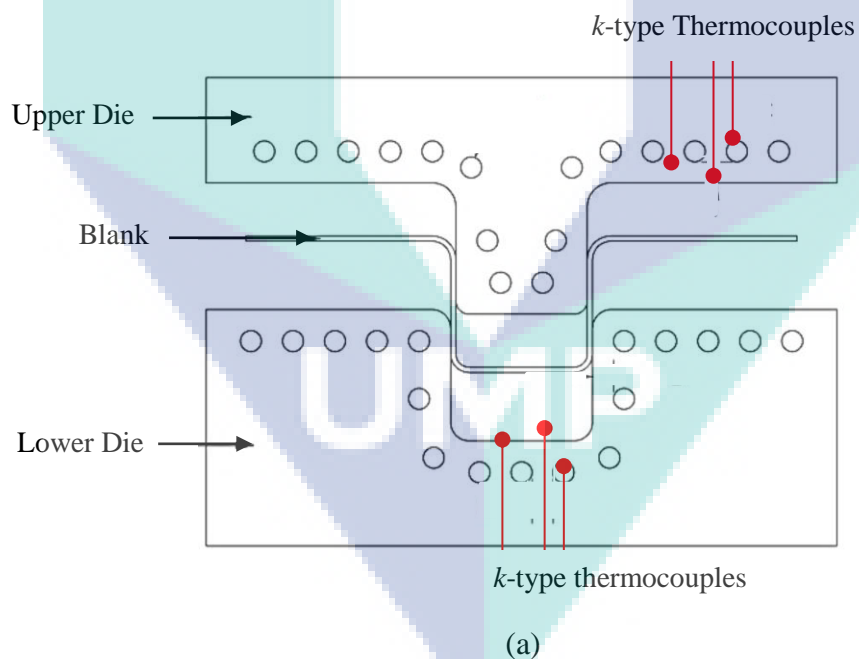


Figure 3.15 Pre-forming process of hat-shaped samples

3.6.2 Location of thermocouples

Thermocouples were located inside the hot press forming (HPF) dies, and *k*-type thermocouples were used in this experiment. Figure 3.16 depicts the *k*-type thermocouples placed at 6 different locations in HPF tool. The function of thermocouples was to measure the actual temperature changed during the quenching process in order to record the data to be analysed. George et al. (2012) and Lin et al. (2015) evaluated the heat transfer distribution of the tool by placing the thermocouple approximately in 4 mm away from the loading counter. The data of temperature changed was collected by using a data logger instrument of model ZR-RX25 Data Logger. The data logger device was used to measure a wide range of temperatures by using *k*-type thermocouples that have a miniature size thermocouple connector. Moreover, the data logger has low conversion time as 10 temperature measurements could be taken for every second. In this experiment, the best location to collect the temperature of HPF dies was 0.05 mm away for the loading counter. The data of the heat transfer distribution enabled to attain in between of 4 mm.



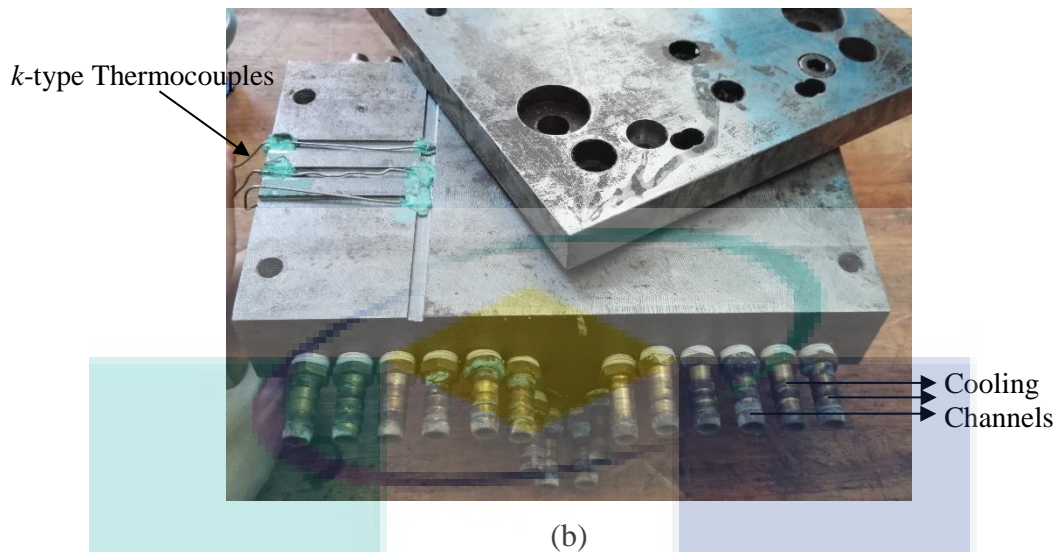


Figure 3.16 Thermocouples location in HPF tool (a) Schematic diagram (b) Three thermocouples in upper tool

3.6.3 Hot press forming of boron steel sheet metal

Hot press forming (HPF) is a process to increase the tensile strength of boron steel by heating it up to austenite transformation temperature and instantly quenched it inside a coolant-cooled die to perform the part drawing (Hu et al., 2013). Several researchers Karbasian et al. 2010 and Naganathan et al. 2012 had elaborated on the HPF process. The sheet metal was heated up to approximately 900 °C for 5 mins heating time and then placed in an enclosure cooled die. The cooling channel has a convection heat transfer coefficient of $7,813 \text{ W}\cdot\text{m}^{-2}\cdot\text{K}^{-1}$ of nanocoolant with a bulk temperature of 25 °C. The chilled water with $4,700 \text{ W}\cdot\text{m}^{-2}\cdot\text{K}^{-1}$ of convection heat transfer coefficient also used to cool down the dies and to allow the quenching operation to transpire.

After attaining the optimum heat transfer distribution data of HPF dies and blank from finite element analysis (FEA), the nanocoolant as a cooling agent of HPF process was synthesised prior to introduction into the experiment. The experiments of comparing two different cooling fluids as coolant with constant flow rate and temperature changed of heat distribution were conducted in this research study. The nanocoolant as an alternative cooling agent was used to compare with chilled water to determine the mechanical properties and microstructure of the drawn part. Merklein et al. (2014) and

Wu et al. (2014) conducted an experiment to determine the mechanical properties in terms of tensile strength and hardness of the formed part by using two different types of cooling fluid such as water and chilled water. Furthermore, the heat transfer distribution experiment was performed to evaluate the cooling rate of the HPF dies.

In the preparation of sheet metal blank, mechanical press machine of model OCP 80 was used to fabricate the hat-shaped sample through the cold forming process as shown in Figure 3.17. After sheet metal blank preparation, hydraulic press machine as shown in Figure 3.18, which was used in conducting the HPF process experiment. The specification of the mechanical press machine and hydraulic press machine were summarized in Table 3.8 and Table 3.9, respectively.

Table 3.8 The features of mechanical press machine model OCP 80

Specifications	Values
Max Die Height (mm)	330
Slide Area (mm X mm)	450 X 550
Stroke Length (mm)	150
Tonnage Capacity (Tonne)	80

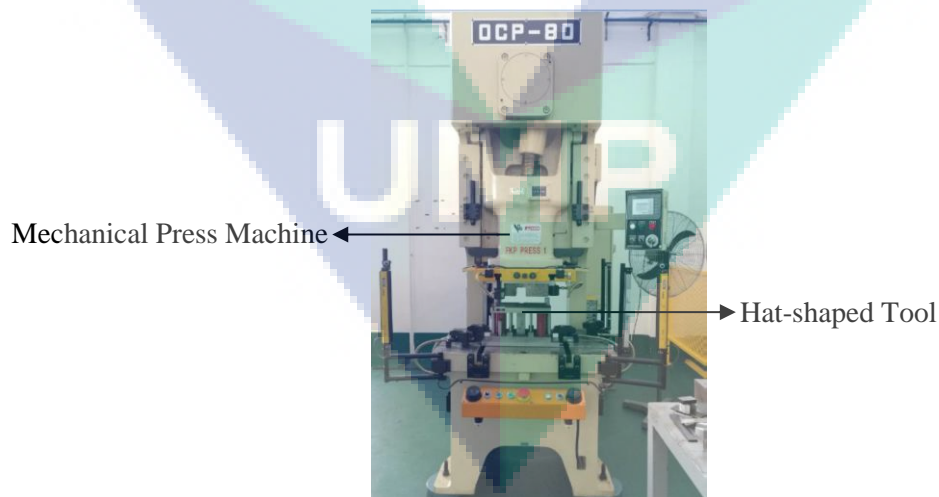


Figure 3.17 Fabrication of hat-shape sample by using mechanical press machine, OCP 80

Table 3.9 The features of hydraulic press machine

Specifications	Values
Bore Diameter Size (mm)	80
Rod Diameter Size (mm)	40
Stroke Length (mm)	200
Tonnage Capacity (Tonne)	10

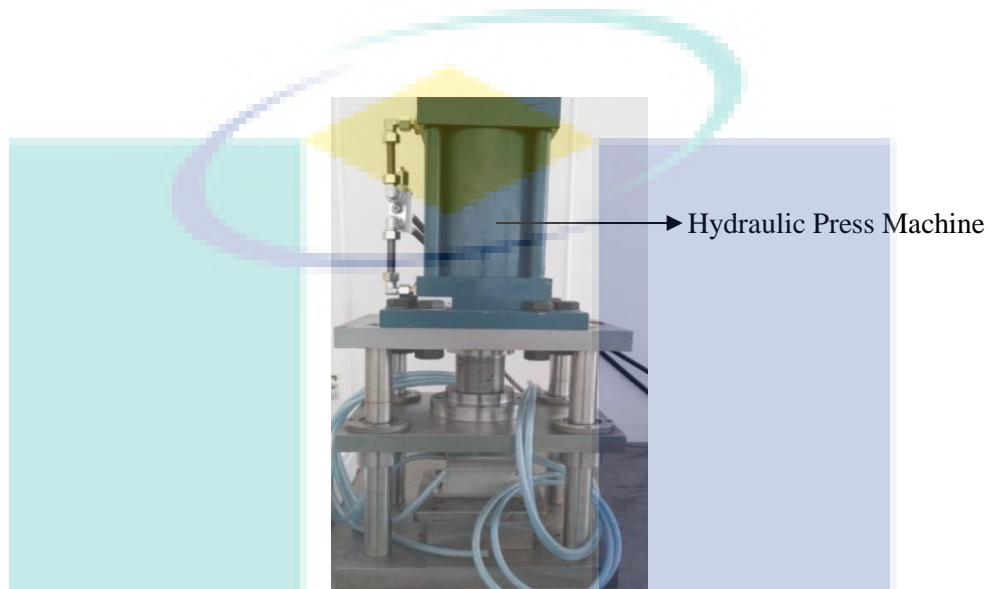


Figure 3.18 Hydraulic press machine used in hot forming operation

3.6.4 Experimental study of heat transfer distribution

Current research project experiments studied several parameters that were used for hot press forming (HPF) process. These parameters such as austenitization temperature, cooling flow rate, pressure and quenching time were used to perform the part drawing in HPF process. As for the cooling flow rate, the value was fixed according to the power of motor water pump used in ACSON model AMAC 40C chiller. The thickness of sheet metal blanks was 1.8 mm and formed to hat-shaped sample through cold forming process. In this experiment, the hat-shaped blank was heated up to 900 °C of temperature for approximately 5 mins time period (Karbasiyan & Tekkaya, 2010). Mori et al. (2012) found that 5 mins of heating time was sufficient to attain the optimum martensitic content in the quenched samples with a maximum hardness of approximately 470 HV. As for the quenching time during HPF process, the time interval was 3 s, 5 s, 8

s and 10 s, respectively. Figure 3.19 presents the experimental setup for the HPF process with chiller and heating furnace. The furnace was used to heat up the boron sheet metal blank to the austenitization temperature and the chiller was used to cool down the HPF die tools to maintain the dies at 25 °C bulk temperature for completing every experiment. As to quench the boron steel sheet metal, the hot forming tool was used. The hydraulic press machine was used to apply the pressure to the boron steel sample. The details of the heat transfer experiment performed were explained in this section.

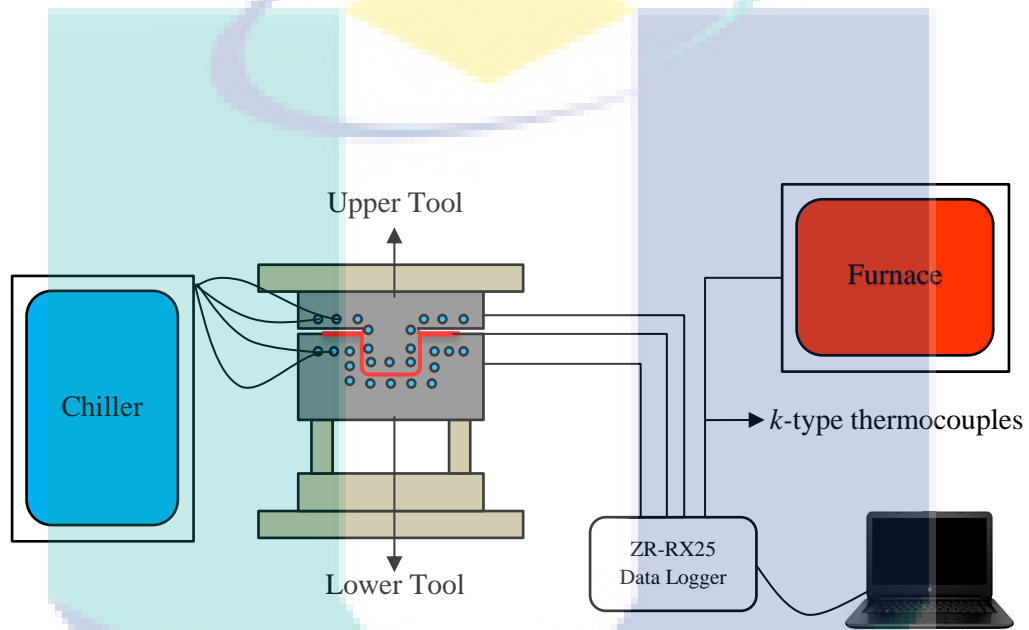


Figure 3.19 The experimental equipment setup for hot press forming tool

UMP

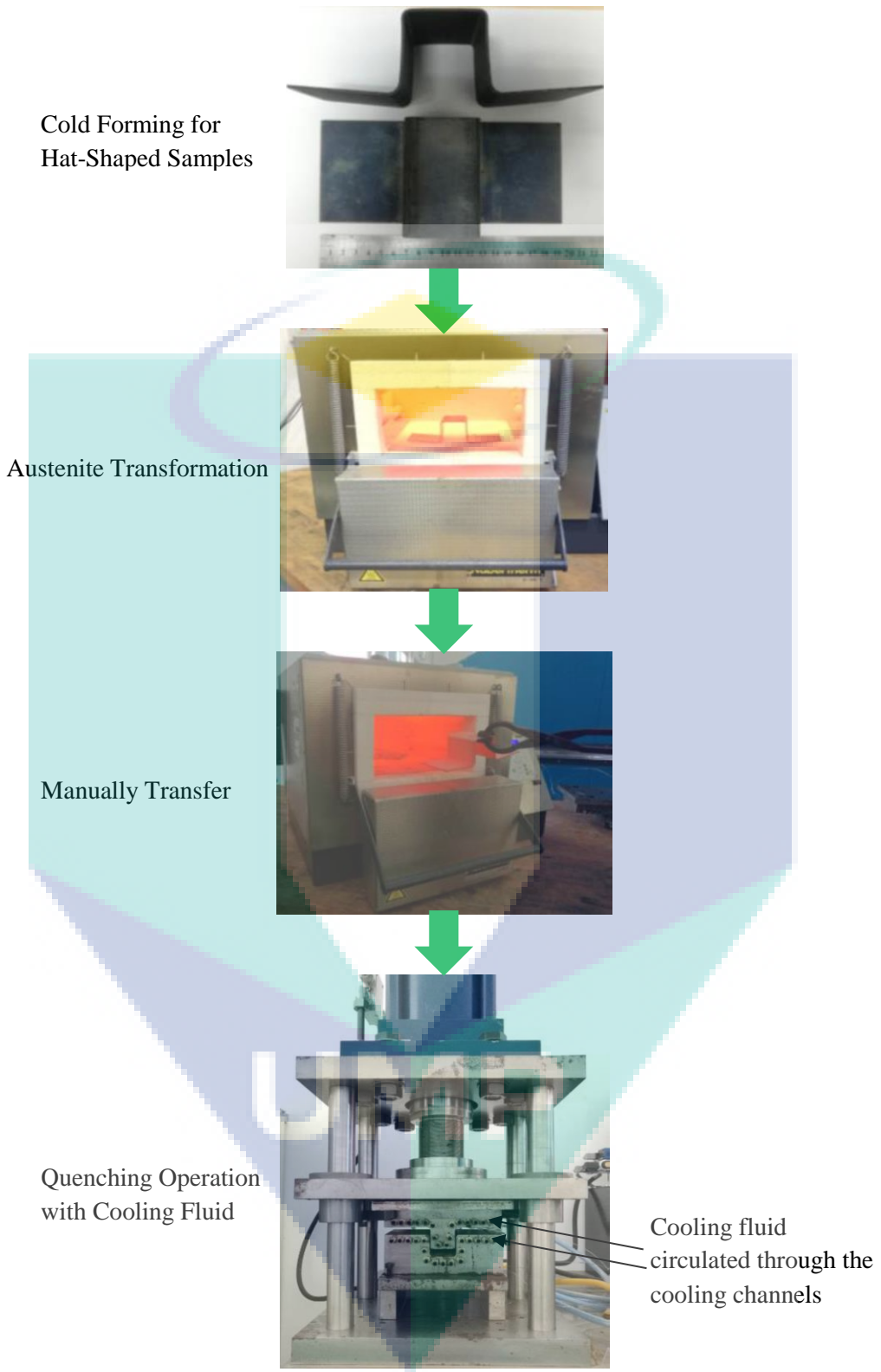


Figure 3.20 Hot press forming process flow of hat-shaped blank

Prior to HPF experiment, the hat-shaped blank was heated to the temperature of 900 °C in the furnace. The austenite blank was then rapidly transferred to the enclosure dies to avoid the heat loss before starting the forming operation. Next, the hat-shaped blank was formed in the HPF dies with a pressure of 20 MPa by using hydraulic press machine. The heat transfer distribution was evaluated during the HPF process. The temperature of the sheet metal blank and the HPF dies were recorded by means of the *k*-type thermocouples. The data collected from experiments were then compared with the simulation results. Figure 3.20 shows the flow of the HPF process of hat-shaped tool. The hot pressed part will be measured and analysed by conducting the hardness measurement, tensile test and metallographic study of the microstructure.

3.6.5 Tensile test measurements

After hot press forming (HPF) experiments, the hot pressed parts were cut into tensile test specimens taken from the wall, bottom and flange locations as illustrated in Figure 3.21. According to the standard of ASTM E 8M, specimens with a total length of 100 mm were cut into 33 mm X 5 mm X 1.8 mm gauge size, which maintained for every tensile test experiment as shown in Figure 3.22. Next, the tensile test specimen was clamped by using the upper and lower jaw of the Universal Tensile Machine (UTM) as depicted in Figure 3.23. Table 3.10 summaries the specifications for UTM machine. The process was stopped when it reached the maximum tensile strength value. The raw results are in the form of force versus elongation. It covers from the elastic phase transition to the plastic deformation until the samples fractures. The data will then be processed to generate the true stress versus true strain curve method regarding ASTM E 8M standard (Merklein et al., 2014; Kim et al., 2015).

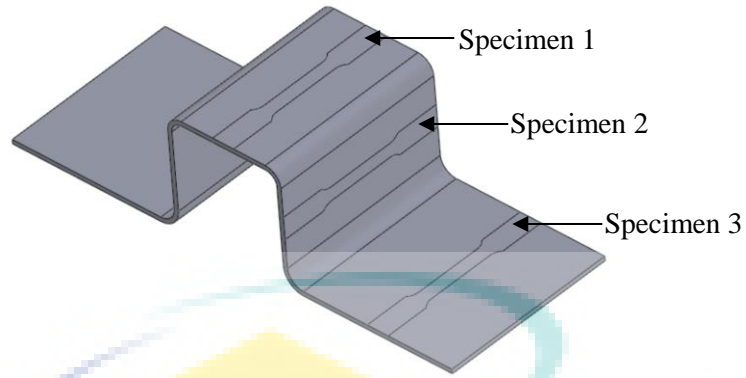


Figure 3.21 Location of hot formed samples for tensile specimen, hardness test and microstructure analysis

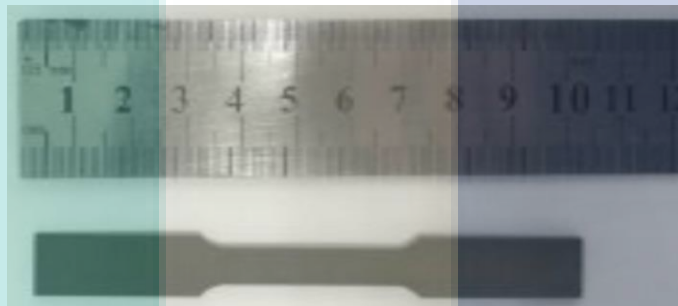


Figure 3.22 Specimen for tensile strength test

Table 3.10 Specifications of Universal Tensile Machine

Parameters	Capacity
Load Capacity (kN)	50
Height (mm)	1,582
Width (mm)	756
Depth (mm)	707
Space between Columns (mm)	420
Total Vertical test Space (mm)	1,193
Total Crosshead Travel (mm)	1,122
Maximum Speed (mm·min ⁻¹)	500
Minimum Speed (mm·min ⁻¹)	0.005
Maximum Force at Full Speed (mm·min ⁻¹)	25
Maximum Force at Full Load (mm·min ⁻¹)	250
Return Speed (mm·min ⁻¹)	500
Weight with Typical Load Cell (kg)	141
Maximum Power Requirement (W)	700

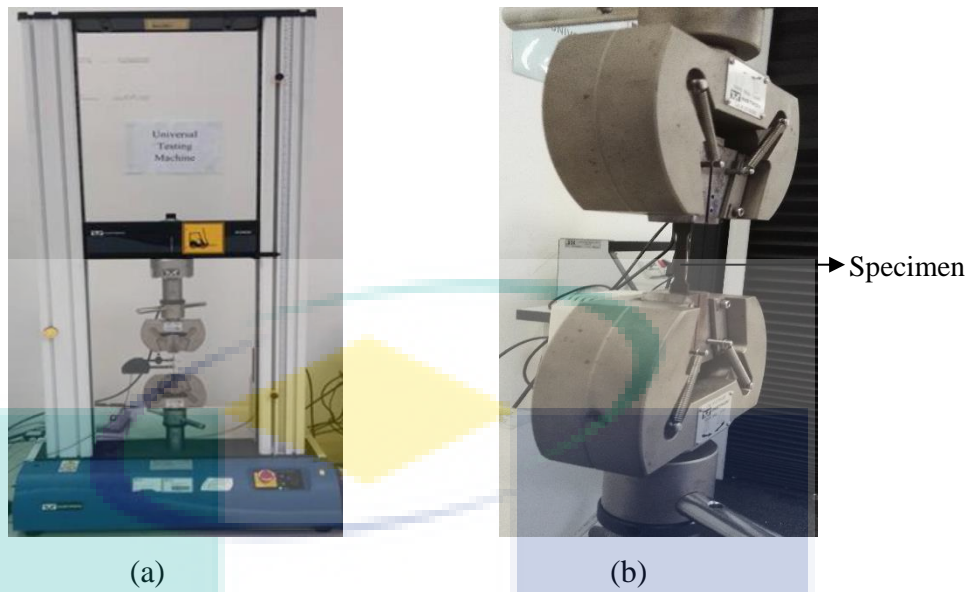


Figure 3.23 Tensile strength measurement with Universal Tensile Machine

3.6.6 Micro-hardness measurements

After the tensile strength test had been done, the sample was then machined into small pieces for the hardness measurement by using Vickers Micro-hardness Machine as shown in Figure 3.24. Table 3.11 lists the specifications of the Vickers Micro-hardness Machine of model Wilson Vickers 402 MVD. The mounting process was followed, where the mixture of 10 mL of resin and 20 mL of powder. The mixture was manually stirred uniformly with a glass rod and held for approximately 3 min after the mixture was poured into the reference sample case. The reference sample was subjected to the grinding and polishing operations. Several grades of sand paper from 800-1,200 grade grain size and liquid of diamond were used to polish and refine the sample. The hardness value was measured by using Vickers method according to DIN EN ISO 6507-1 with the hardness readings measured by a test force of 1 N (Bardelcik et al., 2012, Maeno et al., 2015, Löbbe et al., 2016). The diamond shapes for the reference sample was produced on the surface and it was measured by using the Vickers Micro-hardness Tester Machine.

Table 3.11 Specifications of Wilson Vickers 402 MVD machine

Parameters	Capacity
Hardness Scale	Vickers and Knoop
Test Load (kN)	10-2,000
Dwell Time (s)	5-99
Eyepiece Magnification	10X
Maximum Specimen Height (mm)	85
x-y Stage Dimension (mm)	100 X 100
x-y Stage Travel Range (mm)	25 X 25
Minimum Reading (mm)	0.01
Operating Temperature (°C)	10-38
Machine Dimension, <i>L x W x H</i> (mm)	513 X 320 X 470
Weight (kg)	36
Power Supply (VAC)	110-220

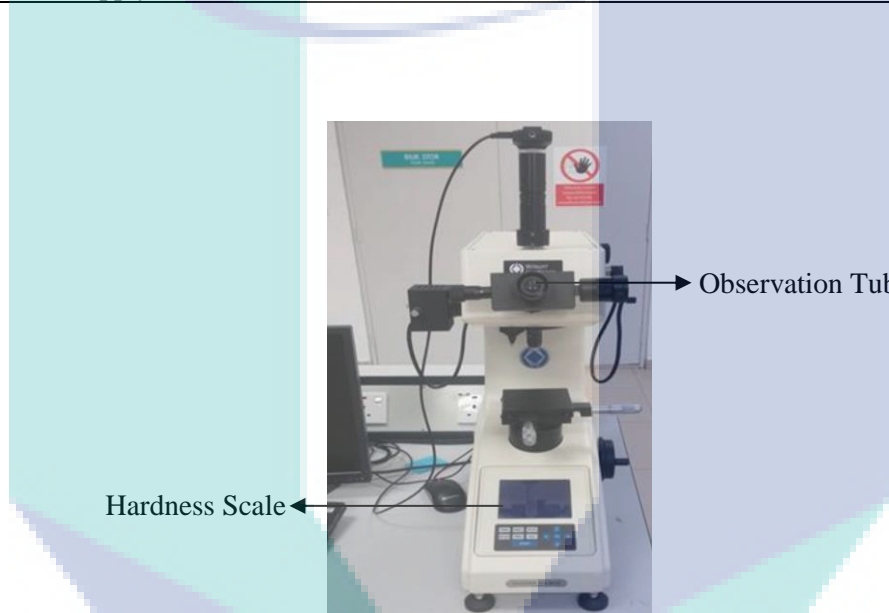


Figure 3.24 Hardness measurement with Vickers Micro-hardness Machine, Wilson Vickers 402 MVD

3.6.7 Metallographic observation study

The obtained microstructures resulting from the samples of hot pressed boron steel were analysed by Light Optical Microscopy (LOM) machine with Progress Capture 28.8 Jenoptik Optical System Image Analyser software as shown in Figure 3.25. The inaccuracy of about $\pm 5\%$ in measuring quantitative area fractions of different phases was reported in the software manual (Nuraini et al., 2013). Table 3.12 lists the specifications of the LOM machine of model Olympus BX51M. The preparation of the reference samples required mounting process as similar to hardness measurement. The reference sample was then subjected to the mechanical polishing procedures with several grades of

sand paper from 100 to 1,500 grade grain size and liquid of diamond were used to polish the reference sample. Lastly, the samples were etched with 3% nitric acid for approximately 2 to 5 s time period (Löbbecke et al., 2016). The microstructure morphology was observed with a magnification of 20X, 50X and 100X with LOM machine. The results of microstructure were captured by using LOM software to generate data and produced the images in the desktop set.

Table 3.12 Specification of LOM, Olympus BX51M machine

Features	Capacity
Optical System	UIS2/UIS (Universal Infinity System) Optical system (featuring infinity correction)
Stroke per Rotation (mm)	0.1 (Fine); 17.8 (Coarse)
Full Stroke Range (mm)	25
Observation Tube Inclination	30°
Distance Adjustment (mm)	50-76
Stage Size, <i>D X W</i> (mm)	156 X 191
Stage Movement, <i>x-y</i> (mm)	76 (Horizontal); 52 (Vertical)
Revolving Nosepiece	Universal 6-position centered revolving nosepiece
Observation Tube	Super widefield trinocular
Magnification Lens	10X-100X (FN 26.5 Super Widefield)
Operating Temperature (°C)	5-40
Operating Environment	Indoor use; Max 2000 m (Altitude)
Power Consumption (W)	140

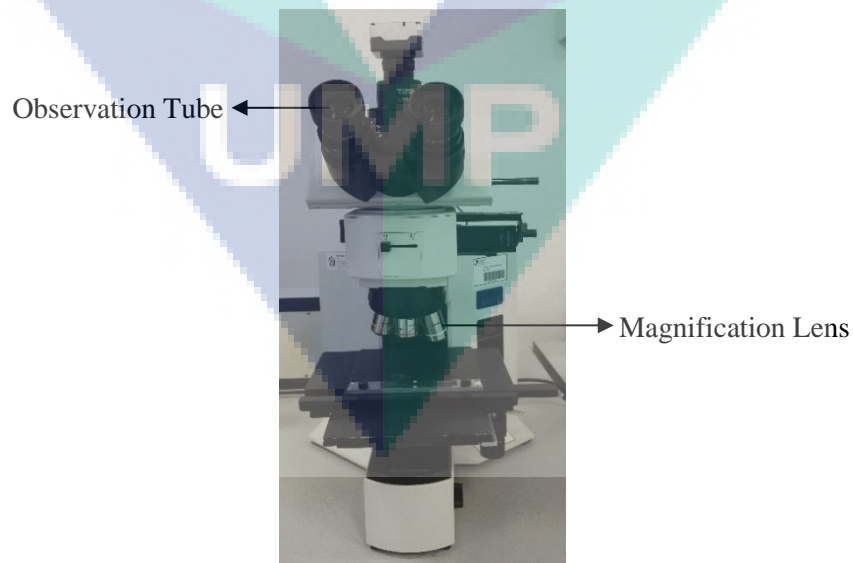


Figure 3.25 Microstructural analysis by using light optical microscopy machine

3.7 Summary

The study of nanocoolants was divided into two major parts, which were measurement of nanocoolants thermal physical properties in terms of thermal conductivity and dynamic viscosity as well as investigation of convective heat transfer coefficient. The measurement was initiated with the validation of the instrument and test rig by using base fluid. For properties measurement, the thermal conductivity and dynamic viscosity were measured at a temperature range of 15 to 55 °C with an interval of 5 °C. The concentrations of the nanocoolants range of 0.2 to 1.0%. The properties evaluations were expected to be affected by the rise in temperature and concentration. The convective heat transfer study was evaluated by the nanocoolants heat transfer performance. The analyses consisted of parameters such as Nusselt number and heat transfer coefficient. The Reynolds number range studied in between 7,000 to 20,000 for bulk temperature of 25 °C. The variation of nanoparticles concentrations and Reynolds number were predicted to affect the Nusselt number and heat transfer coefficient of nanocoolants.

The finite element analysis (FEA) simulation for thermal distribution which involved in obtaining the material data, geometric modelling and meshing in Section 3.5. The hot forming tool was set with k -type thermocouples before the preparation of hat-shaped samples and nanocoolant for the experimental HPF process. The experiment of HPF process by using boron steel was conducted involving several cooling fluids with different cooling rates and heat transfer experiments. The hot pressed part was investigated for microstructure morphology observation by using Light Optical Microscope, the tensile strength test measurement by using Universal Tensile Machine and the Vickers hardness measurement by using Vickers Micro-hardness Machine. The results were presented and discussed briefly in the Chapter 4.

CHAPTER 4

RESULTS AND DISCUSSION

4.1 Introduction

This chapter gathered the data from the thermal conductivity, dynamic viscosity evaluation and convective heat transfer analysis in relation to the objectives. Meantime, the findings of thermal physical properties behaviour with respect to the concentration of nanoparticles and temperature were discussed in this chapter. The discussion began with the validation of data with available literature, and proceeded with the nanocoolant data measurement and evaluation. The evaluation and measurement of thermal physical properties of nanocoolants were crucial as it was adapted into the investigation of convective heat transfer. The data analysis of convective heat transfer involved different engineering parameters such as Reynolds number, Nusselt number and heat transfer coefficient. The significant effect of the nanoparticles concentration to the overall performance of nanocoolant was subjected to the characterization of heat transfer coefficient and Nusselt number. This was the manner that the study included the effect of increment of the nanocoolant concentration and Reynolds number, thus answering the research question and the usage of nanocoolant in real applications of nanocoolants in manufacturing cooling system.

The best finite element analysis (FEA) was discussed as to analyse the best heat transfer distribution between the HPF tools and sheet metal blank by introducing two different cooling agents such as chilled water and nanocoolant. Therefore, the finding of the best FEA method including sizes of meshing and mesh quality criteria was determined. Next, the thermal analysis of nanocoolants based Al_2O_3 for cooling channel performance was conducted with hat-shaped samples at ambient temperature for HPF

process. The temperature distribution results of the experimental heated blank and tools to validate with the FEA heat transfer distribution. Finally, the optimum mechanical properties (tensile strength, Vickers hardness and microstructure) of hot pressed sample was selected and compared with the boron steel as receiving stage and hot pressed part of chilled water. The data and findings collected throughout the study were discussed.

4.2 Thermal Physical Properties

The thermal physical properties of aluminium oxide, Al_2O_3 nanocoolants such as thermal conductivity and dynamic viscosity were measured for the temperature range of 15 to 55 °C and volume concentration range of 0.2 to 1.0%. The measurement values of samples were compared to several references for validation. The thermal conductivity and dynamic viscosity data were plotted against temperature to analyse its patterns and behaviour. The density and specific heat values were predicted by using related parameters as explained in Chapter 2 and 3.

4.2.1 Thermal conductivity of nanocoolant

Figure 4.1 shows the thermal conductivity of the aluminium oxide (Al_2O_3) nanocoolant in the 3 different mixtures (60%:40%; 50%:50%; 40%:60%) of water-EG base fluid at 25 °C for 0.2 to 1.0% volume concentrations. The experimental results of the present study were compared with the estimated values obtained from previously published models. The figure shows that the thermal conductivity of the nanocoolant increased with volume concentration. The experimental values for this study were slightly higher than those of the three models by Hamilton and Crosser (1962); Timofeeva et al. (2011); and Wasp et al. (1977). However, the model by Yu and Choi (2003) agreed with the experimental values to a certain extent. The mean and maximum deviation of the three different percentages of water to ethylene glycol base fluids such as 60%:40%, 50%:50%, and 40%:60% experimental values are compared with the findings of Yu and Choi (2003) are 0.01% and 0.13%; 0.04% and 0.68%; and 0.03% and 1.44%, respectively. Elias et al. (2014) compared the experimental value of thermal conductivity

of the Al_2O_3 /radiator nanocoolant with the Hamilton and Crosser (1962) model. The results showed that their experimental value exhibited a 2.2% deviation from the calculated model. Sonawane et al. (2015) used the Wasp et al. (1977) model that yielded a similar outcome as the Maxwell model for spherical nanoparticles and found that the experimental thermal conductivity values of TiO_2 /water based nanocoolant showed 17.0% deviation from the Wasp model.

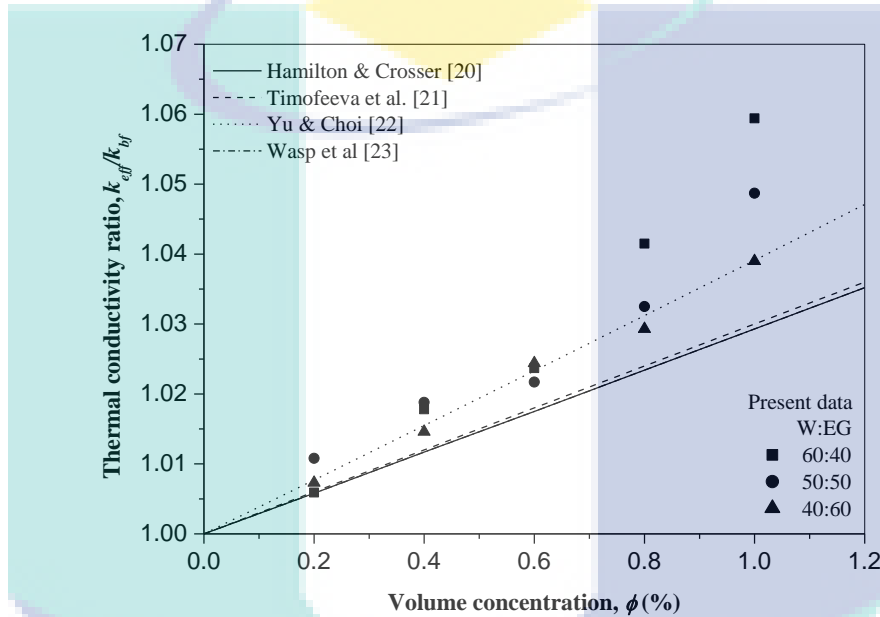
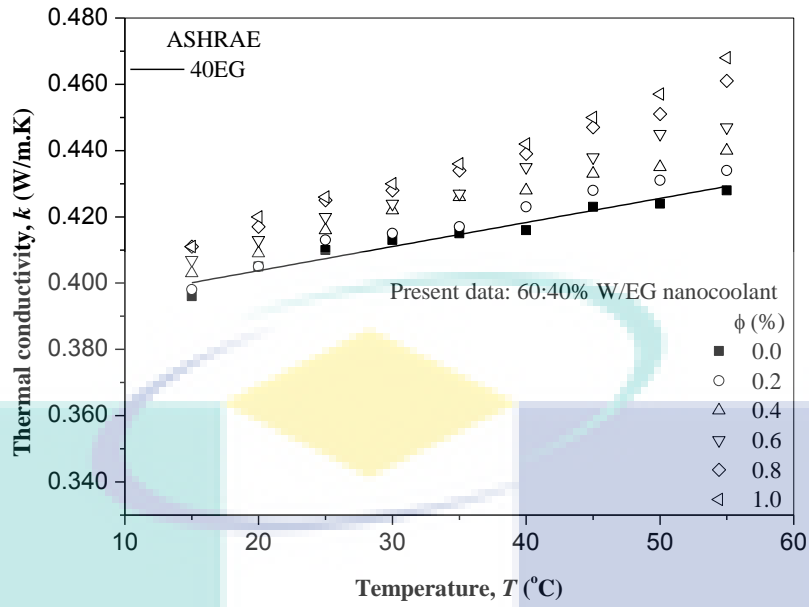


Figure 4.1 Variation of thermal conductivity enhancement as function of nanoparticles volume concentrations in W/EG mixture at 25 °C

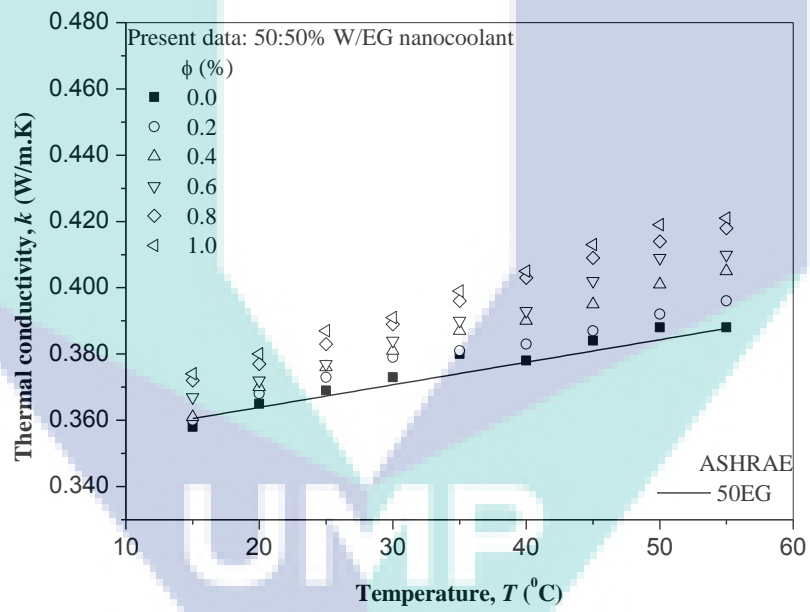
Figure 4.2 shows the thermal conductivity values of three different percentages of base fluids namely 60%:40%, 50%:50%, and 40%:60% water-EG (W/EG) and compared with the values obtained from the ASHRAE handbook (2006). The experimental values of all fluids exhibited $\pm 1.0\%$ deviation with handbook data in the measured temperature range. The nanocoolant with 0.2 to 1.0% volume concentrations were tested with the thermal conductivity instrument. Figure 4.2(a) represents the obtained data of 60%:40% (W/EG) nanocoolant with the data of the base fluid. The figure shows that the thermal conductivity of the nanocoolant increases when temperature and volume concentration are increased. The highest achievable thermal conductivity is $0.468 \text{ W}\cdot\text{m}^{-1}\cdot\text{K}^{-1}$ at 1.0% volume concentration and 55 °C. The thermal conductivity enhancement ratio of the nanocoolant is 1.1 times higher when compared with the base fluid under the same temperature.

Figure 4.2(b) shows the experimental thermal conductivity values of the 50%:50% (W/EG) base fluid. The thermal conductivity increases with the increase of volume concentration and temperature. The thermal conductivity of the nanocoolant with 1.0% volume concentration at 55 °C is $0.421 \text{ W}\cdot\text{m}^{-1}\cdot\text{K}^{-1}$. Thermal conductivity enhancement ratio is 1.07 times at 55 °C and 1.0% volume concentration compared with the base fluid. The experimental thermal conductivity data of 40%:60% (W/EG) base fluid nanocoolant is shown in Figure 4.2(c). A similar thermal conductivity of the nanocoolant trend with increased volume concentrations and temperature were obtained. Thermal conductivity enhancement ratio at 1.0% volume concentration of Al_2O_3 is 1.08 times compared with the base fluid at 55 °C. Experimental thermal conductivity value under the same temperature and same volume concentration of nanoparticles is $0.385 \text{ W}\cdot\text{m}^{-1}\cdot\text{K}^{-1}$. The pattern agrees well with the trend of thermal conductivity enhancement from earlier reported studies (Elias et al., 2014; Sundar et al., 2014; Azmi et al., 2016).

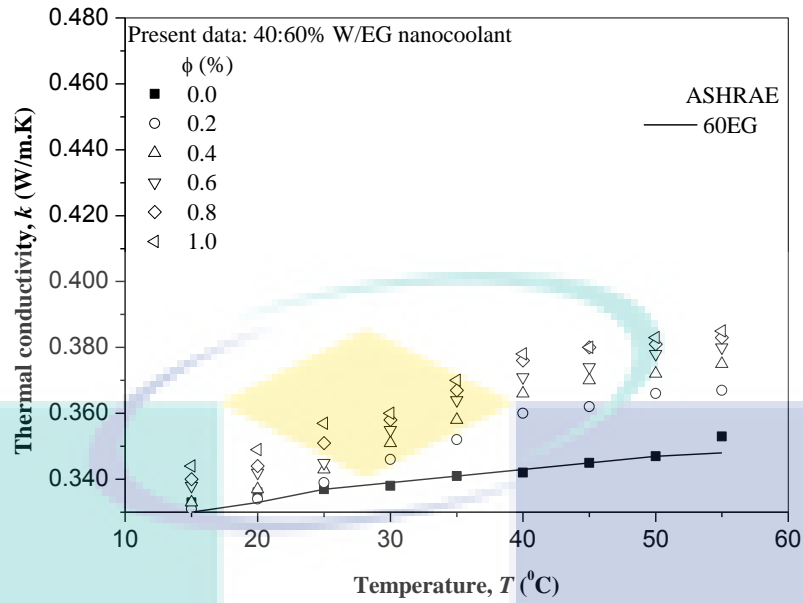
Thermal conductivity augmentation is due to the convection heat transfer of nanoparticles and Brownian motion in the base fluids. The thermal conductivity enhancement also depends on the effect of the base fluid (Azmi et al., 2016). The 60%:40% (W/EG) based nanocoolant has better enhancement of thermal conductivity compared with 50%:50% and 40%:60% (W/EG) based nanocoolants. Water is a better thermal conductivity fluid compared with ethylene glycol. A high percentage of ethylene glycol addition into water reduces the thermal conductivity of water to obtain less thermal conductivity value. The thermal conductivity of 60%:40% (W/EG) base fluid attained the highest experimental value of $0.410 \text{ W}\cdot\text{m}^{-1}\cdot\text{K}^{-1}$ at 25 °C. However, 50%:50% and 40%:60% (W/EG) base fluids are $0.369 \text{ W}\cdot\text{m}^{-1}\cdot\text{K}^{-1}$ and $0.337 \text{ W}\cdot\text{m}^{-1}\cdot\text{K}^{-1}$, respectively. Therefore, the thermal conductivity of the nanocoolant increases with the increase of temperature and volume concentration, but the increase depends on the base fluid. Moreover, the thermal conductivity enhancement of the Al_2O_3 nanocoolant is significant with more than 5% for the volume concentration of higher than 0.6%.



a) 60:40% (W/EG)



b) 50:50% (W/EG)



c) 40%:60% (W/EG)

Figure 4.2 Thermal conductivity of different nanoparticle concentrations for three different mixture of W/EG base fluids

4.2.2 Dynamic viscosity of nanocoolant

Dynamic viscosity of aluminium oxide, Al_2O_3 /water-EG (W/EG) mixture as nanocoolants for 0.2 to 1.0% volume concentrations and 25 °C has been presented in Figure 4.3. The figure shows that the nanocoolant dynamic viscosity increased exponentially with the increment of volume concentration. The models of Pak and Cho (1998); Wang et al. (1999); Sundar et al. (2012); and Batchelor (1977) were utilized to compare with the present data for different volume concentrations at 25 °C. The models of Wang et al. (1999); and Batchelor (1977) largely under predicted the nanocoolants dynamic viscosity. However, the model by Pak and Cho (1998) agrees with the experimental values of 50%:50% and 40%:60% (W/EG) based nanocoolants. The mean and maximum deviation of experimental values compared with that of Pak and Cho are 0.37% and 5.23% for 50%:50% (W/EG); and 0.76% and 7.6% for 40%:60% (W/EG), respectively. The experimental values of 60%:40% (W/EG) based nanocoolant had a similar trend as the dynamic viscosity model of Sundar et al. (2012). The mean and maximum deviation of the experimental values compared with that of Sundar et al. (2012) are 0.74% and 14.35%, respectively.

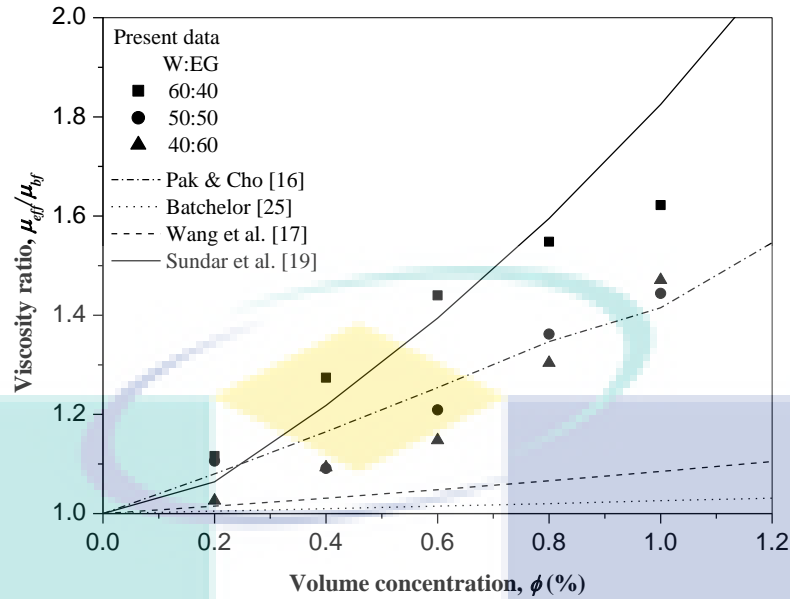


Figure 4.3 Variation of viscosity ratio as fraction of nanoparticle volume concentrations in W/EG mixture at 25 °C

Murshed et al. (2008) compared the experimental values of dynamic viscosity of Al_2O_3 /water based nanofluids with that of Wang et al. (1999). The results showed that their experimental values were higher than those of Wang et al. (1999) by 86% deviation. However, Aladag et al. (2012) used the Batchelor model to calculate the dynamic viscosity of CNT nanofluids. They found that the dynamic viscosity of CNT nanocoolant experimental values showed 26% deviation from the Batchelor (1977) model. Kole et al. (2010) studied the dynamic viscosity of Al_2O_3 in car engine coolant and compared their viscosity results with those of the Batchelor (1977); Brinkman (1952); and K-D model (Azmi et al., 2012). They found that the models failed to predict the measured dynamic viscosity of the nanocoolants. The measured dynamic viscosity values are unpredicted by the two models because of the difference in the size of the particle clusters and the differences in the dispersion techniques in the present study. The models of Wang et al. (1999) and Batchelor (1977) only considered volume concentration, but the nanoparticles can easily form clusters and experience surface adsorption in fluids. The relative dynamic viscosity is increased because the hydrodynamic diameter of nanoparticles increased by the clustering and adsorption of the nanoparticles.

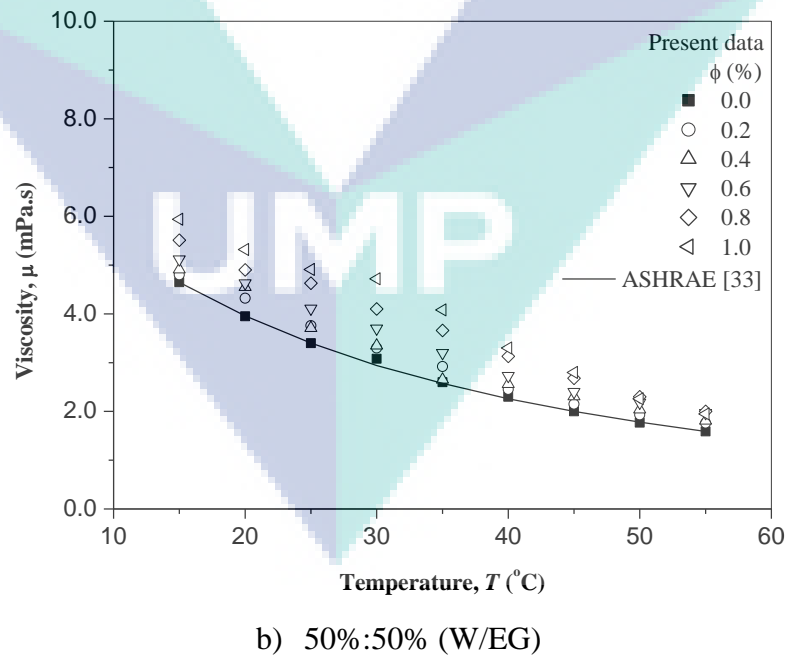
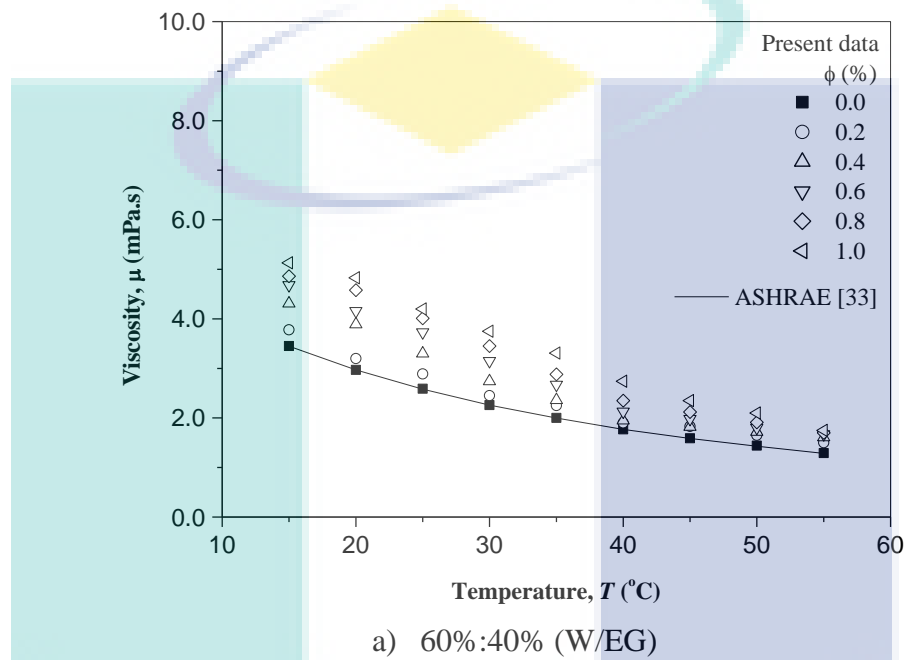
Figure 4.4 shows the dynamic viscosity values of three different mixtures of base fluids, such as 60%:40%, 50%:50%, and 40%:60% (W/EG) compared with the values

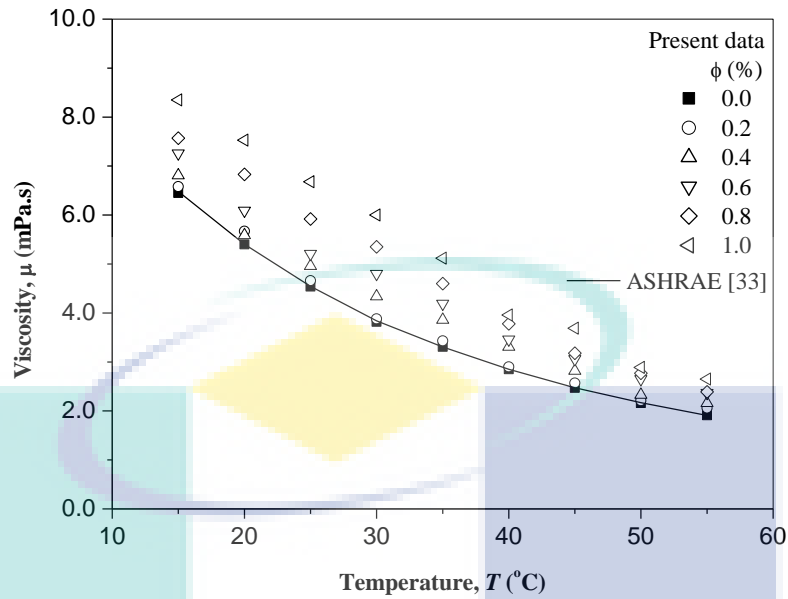
obtained from the ASHRAE handbook (2006). A maximum of $\pm 9.0\%$ deviation was observed between the measured values of all fluids and the handbook data in the experimental range. The nanocoolants were verified in terms of Newtonian or Bringham-like behaviour. Moreover, the shear stress and shear strain rate of all the nanocoolants were observed. The shear strain rate of all the nanoparticle base fluids constantly increased with the increment of shear stress. Thus, nanocoolants exhibit Newtonian behaviour in the experimental temperatures and volume concentrations. A similar experiment of Newtonian behaviour has been investigated by Kole and Dey (2010) with Al_2O_3 /engine oil nanocoolant, Aladag et al. (2012) by considering 50%:50% water mixture-based CNT nanocoolant and Namburu et al. (2007) with 40%:60% (W/EG) based CuO nanocoolant.

Figure 4.4(a) shows the experimental dynamic viscosity of Al_2O_3 nanocoolant and 60%:40% (W/EG) base fluid. The figure shows that the dynamic viscosity of nanocoolants decreases with the increase of temperatures, but the increment of volume concentrations increases the dynamic viscosity compared with the base fluid. At 1.0% volume concentration, the dynamic viscosity enhancement ratio is 1.35 times at 55 °C compared with that of the base fluid. The experimental dynamic viscosity value of 50%:50% (W/EG) nanocoolant is shown in Figure 4.4(b) along with the base fluid. The dynamic viscosity enhancement ratio for 1.0% volume concentration is 1.23 times at 55 °C compared with that of the base fluid. Figure 4.4(c) shows the experimental dynamic viscosity values of 40%:60% (W/EG) base fluid. The dynamic viscosity enhancement of the nanocoolant with 1.0% volume concentration at 55 °C is 1.39 times compared with that of the base fluid.

The enhancement of dynamic viscosity owing to the dispersion of nanoparticles in water-EG mixture based Al_2O_3 nanocoolant causes resistance between the fluid layers. Moreover, the present analysis for the dynamic viscosity of nanocoolant with the effect of base fluids shows that the 40%:60% (W/EG) based Al_2O_3 nanocoolant provides more viscosity than the 50%:50% and 60%:40% (W/EG) based Al_2O_3 nanocoolants in the measured volume concentrations and temperatures. The ASHRAE handbook (2006) also proves that the 40%:60% (W/EG) is more viscous than the 50%:50% and 60%:40% (W/EG) base fluids. Therefore, the high amount of ethylene glycol base fluid attains greater dynamic viscosity value compare with the low amount of ethylene glycol base

fluids. Sundar et al. (2014) detected the same behaviour of Al_2O_3 nanoparticles dispersed in water and ethylene glycol. Their data showed that the ethylene glycol based nanocoolants were higher dynamic viscosity than water based nanocoolants. The results in Figure 4.4(a)-(c) shows that the enhancement of dynamic viscosity is insignificant for volume concentrations of less than 0.4% using the Al_2O_3 /water-EG mixture nanocoolant.





c) 40%:60% (W/EG)

Figure 4.4 Viscosity of different nanoparticle concentrations for three different mixture of water-EG base fluids

4.2.3 Heat transfer coefficient of nanocoolant

The experimental data on thermal conductivity of the aluminium oxide, Al_2O_3 /water-EG mixture with volume concentration from 0.2 to 1.0% at three different base mixtures is shown in Figure 4.5. The figure indicated that thermal conductivity increased with the decrease of the percentage of ethylene glycol mixed as the base fluid. Similar patterns agreed well with the findings of Sundar et al. (2013), who conducted the suspension of Fe_3O_4 in ethylene glycol to water mixtures for three different mixture percentages and at higher temperature range. Azmi et al. (2013) analysed the condition that a nanocoolant does aid the improvement in heat transfer when the ratio of enhancement in dynamic viscosity to thermal conductivity compared to the base fluid which is lower than 4.0. The thermal physical properties evaluation in the present study concluded that with the use of Al_2O_3 nanocoolant in 60%:40% (W/EG) based fluid will maximize the enhancement of thermal conductivity and simultaneously minimize the dynamic viscosity increment of nanocoolant. Therefore, the 60%:40% (W/EG) nanocoolant properties are advantages for heat transfer application and were used in the

further evaluation of heat transfer coefficient for hot press forming (HPF) cooling application.

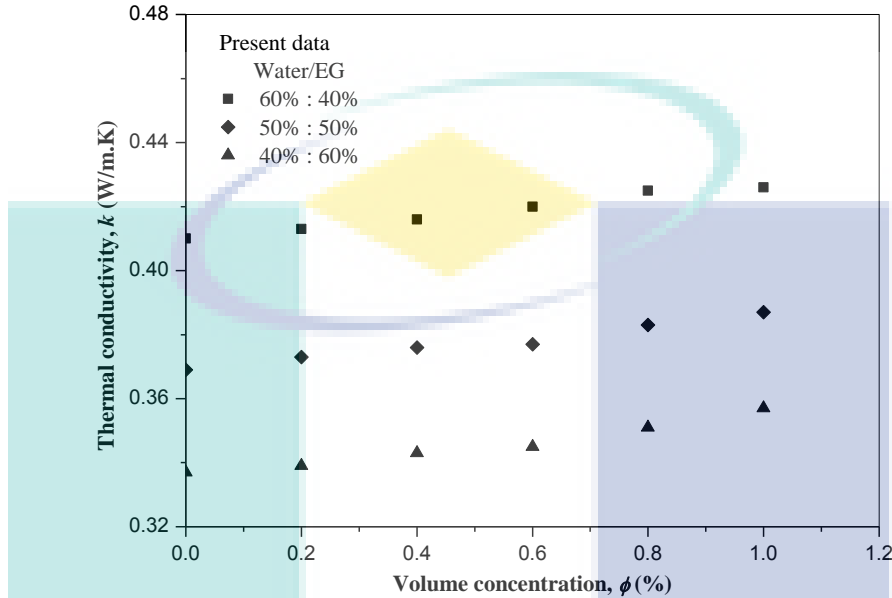


Figure 4.5 Relationship between thermal conductivity as function of nanoparticles volume concentration for three different mixture base fluids

Nusselt number of base fluid 60%:40% of water-EG mixture was estimated using equations of Lim et al. (2016). Chandrasekar et al. (2010); and Sereelakshmy et al. (2014) highlighted that larger Nusselt number caused the higher efficiency of convection process due to more suspended nanoparticles near the wall. Thus, Al_2O_3 nanocoolant in 60%:40% water-EG mixture base fluid could be implemented at volume concentration less than 1.0% and temperature of 25 °C for application in HPF die. The equation of Usri (2016) is used for the estimation of the Nusselt number of Al_2O_3 nanocoolants flow in a tube as shown in Equation 4.1. It is applicable for Al_2O_3 nanocoolants with the different base ratio (BR) of water-EG mixture at volume concentrations less than 1.0% and maximum temperatures of 70 °C. Further, the convective heat transfer coefficient is calculated from Equation 4.2.

$$Nu_{nf} = 0.025 Re_{nf}^{0.76} Pr_{nf}^{0.45} \times \left[(0.01 + BR)^{-0.1} \times \left(1 + \frac{T_{nf}}{70} \right)^{0.14} \right] \quad 4.1$$

$$h_{nf} = \frac{Nu_{nf} \times k_{nf}}{D} \quad 4.2$$

Prandtl number of nanocoolant is obtained from Equation 4.3, while, the Reynolds number is obtained from Equation 2.1 in Section 2.9.2 with the properties referred at the bulk temperature, T_b .

$$Pr_{nf} = \frac{C_{nf} \mu_{nf}}{k_{nf}} \quad 4.3$$

Thermal conductivity and dynamic viscosity for every concentration of Al_2O_3 nanocoolants were investigated initially in the present work. Whereas, the density and specific heat of nanocoolant are determined by the classical model solid-liquid relation as in Equation 4.4 and Equation 4.5, respectively.

$$\rho_{nf} = \left(\frac{\phi}{100}\right)\rho_p + \left(1 - \frac{\phi}{100}\right)\rho_{bf} \quad 4.4$$

$$C_{nf} = \frac{\left(1 - \frac{\phi}{100}\right)(\rho C)_{bf} + \left(\frac{\phi}{100}\right)(\rho C)_p}{\left(1 - \frac{\phi}{100}\right)\rho_{bf} + \left(\frac{\phi}{100}\right)\rho_p} \quad 4.5$$

The heat transfer coefficient of Al_2O_3 nanocoolant in 60%:40% (W:EG) at the temperature of 25 °C is higher compared to the base fluid as shown in Figure 4.6. At lower Reynolds number of 7,000, the heat transfer coefficient of the nanocoolant with 0.2% volume concentration is $4498.4 \text{ W}\cdot\text{m}^{-2}\cdot\text{K}^{-1}$ and it is enhanced by 2.9%. Besides, the heat transfer coefficient of 0.8% volume concentration is improved by 18.7% at the same Reynolds number compared to the base fluid. At higher Reynolds number of 20,000, the heat transfer enhancement of the nanocoolant at 0.2% and 0.8% volume concentrations are 4.0% and 24.9%, respectively. The convective heat transfer coefficient of 1.0% concentration in 60%:40% (W:EG) base fluid at 25 °C is enhanced by 25.4% better than that of 50%:50% and 40%:60% (W:EG) base fluid for Reynolds number of 20,000. Figure 4.6 describes that with the addition of nanoparticles to water-EG mixture base fluid will significantly improve the heat transfer coefficient of the nanocoolant. The

similar pattern was also found by Yu et al. (2012). They stated that the increment of heat transfer performance is due to the increase of the effective thermal conductivity of nanocoolant. Therefore, the use of nanocoolant for application in the cooling channel of HPF die is significant to increase its heat transfer performance.

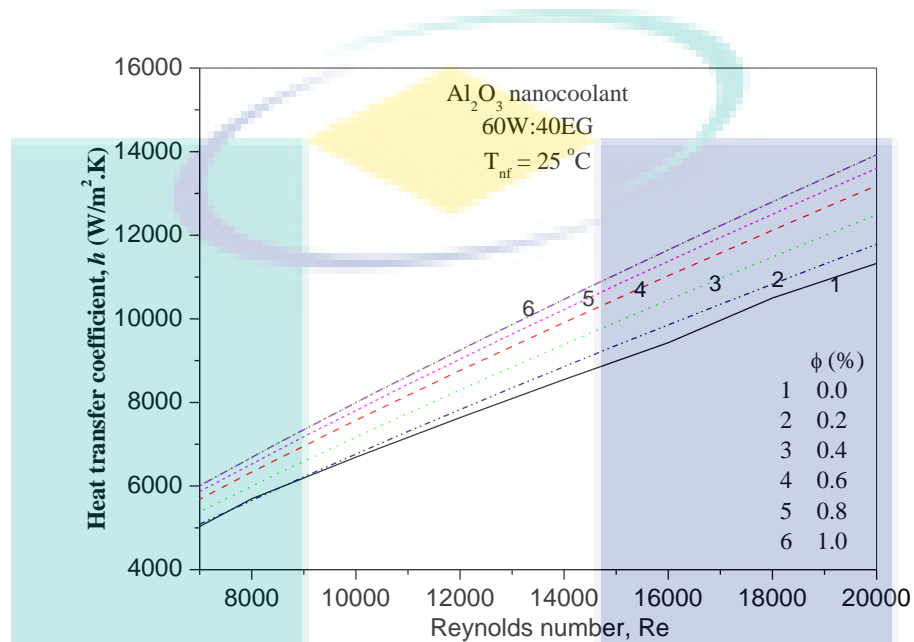


Figure 4.6 Distribution of heat transfer coefficient of 60%:40% water-EG mixture based Al_2O_3 nanocoolant

4.3 Thermal Analysis Results and Validation with Hat-Shaped Tools

The temperature value of the heated sheet metal and the hot press forming (HPF) dies were initially given as input to the ANSYS simulation software. The initial temperature of heated sheet metal was 900 °C during thermal analysis and the initial temperature for dies were 25 °C. Figure 4.7 depicts the steady state condition for HPF tool and hot blank sheet.

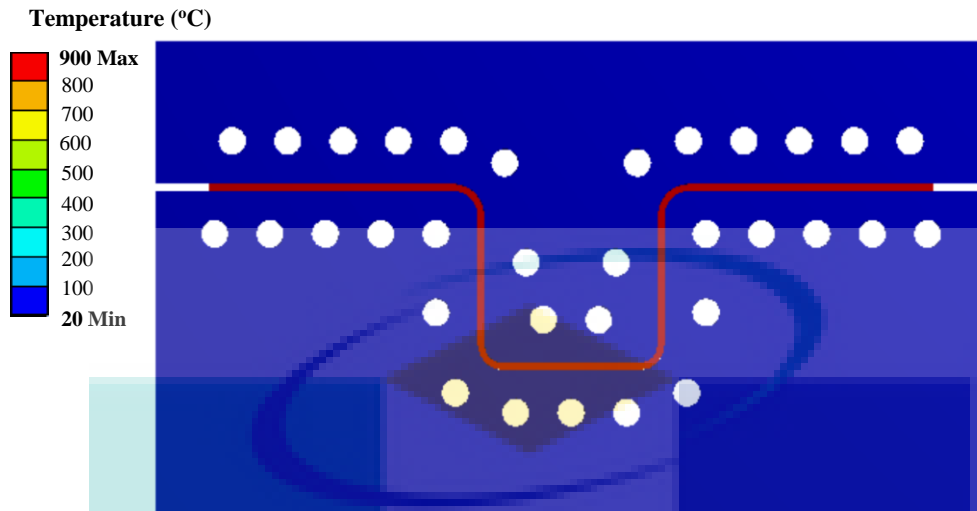
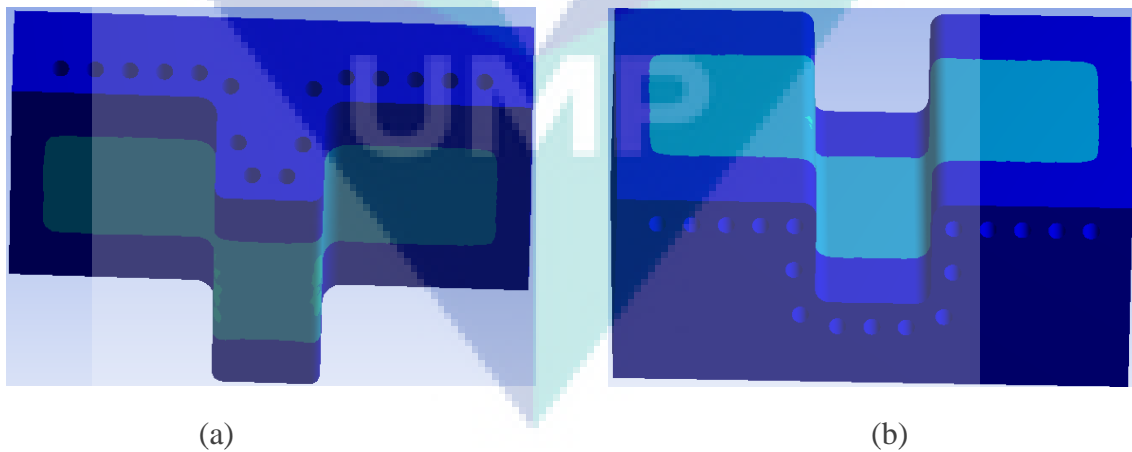


Figure 4.7 Thermal analysis at steady state condition for HPF simulation

The data of the temperature changed from HPF simulation was recorded in several periods of time such as 3 s, 5 s, 8 s and 10 s. Then, two different cooling fluids of nanocoolant and chilled water were compared during simulation and the cooling rate of the sample was attained to validate with the experimental results. The temperature distribution for the HPF sample was evaluated and the cooling rate was calculated based on the Equation 3.3 to 3.6 in Section 3.5.5. Figure 4.8 presents an example of temperature distribution for the cooling channel after 5 s of holding time.



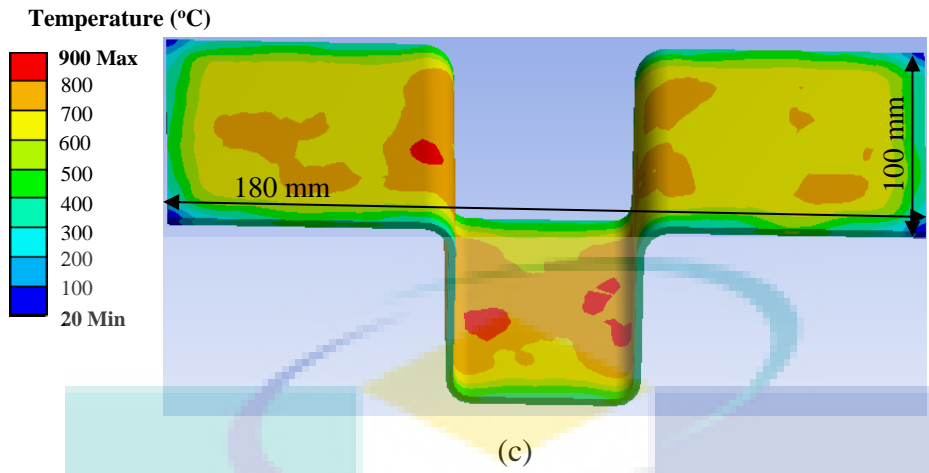


Figure 4.8 Transient thermal analysis for HPF simulation by introducing nanocoolant

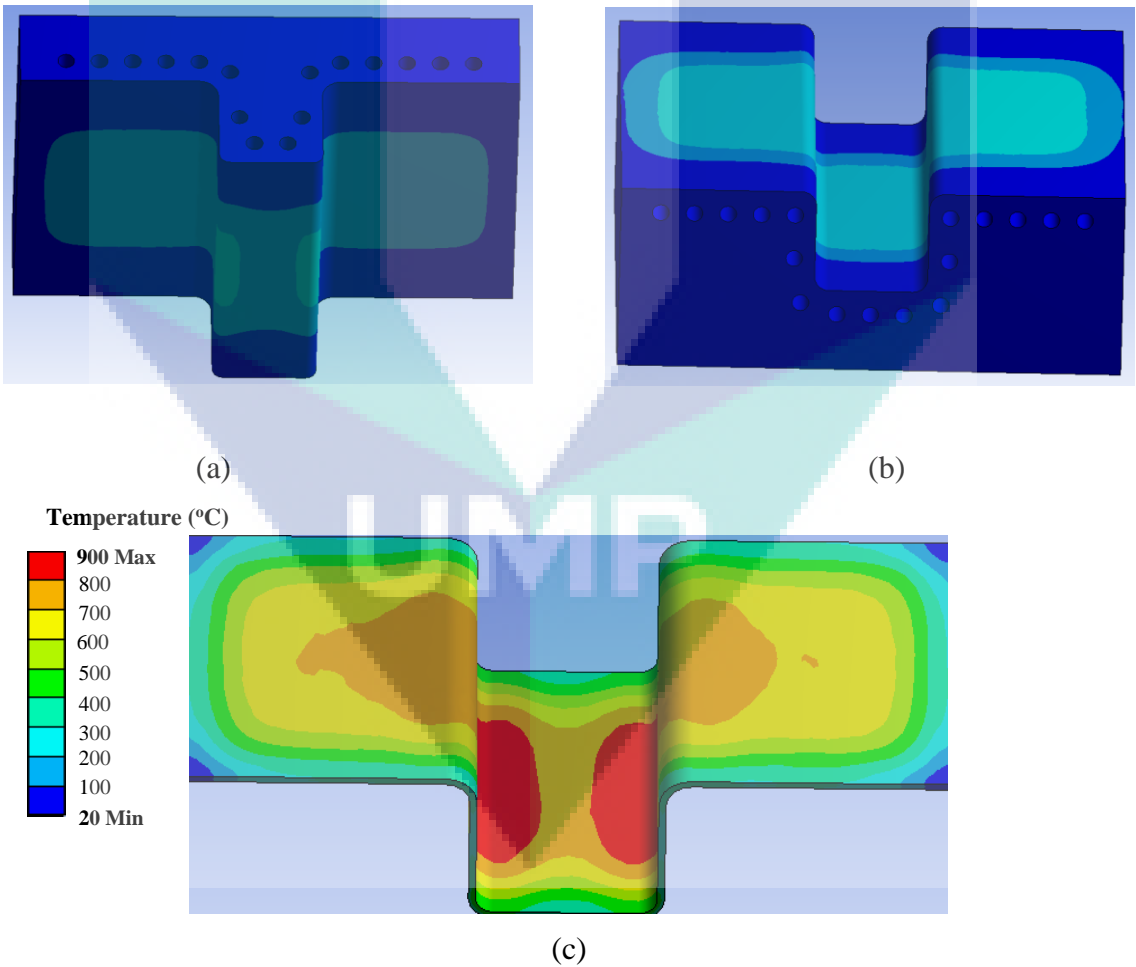


Figure 4.9 Transient thermal analysis for HPF simulation by introducing chilled water

4.3.1 Comparison of nanocoolant with chilled water in simulation

The thermal analysis simulation of hot press forming (HPF) process was conducted by introducing two different cooling agents such as nanocoolant and chilled water separately to compare the heat transfer distribution values. The materials mentioned in Section 3.5.1 and its thermal properties were applied for the finite element analysis (FEA). The temperature changed of the sheet metal blank and HPF dies during the process was measured by the FEA simulation and compared between nanocoolant and chilled water as tabulated in Table 4.1. The cooling rate of nanocoolant was slightly higher than chilled water in this simulation. However, both of the coolants have a similar cooling pattern for blank and tool to a certain extent. The pattern agrees well with the trend of cooling performance in HPF process studied by several researchers (Merklein et al., 2014; Karbasian and Tekkaya, 2010; Mori et al., 2015).

Table 4.1 Temperature distribution for HPF tools and heated blank

Time, (s)	Nanocoolant			Chilled Water		
	Upper die	Lower die	Blank	Upper die	Lower die	Blank
0.0	25.00	25.00	900.00	61.58	73.81	900.00
0.5	55.00	50.00	537.40	134.64	139.07	637.99
1.0	83.43	83.26	395.91	207.70	204.32	544.32
1.5	110.34	111.00	308.88	200.88	197.19	466.00
2.0	134.74	140.00	266.09	194.06	190.06	375.67
2.5	149.03	149.13	249.37	192.36	186.69	345.40
3.0	160.32	160.00	227.77	190.66	183.32	315.13
3.5	164.20	159.45	206.07	185.63	178.03	292.75
4.0	155.25	152.00	189.97	180.61	172.73	270.37
4.5	146.32	146.10	179.57	174.66	167.28	246.13
5.0	142.72	140.00	166.77	168.70	161.83	221.88
5.5	134.10	133.90	159.67	162.94	156.38	204.65
6.0	127.23	130.03	144.87	157.18	150.93	187.41
6.5	121.31	123.00	139.57	151.98	145.75	174.88
7.0	116.84	116.60	134.57	146.78	140.56	162.35
7.5	109.77	108.50	120.13	142.17	135.76	153.03
8.0	104.50	104.00	112.57	137.56	130.95	143.71
8.5	100.15	99.90	105.98	127.53	124.85	135.61
9.0	94.10	93.78	98.56	117.50	118.75	127.50
9.5	91.94	91.00	96.57	115.06	115.62	123.13
10.0	89.71	89.50	95.33	112.62	112.50	118.75

Figure 4.10 shows the mean and maximum enhancement of nanocoolants cooling rate value compared with the chilled water are 30.2% and 42.3%, respectively. Merklein et al. 2014 compared the three different types of the cooling agents such as pure air, water and atmospheric condition. The results showed that their experimental value obtained a 66.3% augmentation of cooling rate from atmospheric condition to pure air with the controlled air blowing system. Nanocoolants had optimum cooling rate because the convection heat transfer of nanoparticles and Brownian motion in the base fluids (Sundar et al., 2014; Lim et al., 2016). The thermal conductivity of nanocoolant enhancement also depends on the effect of the base fluid (Lim et al., 2016). Nevertheless, chilled water only exhibited convection heat transfer mechanism with the cooling rate around $50 \text{ K}\cdot\text{s}^{-1}$ (Karbasiyan and Tekkaya, 2010).

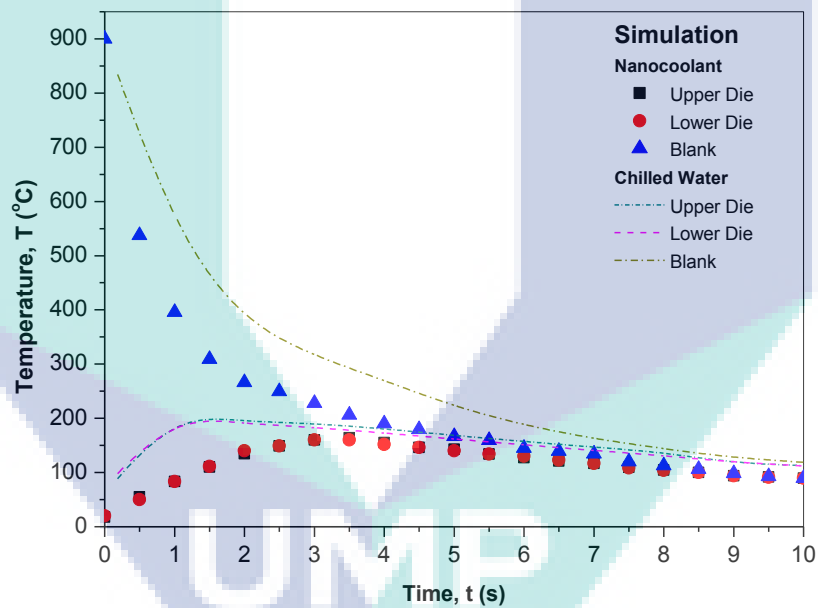


Figure 4.10 Heat transfer distribution between nanocoolant and chilled water for hat-shaped tool

4.3.2 Temperature validation of hot press forming with thermal analysis

As discussed in Sections 3.5.1 to 3.5.3 before that finite element analysis (FEA) simulation of the hot press forming (HPF) process were conducted by implementing all mentioned material and thermal properties. The temperature evolutions of the HPF dies and blank during the process were measured by experiments and computed by simulations; further both the values were compared and depicted as shown in Figure 4.11. The graph below showed the results of the temperature changed for tool and boron steel blank. The experimental results were validated with the temperature data of thermal analysis simulation for upper die, lower die and boron steel blank. The results of the experiments indicated that the heat transfer distribution trend was almost identical with FEA for tool and boron steel blank.

The average percentage errors of the heat transfer distribution between experimental results and FEA thermal analysis data were 7.50%, 3.62% and 8.82% for the HPF upper die, lower die and boron steel blank, respectively. In 2017, a researcher compared the heat transfer distribution of FEA simulation of the HPF process with experimental results to determine the percentage error values for upper die, lower die and sheet metal blank were 16.65%, 17.95% and 7.92%, respectively (Zamri, 2017; Namklang et al., 2016). The reason for deviation happened between FEA and experimental results were attributed to the longer time taken to transfer the heated blank to the hat-shaped tool and the greater time taken to close the hat-shaped tool. Wang and Lee, (2013) stated that the FEA results were affected if more than 10 s of the transferring time of heated blank to the hot forming die. During the HPF experiments, the upper die was opened space widely due to the punch stroke for the hat-shaped tool was 50 mm. As the speed of hydraulic press machine was slow, the austenite blank no longer at optimum temperature condition due to the reduction of temperature by air exposure. The results of the experimental HPF process and FEA simulation showed an acceptable agreement with Namklang et al. (2016), who had lower values of percentage error and similar pattern distribution.

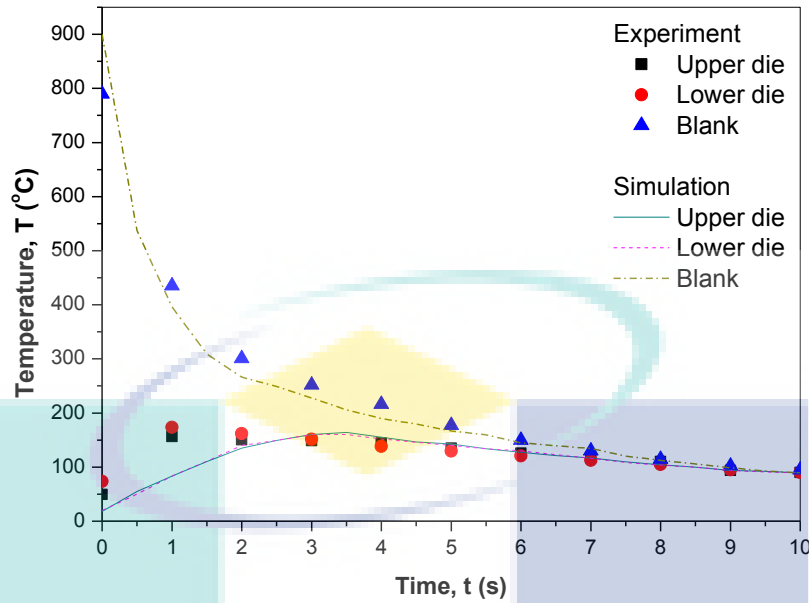


Figure 4.11 Comparison of heat transfer distribution between FEA and experiments for hat-shaped tool

4.4 Experimental Analysis of Hot Pressed Boron Steel

4.4.1 Microstructural transformation analysis

When the austenitization was applied on boron steel, higher temperature for homogenization was mandatory. Since the transformation was strongly dependent on the microstructure in terms of the chemical composition, the present phases and the grain size (Lolla et al., 2011). The micrographs of as-received and hot pressed boron steel blanks were tabulated according to the period of quenching time or holding time taken and types of cooling fluids as shown in Table 4.2. At 100X magnification, the as-received sample contained the mixture of pearlite phase and 73 to 77% ferrite and a small amount of carbide. Nuraini et al. (2013) stated that as-received boron steel exhibited pearlite phase located at ferrite grain boundaries. In this phase, ferrite-pearlite microstructure existed and brittle fracture in the sheet metal steel in the state (Frydman et al., 2012). For hot pressed samples at 100X magnification, they showed the martensitic microstructure and grain refinement occurred in the blank samples as shown in micrographs of the table below.

Table 4.2 Micrographs of boron steel blank with several quenching time periods

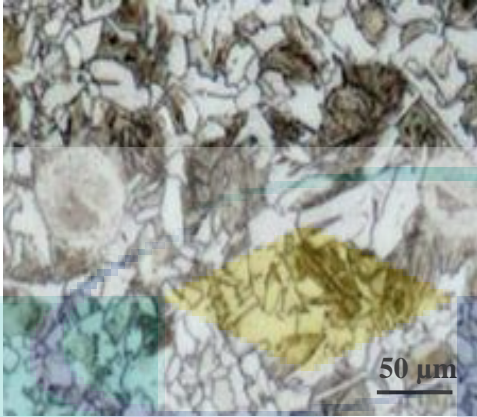
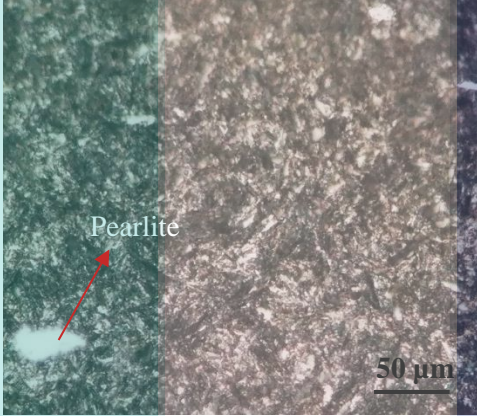

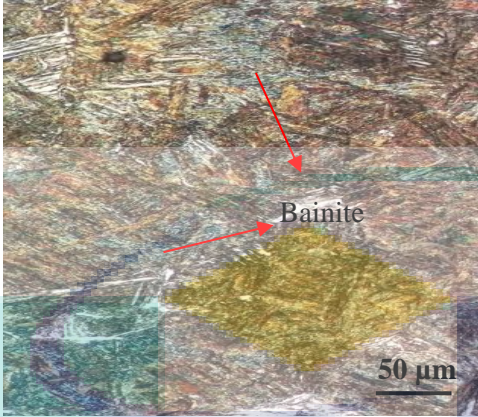
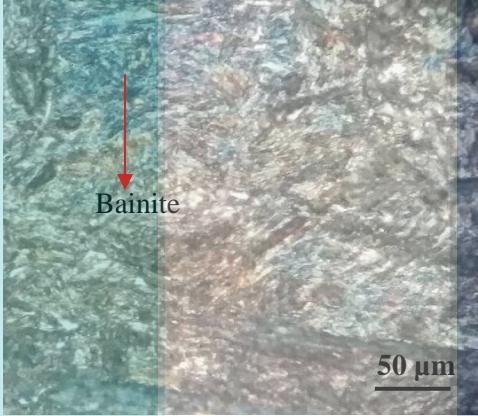
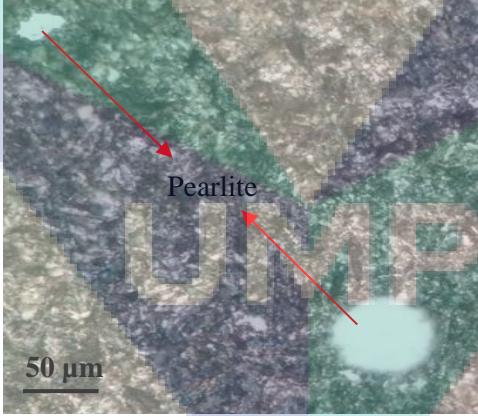
Cooling Fluid	Microstructure	Evaluation
As-delivery		Material : Boron steel Temperature : Ambient temperature Microstructure : Ferrite and Pearlite
Nanocoolant		Material : Boron steel Temperature : 900 °C Holding Time : 3 s Microstructure : Pearlite and Martensite
Nanocoolant		Material : Boron steel Temperature : 900 °C Holding Time : 5 s Microstructure : Martensite

Table 4.2 Continued

Cooling Fluid	Microstructure	Evaluation
Nanocoolant		Material : Boron steel Temperature : 900 °C Holding Time : 8 s Microstructure : Martensite and Bainite
Nanocoolant		Material : Boron steel Temperature : 900 °C Holding Time : 10 s Microstructure : Bainite and Martensite
Chilled Water		Material : Boron steel Temperature : 900 °C Holding Time : 10 s Microstructure : Pearlite and Martensite

After hot pressed and nanocoolant quenched for 3 s of holding time, the sample contained pearlite and martensitic microstructure. The pearlite content was around 2%, and the martensite content was approximately 90%. Srithananan et al. (2016) stated that brown colour represented martensitic phase after the image was taken to quantify the area fraction. The figure indicated that short holding time was insufficient to enable a martensitic transformation. Löbbeck et al. (2016) demonstrated an experiment to study the

first phase transformation of boron steel at each dwell time and cooling rate. They found that longer holding time and a cooling rate above the critical cooling rate of $45 \text{ K}\cdot\text{s}^{-1}$ were feasible to reach the martensite start and develop a martensitic microstructure, which was determined and agreed by Naderi et al. (2011).

In contrast to the 3 s of holding time, the sample of nanocoolant quenched for 5 s of quenching time contained a nearly total martensitic microstructure. The martensite content was more than 97% and only approximately 0.01% of bainite content in the transformation phase. The microstructure result showed that the nanocoolant with high cooling rate used was sufficient for 5 s quenching time to produce a fully martensitic microstructure with large needles shaped martensite were oriented in different angles and observed in almost every part of the sample, which suggested an increase of strength with sufficient cooling rate and holding times. This result was in accordance with Nikravesh et al. (2012) and L bbeck et al. (2016), who showed that higher cooling rate and sufficient or long holding times cause a reduction of the martensite start temperature. Sufficient quenching time led to a formation of martensite than a diffusion controlled formation of the cementite because of the increasing diffusion length (Naderi et al., 2011). This mechanism finally required a higher driving force for the martensite transformation, which was obtained at a lower temperature of hot forming tools with a cooling fluid of high convection heat transfer coefficient (L bbeck et al., 2016).

The phase transformation of hot pressed boron steel by 8 s and 10 s quenching period of time as shown in figures. The results presented that the microstructure exhibited a slight content of bainite microstructure, which blue colour represented bainitic phase (Sriathananan et al., 2016) after 8 s of quenching time. The martensite content was approximately 95%, while bainite content was around 3%. However, in 10 s quenching period of times, the hot pressed sample exhibited an increasing content of bainite microstructure. The bainite content was more than 15% and the martensite content decreased to only 74%. The reason for longer holding times promoted high bainitic fractions, because of the martensite transformations were impoverished of carbon so that a recombination of martensite was impeded (Bargel et al., 2012). L bbeck et al., (2016) stated that the higher temperature and longer holding time caused a grain growth of hot formed sample. Thus, the diffusion of carbon was reduced and fewer lattice defects were available for the nucleation of carbides so that the diffusionless transformation of ferrite

and bainite was favoured. Obviously, the amount of martensite significantly decreased when the applied quenching time was increased, while the amount of bainite increased in contrast.

Lastly, the cooling rate of chilled water was not sufficient to transform the hot pressed sample to a fully martensitic microstructure. Two phases of the pearlite and mixture of bainitic/martensitic microstructures obtained by lower cooling rate was anticipated. Nevertheless, with the realized higher cooling rate from the austenitization temperature in these heat treatments, ferrite and pearlite could be prevented (Bardelcik et al., 2014). After hot pressed and water quenched in 10 s period of holding time, the sample contained the mixture of pearlite phase and bainitic/martensitic microstructure. The pearlite content was around 5%, the bainite content was more than 40% and the martensite content was decreased to approximately 50%. L bbe et al., (2016) concluded that the reason for the cooling rate-dependent phase transformation was an inhomogeneous carbon distribution, so that a critical concentration allowed the diffusion control transformation. Hence, the critical cooling rate was the major controlling factor of martensite formation but rather increasing of short holding time and temperature.

4.4.2 Tensile strength analysis

The experimental results obtained from the tensile strength test was tabulated according to the periods of quenching time taken and types of cooling fluids as shown in Table 4.3. The graph reflected the data recorded in the table below were plotted accordingly as displayed in Figure 4.12. The figure shows the ultimate tensile strength of hot formed samples in two different cooling mediums such as nanocoolant and chilled water with several quenching durations.

Table 4.3 Tensile strength value for several specimens of hot formed boron steel

Cooling Fluids	Quenching Duration (s)	Ultimate Tensile Strength (MPa)		
		<i>Specimen 1</i>	<i>Specimen 2</i>	<i>Specimen 3</i>
Nanocoolant	3	1282.67	1340.46	1295.35
	5	1500.08	1521.93	1501.79
	8	1421.66	1419.84	1440.55
	10	1378.11	1396.21	1451.62
Chilled Water	10	1110.67	1030.55	1104.65
As-received	0	545.28	541.32	523.67

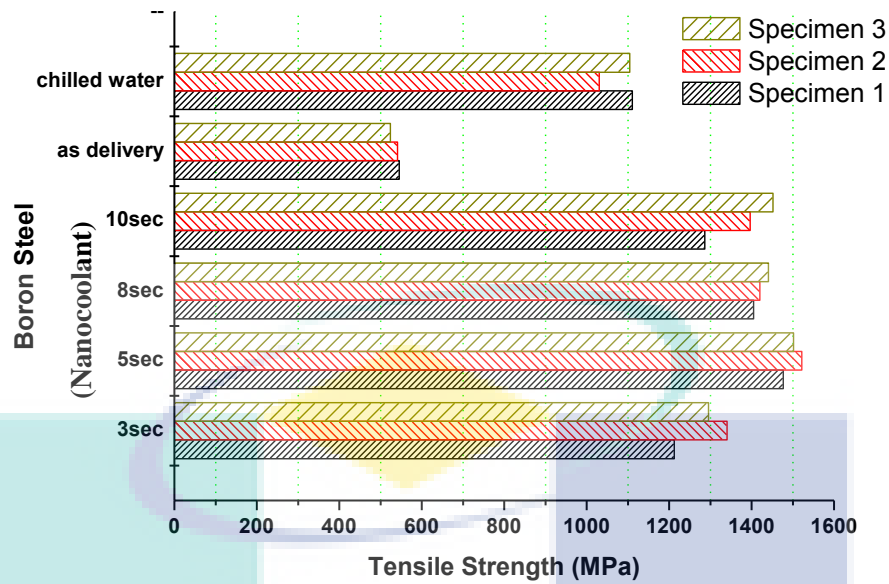


Figure 4.12 Ultimate tensile strength of blank samples at several cooling conditions

Since a nearly total martensitic microstructure was obtained at 5 s period of holding time with nanocoalant quenched, the maximum tensile strength 1,521.93 MPa was attained with higher convection heat transfer coefficient and cooling rate at sufficient period of holding time which was 5 s quenching duration. This effect was driven by the large martensitic needles oriented in different angles, which increased for higher convection heat transfer coefficient in order to increase the cooling rate and not more than 5 s holding duration. Bardelcik et al. (2010) experimentally investigated the effect of cooling rate on the high strain rate properties of boron steel and they proposed that the cooling rate was accelerated by increasing the convection heat transfer coefficient, more nucleation points were utilized and hence, a finer and disordered martensitic microstructure was formed. However, the tensile strength value of the boron steel was decreased gradually when increased the quenching time. According to L bbe et al. (2016) for setting mechanical properties of high strength steels in rapid hot forming processes, the ultimate tensile strength of boron steel was decreased gradually when the holding time increased. This phenomenon could be explained by the producing lath-shaped structure because a finer structure and grain boundaries impede dislocation motions.

The ultimate tensile strength of hot pressed boron steel with chilled water quenched was only 1,030.55 MPa. Since the micrograph of sample enforced a slight pearlite fraction and mixture phase of bainitic/martensitic microstructures. It was not only

the corresponding tensile strength which was unfavourably low but also the small uniform strain indicated a brittle microstructure (Löbbe et al., 2016). The comparison of the tensile strength of the hot pressed boron steel with nanocoolant quenched and the hot pressed boron steel with chilled water quenched and the as received boron steel before the quenching process. The tensile strength increased with the increasing of convection heat transfer coefficient in order to increase the cooling rate. The ultimate tensile strength enhancement ratio was 47.5% with nanocoolant quenched compared with the chilled water quenched of the hot pressed boron steel. Furthermore, the tensile strength of boron steel as received was only 545.28 MPa. The tensile strength of hot pressed boron steel with nanocoolant quenched had increased up to 179.1% enhancement when compared with the raw material.

According to Merklein et al. (2014), the value of tensile strength after quenching process was around 1,400 MPa due to the specimen showed an increase of the martensitic microstructure. Srithananan et al. (2016) experimental study the stress-strain and fracture behaviour of heat-treated boron steels for HPF process and they stated that stress-strain curves of the heat-treated boron steels were strongly influenced by the occurring microstructure constituents. The tensile strength of boron steel as received stage was low due to the bigger portions of ferrite phase microstructure were detected (Naderi et al., 2011). However, the ultimate tensile strength value variations of the investigated hot pressed specimens had been anticipated. Naderi et al. (2011) presented that a decreased in tensile strength value, because of the martensite volume fraction reduction. The martensitic phase microstructure due to its high hardness was brittle and low ductility. Moreover, Wang et al. (2013) conducted an investigation of the die quench properties of hot forming, and they found that if the transferring time of austenite boron steel to the hot forming tools more than 15 s could affect the strength of hot pressed boron steel around 400 MPa reduction. Therefore, in this research project, hot pressed boron steel with nanocoolant quenched in 5 s die holding duration would increase the ultimate tensile strength up to 2,000 MPa by using robotic arm transferred the austenite boron steel.

4.4.3 Hardness analysis of hot formed boron steel

The Vickers hardness results of the hot pressed boron steel in several periods of quenching time taken and types of cooling fluids were displayed in Table 4.4. The hardness values were measured by using Vickers method according to DIN EN ISO 6507-1 with the diamond shaped was produced on the surface of the sample as depicted in Figure 4.13. The graph reflected the data recorded in the table below were plotted accordingly as shown in Figure 4.14. The figure shows the hardness value of as-received boron steel and hot pressed samples in two different cooling fluids such as nanocoolant and chilled water.

Table 4.4 Hardness value for several specimens of hat-shaped boron steel

Cooling Mediums	Quenching Duration (s)	Vickers Hardness (HV1)		
		Specimen 1	Specimen 2	Specimen 3
Nanocoolant	3	491	421	436
	5	588	543	552
	8	579	526	520
	10	570	540	549
Chilled Water	10	567	578	509
As-received	0	105	106	105

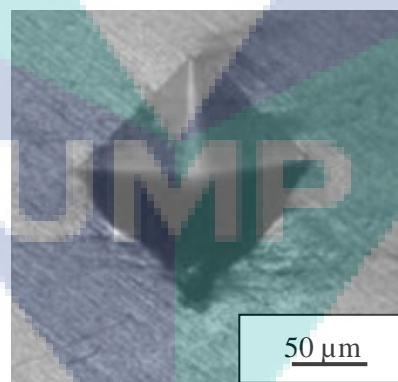


Figure 4.13 Vickers hardness reading HV1 with diamond shaped indent 50 μm

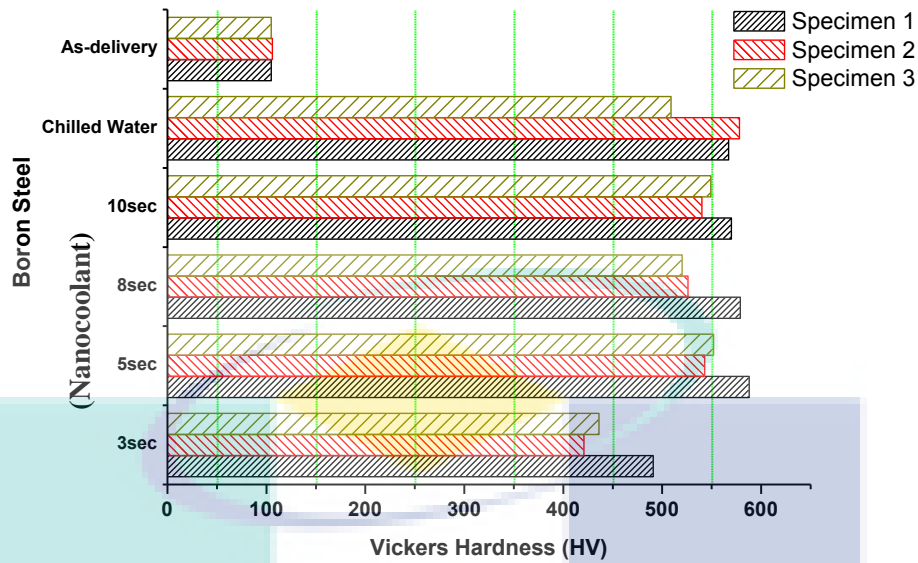


Figure 4.14 Hardness value of hot pressed samples at several cooling conditions

Hardness properties of the hot pressed boron steels as different quenching mediums and quenching duration were responding to micrograph as shown in Table 4.4. The highest Vickers hardness value of 588 HV1 was measured in nanocoolant with the quenching time period of 5 s. Note that the as-delivered boron steel had the average micro-hardness of 105 HV1. The quenching in the nanocoolant led to significant increase in ratio of 4.6 times in hardness of the sample due to the presence of large martensitic needles structure in the entire region (Namklang et al., 2016). The martensitic structure would lead to an elevated strength of the boron steel due to an increase in dislocation impedances (Bardelcik et al., 2010 & Wang et al., 2013).

The hot pressed samples with the presence of bainitic microstructure phase exhibited a marginal increase in the hardness value. The lowest hardness was only 421 HV1 among these samples, when hot pressed in chilled water and long period of quenching time. Eller et al. (2014) highlighted that as the hardness value was higher than 470 HV or 47.5 HRC, then it could be identified as a resulting of martensitic microstructure phase. As the hardness value was below 450 HV, then it could be related to ferrite/pearlite mixed phase, and it was expected that some pearlite zone had been formed in the microstructure of hot pressed sample with 3 s quenching time period. It was in agreement with the results presented in Table 4.4. Merklein et al. (2014) found that the hardness value of hot pressed part was around 514 HV. Naderi et al. (2011) obtained the highest hardness value of approximately 600 HV in their sample of steel-A

with different carbon contents. Namklang et al. (2016) produced the hot pressed part with Vickers hardness value of 550 HV in the bottom area region. Since, the hardness value obtained was higher compared to the normal trend, the results were acceptable.

4.5 Summary

The thermal conductivity and dynamic viscosity of aluminium oxide, Al_2O_3 /water-EG mixture nanocoolants were investigated. The results show that thermal conductivity increases with the increment of volume concentrations and temperature. However, the thermal conductivity of nanocoolant decreases with the increase of ethylene glycol percentage in the base fluid. Temperature and volume concentration contribute significant effects on the effective thermal conductivity of nanocoolants. The experimental analysis found that dynamic viscosity of nanocoolants increases with the increment of volume concentration. However, the dynamic viscosity of nanocoolants decreases with the increase of temperature.

The dynamic viscosity enhancement was investigated to be greater than the enhancement of thermal conductivity. The highest dynamic viscosity enhancement increased by 39% compared to the base fluid. However, the highest thermal conductivity enhancement increased by 10% compared with the base fluid. At 1.0% volume concentration, the heat transfer enhancement is 25.4% estimated for the nanocoolant bulk temperature of 25 °C. Therefore, finding the ideal volume concentration of Al_2O_3 /water-EG mixture nanocoolant is very important to increase the productivity of hot press forming (HPF) processes. The use of Al_2O_3 /water-EG mixture nanocoolants of 60%:40% (W/EG) with the volume concentration of less than 1.0% is recommended for application in the cooling system of HPF process.

In FEA simulation, the medium sized mesh was utilized in the hot forming tool as it provided reasonable accuracy with a bearable computational burden. Moreover, by choosing a refined mesh which focused on the cooling channel, it resulted in higher quality of FEA. In this study, thermal analysis was able to measure the heat transfer distribution of the austenite blank and hot pressed tool by introducing nanocoolant and chilled water into the cooling channel system. In order to validate the simulation data

with the experimental results, the temperature distribution was evaluated and compared. Based on the hat-shaped tool, the average percentage error for the upper die, lower die and austenite blank were 7.50%, 3.62% and 6.47%, respectively. The results attained demonstrate an acceptable agreement with Namklang et al. (2016), between the experimental and FEA simulation data.

The metallographic studies of the hot pressed parts were performed by using Light Optical Microscope (LOM) machine with Progress Capture 28.8 Jenoptik Optical System Image Analyser software. The microstructure transformation of the hot pressed part with 5 s quenching period of time by using nanocoolant exhibited nearly total martensitic phase. Therefore, the value of the tensile strength and Vickers hardness were also measured. The tensile strength of the final part was observed to increase up to 47.5% with nanocoolant quenched compared with the chilled water, and approximately 179.1% enhancement in tensile strength when compared with the as-received boron steel. The enhancement ratio of hardness was about 4.6 times for the hot pressed part compared with the initial condition of boron steel. As a concluding remark, it was apparent that the nanocoolant which obtained higher heat transfer coefficient in order to produce higher cooling rate compared with chilled water were able to achieve better mechanical properties such as tensile strength and hardness values of the output sample.



UMP

CHAPTER 5

CONCLUSION

5.1 Conclusion

The overall objectives of the research project were achieved in which the potential of the selected aluminium oxide, Al_2O_3 nanoparticles suspended in aqueous ethylene glycol solution of base fluid has been investigated through a series of methods and analyses. The three research objectives were achieved through three different stages of experiments and summarised into three different paragraphs.

The analyses in the first stage of the experiment were conducted to fulfil the objective one. From this first stage of the experiment, the nanocoolants produced from nanoparticles of Al_2O_3 was uniformly dispersed in water-EG mixture could sustain in sedimentation evaluation after being synthesized by using the ultrasonic hot-air machine. Besides that, increasing of nanoparticle concentrations and a reduction of ethylene glycol base fluids was proven to enhance thermal conductivity property in order to increase the convection heat transfer coefficient value. The enhancement of heat transfer coefficient could attain 66.2% compared with chilled water as a cooling agent in the HPF process at the bulk temperature condition of 25 °C. Also, the results showed that the several volume fractions of Al_2O_3 nanoparticles and different concentrations of ethylene glycol as base fluids owned their respective enhancement and weaknesses of convection heat transfer for application in the cooling system of HPF process. Therefore, finding the ideal volume fraction of Al_2O_3 base water-EG mixture nanocoolant is important to increase the productivity of HPF processes. The use of Al_2O_3 /water-EG mixture nanocoolant of 60%:40% (W/EG) with a volume concentration of 0.8% is recommended as cooling nanofluids for application in HPF process.

Through the second stage of simulation analysis, the second objective was achieved. Thermal analysis in the HPF process of heat transfer distribution for the upper tool, lower tool and heated blank were conducted at the optimum mesh quality, with refinement control meshed and suitable medium size of meshing decided from the simulation analysis which was done previously. The temperature changed of hat-shaped tools and heated blank were analysed with respect to the several periods of quenching time by using heat transfer coefficient values of the nanocoolants and chilled water. It was found that the results obtained at this stage corresponded well with those stated in the literature and hypothesis in which nanocoolants of Al_2O_3 base fluid could help to rapidly reduce the temperature of tools and heated sheet metal blank by improving the convection heat transfer coefficient value to increase the cooling rate. Also, the optimum quenching time and heat transfer enhancement of nanocoolant compared with chilled water were collected from the analysis. As for the validation of simulation data with experimental results, the percentage deviations of heat distribution for the upper tool, lower tool and heated blank were able to fulfil the requirements and agreed with the experimental hat-shaped and FEA simulation results.

The analyses in the final stage of the experiment were conducted to achieve objective three. From this final stage of the experiment, the tensile strength of test specimens produced from three different locations such as flange, wall and bottom of the austenite boron steel blank after being manufactured from wire cut machine. Moreover, the specimen was cut into a small piece of samples after the tensile strength test had been performed. The samples were mounted for Vickers hardness measurement after the grinding and polishing operations had been performed for the samples. Also, the microstructure analysis of the samples was conducted to evaluate the result of heated boron steel from austenite phase transformed to fully martensitic behaviour. The result showed that the mechanical properties of hot pressed boron steel were improved by introducing nanocoolant compared with chilled water to a certain extent. The nanocoolant as a cooling agent for HPF experiment obtained fully martensitic microstructure of boron steel and thus contributing to the higher tensile strength and Vickers hardness value compared with boron steel as received condition. Chilled water for HPF experiment, on the other hand, showed the pearlite microstructure transformation due to the lower convection heat transfer value and cooling rate. Therefore, the tensile strength of hot formed boron steel was able to fulfil the minimum requirement of HPF value with 1,400

MPa, but the hardness value was still in acceptance limit which was above 470 HV. In addition, the strength of boron steel from nanocoolants was evaluated to increase up to 190.90% after the quenching operation, while the hardness was approximately enhanced 414.28% from the as delivered condition. As compared with chilled water, the tensile strength was approximately improved 47.5%, but the Vickers hardness value was reminded satisfactory limit rate as hot formed part. The value of the tensile strength measured would be slightly higher than 1,600MPa from the usual trend. This was mainly due to the longer transfer time of the blank product from the furnace to the hydraulic press machine, in addition to the waiting time for the machine to press the heated boron steel.

5.2 Contributions to Knowledge

The significant contributions of this research study were to synthesise the nanocoolants as alternative cooling fluid for hot press forming (HPF) applications and optimised the cooling system to develop a high productivity HPF system for automotive industry market in ASEAN region countries. In addition to the nanocoolants application, this research also studied the heat transfer distribution in order to optimise the power consumption by the chiller. The mechanical properties enhancement of hot pressed parts was investigated and analysed in order to introduce to the commercial car chassis. This summarises the four original contributions of this research project which are as follows:

- The effect of several concentrations of nanocoolant on the convection heat transfer coefficient with optimization the thermal physical properties in terms of thermal conductivity and dynamic viscosity had been analysed and consequently, the augmentation of heat transfer coefficient value and optimum concentration of nanocoolant could be selected.
- The investigation of thermal analysis on the HPF process by introducing nanocoolant and chilled water as cooling fluids through finite element analysis (FEA) simulation had been computed and evaluated. The simulation data would be collected and validated by the experimental results of the hat-shaped tool.

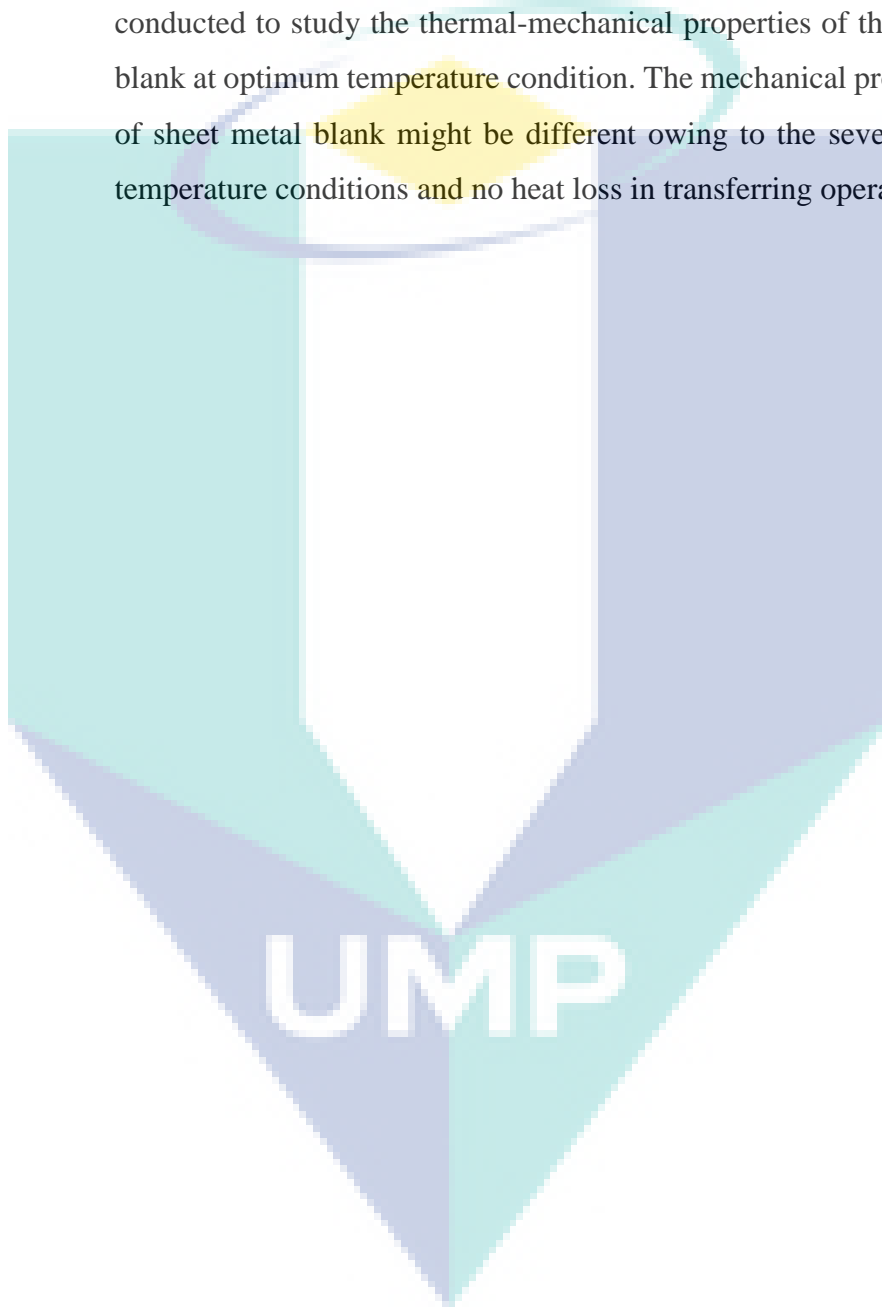
- The effect of nanocoolants and chilled water for the hot pressed part on the mechanical properties in terms of tensile strength and Vickers hardness; and microstructure transformation of several periods of quenching time.
- The successful study of this research could lead to better understanding and optimized the HPF process. The knowledge and data defined for the characteristic of ultra-high strength steel (UHSS) and nanocoolants could be widely used to gain its best performance in the hot forming operation, improved cycle time of production and die life duration.

5.3 Future Works

Several suggestions are proposed as follows for future work:

- 1) Similar methodologies adopted in this research could be referred and applied for the optimization design of cooling channels. Due to the availability of advanced engineering methods such as Heuristic method, Taguchi method or Neural Networks, the cooling rate of hot press forming (HPF) tools and austenite boron steel blank might be increased during the quenching process. Therefore, the research could be conducted to study the optimization of cooling channel design for the HPF tool process. The results might be improved with nanocoolants compared to the conventional process.
- 2) The automated robotic arm replaced the manually transfer method to transfer the heated blank from the heating furnace to the HPF tools. This robotic arm could be used to reduce the temperature of heated blank lost through atmosphere condition by rapidly transferring the heated blank. Instead of the very slow press speed of hydraulic press machine, this might result in a cooler blank before the quenching operation transpires.

- 3) In order to ensure a sustainable and continuous production of hot formed parts, the directly HPF method could be conducted to eliminate the transfer time of the heated blank. In this process, the blank was formed and hardened in one mold which saved the cost of preforming and accelerated the pace of production. Therefore, research could be conducted to study the thermal-mechanical properties of the sheet metal blank at optimum temperature condition. The mechanical property results of sheet metal blank might be different owing to the several austenitic temperature conditions and no heat loss in transferring operation.



REFERENCES

- Abbassi, Y., Talebi, M., Shirani, A. S. and Khorsandi, J. (2014). Experimental investigation of TiO₂/water nanofluid effects on heat transfer characteristics of a vertical annulus with non-uniform heat flux in non-radiation environment. *Annals of Nuclear Energy*, 69, 7-13.
- Abdul-Hay, B., Bourouga, B. and Dessain, C. (2010). Thermal contact resistance estimation at the blank/tool interface: experimental approach to simulate the blank cooling during the hot stamping process. *International Journal of Material Forming*, 3(3), 147–163.
- Akhavan-Behabadi, M., Hekmatipour, F., Mirhabibi, S. and Sajadi, B. (2015). Experimental investigation of thermal–rheological properties and heat transfer behaviour of the heat transfer oil–copper oxide (HTO–CuO) nanofluid in smooth tubes. *Experimental Thermal and Fluid Science*, 68, 681-688.
- Altan, T. and Tekkaya, A. E. (2012). *Sheet Metal Forming Processes and Application*. New York: ASM International, 133–156.
- Amiri, A., Shanbedi, M., Yarmand, H., Arzani, H. K., Gharehkhani, S., Montazer, E., Sadri, R., Sarsam, W., Chew, B.T. and Kazi, S.N. (2015). Laminar convective heat transfer of hexylamine-treated MWCNTs-based turbine oil nanofluid. *Energy Conversion and Management*, 105, 355-367.
- Anoop, K., Sadr, R., Yu, J., Kang, S., Jeon, S. and Banerjee, D. (2012). Experimental study of forced convective heat transfer of nanofluids in a microchannel. *International Communications in Heat and Mass Transfer*, 39 (9), 1325-1330.
- Ansari, M. S., Shukla, S. and Awasthi, S. (2014). A review on nano fluid: Synthesis characterization and application. *Journal of Basic and Applied Engineering Research*, 1, 23-38.
- ANSYS. (2016). ANSYS Meshing. Retrieved from <http://www.ansys.com/products/platform/ansys-meshing> (11 JUNE 2017)
- Arani, A. A. and Amani, J. (2012). Experimental study on the effect of TiO₂–water nanofluid on heat transfer and pressure drop. *Experimental Thermal and Fluid Science*, 42, 107-115.

- Arulprakasajothi, M., Elangovan, K., Reddy, K.H. and Suresh, S. (2015b). Heat transfer study of water-based nanofluids containing titanium oxide nanoparticles. *Materials Today: Proceedings*, 2 (4), 3648-3655.
- ASHRAE. (2009). *ASHRAE Handbook - Fundamentals (SI Edition)*. Atlanta, GA: American Society of Heating, Refrigerating and Air-Conditioning Engineers, Inc.
- Azmi, W. H., Sharma, K. V., Mamat, R., Alias, A. B. S. and Izwan Misnon, I. (2012). Correlations for thermal conductivity and viscosity of water based nanofluids *IOP Conf. Series: Materials Science and Engineering*, 36, 1 - 6.
- Azmi, W. H., Sharma, K. V., Mamat, R., Najafi, G. and Mohamad, M. S. (2016). The enhancement of effective thermal conductivity and effective dynamic viscosity of nanofluids - A review. *Renewable and Sustainable Energy Reviews*, 53, 1046-1058.
- Azmi, W. H., Sharma, K. V., Sarma, P. K., Mamat, R. and Anuar, S. (2014). Comparison of convective heat transfer coefficient and friction factor of TiO₂ nanofluid flow in a tube with twisted tape inserts. *International Journal of Thermal Sciences*, 81(0), 84-93.
- Azmi, W. H., Sharma, K. V., Sarma, P. K., Mamat, R., Anuar, S. and Dharma Rao, V. (2013). Experimental determination of turbulent forced convection heat transfer and friction factor with SiO₂ nanofluid. *Experimental Thermal and Fluid Science*, 51 (0), 103-111.
- Banabic, D. (2010). *Sheet Metal Forming Processes*. 1st Edition. London: Springer.
- Bardelcik, A., Worswick, M. J., Winkler, S., and Wells, M. A. (2012). A strain rate sensitive constitutive model for quenched boron steel with tailored properties. *International Journal of Impact Engineering*, 50, 49-62.
- Bardelcik, A., Worswick, M. J., and Wells, M. A. (2014). The influence of martensite, bainite and ferrite on the as-quenched constitutive response of simultaneously quenched and deformed boron steel – Experiments and model, *Journal of Materials and Design*, 55, 509–525.
- Bayat, J. and Nikseresht, A. H. (2012). Thermal performance and pressure drop analysis of nanofluids in turbulent forced convective flows. *International Journal of Thermal Sciences*, 60, 236-243.

- Beck, M., Yuan, Y., Warriar, P. and Teja, A. (2010). The thermal conductivity of alumina nanofluids in water, ethylene glycol, and ethylene glycol + water mixtures. *Journal of Nanoparticle Research*, 12 (4), 1469-1477.
- Bhanvase, B. A., Sarode, M. R., Putterwar, L. A., K. A, A., Deosarkar, M. P. and Sonawane, S. H. (2014). Intensification of convective heat transfer in water/ethylene glycol based nanofluids containing TiO₂ nanoparticles. *Chemical Engineering and Processing: Process Intensification*, 82, 123-131.
- Bianco, V., Manca, O. and Nardini, S. (2014). Performance analysis of turbulent convection heat transfer of Al₂O₃ water-nanofluid in circular tubes at constant wall temperature. *Energy*, 77, 403-413.
- Boljanovic, V. and Paquin, J. (2006). *Die Design Fundamental*. 3rd Edition. Pennsylvania State University: Industrial Press
- Bolz, R. E. and Tuve, G. L. (2007). *Handbook of Tables for Applied Engineering Science*. 2nd Edition. Boca Raton: CRC press.
- Bosetti, P., Bruschi, S., Stoehr, T., Lechler, J., and Merklein, M. (2010). Interlaboratory comparison for heat transfer coefficient identification in hot stamping of high strength steels. *International Journal of Material Forming*, 3(S1), 817–820.
- Cabaleiro, D., Gracia-Fernández, C., Legido, J. and Lugo, L. (2015). Specific heat of metal oxide nanofluids at high concentrations for heat transfer. *International Journal of Heat and Mass Transfer*, 88, 872-879.
- Cengel, Y. A. and Ghajar, A. J. (2011). *Heat and Mass Transfer: In Fundamental and Application*, 4th Edition. New York: MacGraw Hill, pp. 9-16,25-28,423-426,488,489.
- Cengel, Y. A. (2010). *Fluid Mechanics*. 2nd Edition. New York: MacGraw Hill.
- Chandra Sekhara Reddy, M. and Vasudeva Rao, V. (2014). Experimental investigation of heat transfer coefficient and friction factor of ethylene glycol water based TiO₂ nanofluid in double pipe heat exchanger with and without helical coil inserts. *International Communications in Heat and Mass Transfer*, 50, 68-76.
- Chandrasekar, M., Suresh, S. and Bose, A. C. (2010a). Experimental investigations and theoretical determination of thermal conductivity and viscosity of Al₂O₃/water nanofluid. *Experimental Thermal and Fluid Science*, 34 (2), 210-216.

- Chandrasekar, M., Suresh, S. and Chandra Bose, A. (2010b). Experimental studies on heat transfer and friction factor characteristics of Al₂O₃/water nanofluid in a circular pipe under laminar flow with wire coil inserts. *Experimental Thermal and Fluid Science*, 34 (2), 122-130.
- Chang, Y., Meng, Z. H., Ying, L., Li, X. D., Ma, N. and Hu, P. (2011). Influence of hot press forming techniques on properties of vehicle high strength steels. *Journal of Iron and Steel Research International*, 18(5), 59–63.
- Choi, S. U. S., Zhang, Z. G. and Keblinski, P. (2004). (Nanofluids). In: Nalwa, S. H. (ed.) *Encyclopedia of Nanoscience and Nanotechnology*. New York: Scientific Publishers.
- Chun, S. Y., Bang, I. C., Choo, Y. J. and Song, C. H. (2011). Heat transfer characteristics of Si and SiC nanofluids during a rapid quenching and nanoparticles deposition effects. *International Journal of Heat and Mass Transfer*, 54 (5-6), 1217-1223.
- Cui, J., Sun, G., Xu, J., Huang, X. and Li, G. (2015). A method to evaluate the formability of high-strength steel in hot stamping. *Materials and Design*, 77, 95–109.
- Decagon Devices, I. (2014). *KD2 Pro Thermal Properties Analyzer Operator's Manual*. Pullman WA: Decagon Devices, Inc.
- Denkena, B., Helmecke, P. and Hülsemeyer, L. (2014). Energy Efficient Machining with Optimized Coolant Lubrication Flow Rates. *Procedia CIRP*, 24 (0), 25-31.
- Efevbokhan, V. E. and Ohiozua, O. N. (2013). Comparison of the cooling effects of a locally formulated car radiator coolant with water and a commercial coolant. *The International Journal Of Engineering And Science*, 2 (1), 254-262.
- Elias, M. M., Mahbubul, I. M., Saidur, R., Sohel, M. R., Shahrul, I. M., Khaleduzzaman, S. S. and Sadeghipour, S. (2014a). Experimental investigation on the thermophysical properties of Al₂O₃ nanoparticles suspended in car radiator coolant. *International Communications in Heat and Mass Transfer*, 54, 48-53.
- Esfe, M. H., Karimipour, A., Yan, W. M., Akbari, M., Safaei, M. R. and Dahari, M. (2015). Experimental study on thermal conductivity of ethylene glycol based nanofluids containing Al₂O₃ nanoparticles. *International Journal of Heat and Mass Transfer*, 88, 728-734.

- Fani, B., Kalteh, M. and Abbassi, A. (2015). Investigating the effect of Brownian motion and viscous dissipation on the nanofluid heat transfer in a trapezoidal microchannel heat sink. *Advanced Powder Technology*, 26 (1), 83-90.
- Fontes, D. H., Ribatski, G. and Bandarra Filho, E. P. (2015). Experimental evaluation of thermal conductivity, viscosity and breakdown voltage AC of nanofluids of carbon nanotubes and diamond in transformer oil. *Diamond and Related Materials*, 58, 115-121.
- Ganeshkumar, J., Kathirkaman, D., Raja, K., Kumaresan, V. and Velraj, R. (2015). Experimental study on density, thermal conductivity, specific heat and viscosity of water-ethylene glycol mixture dispersed with carbon nanotubes. *Thermal Science*, (00), 28-28.
- Gao, W., Kong, L. and Hodgson, P. (2012). Atomic interaction of functionalized carbon nanotube base nanofluids with a heating surface and its effect on heat transfer. *International Journal of Heat and Mass Transfer*, 55 (19-20), 5007-5015.
- George, R., Bardelcik, A. and Worswick, M. J. (2012). Hot forming of boron steels using heated and cooled tooling for tailored properties. *Journal of Materials Processing Technology*, 212(11), 2386–2399.
- Ghadimi, A., Saidur, R. and Metselaar, H. S. C. (2011). A review of nanofluid stability properties and characterization in stationary conditions. *International Journal of Heat and Mass Transfer*, 54 (17–18), 4051-4068.
- Hadadian, M., Samiee, S., Ahmadzadeh, H. and Goharshadi, E. K. (2013). Nanofluids for heat transfer enhancement—A review. *Physical Chemistry Research*, 1 (1), 1-33.
- Haddad, Z., Abid, C., Oztop, H. F. and Mataoui, A. (2014). A review on how the researchers prepare their nanofluids. *International Journal of Thermal Sciences*, 76 (0), 168-189.
- Hafizuddin. (2014). *Dies Design Structure & Manufacturing Concept*.
- Hajjar, Z., Rashidi, A. M. and Ghozatloo, A. (2014). Enhanced thermal conductivities of graphene oxide nanofluids. *International Communications in Heat and Mass Transfer*, 57, 128-131.

- Hatami, F. and Okhovati, F. (2014). Analysis of turbulent flow of nanofluids in a pipe. *European Online Journal of Natural and Social Sciences*, 3 (3), pp. 72-85.
- Hayduk, W. and Malik, V.K. (1971). Density, viscosity, and carbon dioxide solubility and diffusivity in aqueous ethylene glycol solutions. *Journal of Chemical & Engineering Data*, 16 (2), 143-146.
- Heris, S. Z., Shokrgozar, M., Poorpharhang, S., Shanbedi, M. and Noie, S. H. (2013). Experimental study of heat transfer of a car radiator with CuO/ethylene glycolwater as a coolant. *Journal of Dispersion Science and Technology*, 35 (5), 677-684.
- Heyhat, M. M., Kowsary, F., Rashidi, A. M., Momenpour, M. H. and Amrollahi, A. (2013). Experimental investigation of laminar convective heat transfer and pressure drop of water-based Al₂O₃ nanofluids in fully developed flow regime. *Experimental Thermal and Fluid Science*, 44, 483-489.
- Hoffmann, H., So, H. and Steinbeiss, H. (2007). Design of hot stamping tools with cooling system. *CIRP Annals - Manufacturing Technology*, 56(1), 269–272.
- Hu, P. and Ying, L. (2017). *Hot Stamping Advanced Manufacturing Technology of Lightweight Car Body*. 1st Edition. Beijing: Science Press.
- Hu, P., Ma, N., Liu, L. and Zhu, Y. (2013). *Theories, Methods and Numerical Technology of Sheet Metal Cold and Hot Forming*. 1st Edition. New York: Springer-Verlag London.
- Hung, Y. H., Teng, T. P. and Lin, B. G. (2013). Evaluation of the thermal performance of a heat pipe using alumina nanofluids. *Experimental Thermal and Fluid Science*, 44, 504-511.
- Hussein, A. M., Sharma, K. V., Bakar, R. A. and Kadirgama, K. (2014). A review of forced convection heat transfer enhancement and hydrodynamic characteristics of a nanofluid. *Renewable and Sustainable Energy Reviews*, 29, 734-743.
- Jarahnejad, M., Haghghi, E., Saleemi, M., Nikkam, N., Khodabandeh, R., Palm, B., Toprak, M. and Muhammed, M. (2015). Experimental investigation on viscosity of water-based Al₂O₃ and TiO₂ nanofluids. *Rheologica Acta*, 54 (5), 411-422.
- Javadi, F. S., Sadeghipour, S., Saidur, R., Boroumandjazi, G., Rahmati, B., Elias, M. M. and Soheli, M. R. (2013). The effects of nanofluid on thermophysical properties and heat transfer characteristics of a plate heat exchanger. *International Communications in Heat and Mass Transfer*, 44, 58-63.

- Jiang, C., Shan, Z., Zhuang, B., Zhang, M. and Xu, Y. (2012). Hot stamping die design for vehicle door beams using ultra-high strength steel. *International Journal of Precision Engineering and Manufacturing*, 13(7), 1101–1106.
- Kamalgharibi, M., Hormozi, F., Zamzamian, S. and Sarafraz, M. M. (2015). Experimental studies on the stability of CuO nanoparticles dispersed in different base fluids: influence of stirring, sonication and surface active agents. *Heat and Mass Transfer*, 52(1), 1-8.
- Karbasian, H. and Tekkaya, A. E. (2010). A review on hot stamping. *Journal of Materials Processing Technology*, 210(15), 2103–2118.
- Kayhani, M. H., Soltanzadeh, H., Heyhat, M. M., Nazari, M. and Kowsary, F. (2012). Experimental study of convective heat transfer and pressure drop of TiO₂/water nanofluid. *International Communications in Heat and Mass Transfer*, 39 (3), 456-462.
- Khedkar, R. S., Sonawane, S. S. and Wasewar, K. L. (2012). Influence of CuO nanoparticles in enhancing the thermal conductivity of water and monoethylene glycol based nanofluids. *International Communications in Heat and Mass Transfer*, 39 (5), 665-669.
- Kim, D. Y., Kim, H. Y., Lee, S. H., and Kim, H. K. (2015). Life estimation of hot press forming die by using interface heat transfer coefficient obtained from inverse analysis. *International Journal of Automotive Technology*, 16(2), 285–292.
- Kim, H. J., Lee, S. H., Lee, J. H. and Jang, S. P. (2015). Effect of particle shape on suspension stability and thermal conductivities of water-based bohemite alumina nanofluids. *Energy*, 90(2), 1290-1297.
- Kole, M. and Dey, T. K. (2011). Effect of aggregation on the viscosity of copper oxide–gear oil nanofluids. *International Journal of Thermal Sciences*, 50 (9), 1741-1747.
- Kole, M. and Dey, T. K. (2012a). Investigations on the pool boiling heat transfer and critical heat flux of ZnO-ethylene glycol nanofluids. *Applied Thermal Engineering*, 37, 112-119.
- Kole, M. and Dey, T. K. (2010). Thermal conductivity and viscosity of Al₂O₃ nanofluid based on car engine coolant. *Journal of Physics D: Applied Physics*, 43, 315501.

- Kole, M. and Dey, T. K. (2012b). Thermophysical and pool boiling characteristics of ZnO-ethylene glycol nanofluids. *International Journal of Thermal Sciences*, 62 (0), 61-70.
- Konakanchi, H., Vajjha, R. S., Chukwu, G. A. and Das, D. K. (2015). Measurements of μ h of three nanofluids and development of new correlations. *Heat Transfer Engineering*, 36 (1), 81-90.
- Kumaresan, V. and Velraj, R. (2012). Experimental investigation of the thermo-physical properties of water-ethylene glycol mixture based CNT nanofluids. *Thermochimica Acta*, 545, 180-186.
- Kumar, D. D., Shirsat, V. Sharma, V. and Sarpate, C. (2011). Design optimization of hot forming tools by numerical thermal analysis. *KLT Automotive and Tubular Product LTD*.
- Li, H., He, Y., Hu, Y., Jiang, B. and Huang, Y. (2015). Thermophysical and natural convection characteristics of ethylene glycol and water mixture based ZnO nanofluids. *International Journal of Heat and Mass Transfer*, 91, 385-389.
- Li, Y., Fernández-Seara, J., Du, K., Pardiñas, Á. Á., Latas, L. L. and Jiang, W. (2016). Experimental investigation on heat transfer and pressure drop of ZnO/ethylene glycol-water nanofluids in transition flow. *Applied Thermal Engineering*, 93, 537-548.
- Lim, S. K., Azmi, W. H. and Yusoff, A. R. (2016). Investigation of thermal conductivity and viscosity of Al₂O₃/water-ethylene glycol mixture nanocoolant for cooling channel of hot press forming die application. *International Communications in Heat and Mass Transfer*, 78, 182-189.
- Lim, W. S., Choi, H. S., Ahn, S. Y. and Kim, B. M. (2014). Cooling channel design of hot stamping tools for uniform high-strength components in hot stamping process. *International Journal of Advanced Manufacturing Technology*, 70(5-8), 1189-1203.
- Lin, T., Song, H., Zhang, S., Cheng, M. and Liu, W. (2014). Cooling systems design in hot stamping tools by a thermal-fluid-mechanical coupled approach. *Advances in Mechanical Engineering*, 2, 1-13.
- Liu, H., Lei, C. and Xing, Z. (2013). Cooling system of hot stamping of quenched steel BR1500HS: optimization and manufacturing methods. *The International Journal of Advanced Manufacturing Technology*, 69(1-4), 211-223.

- Liu, M. S., Lin, M. C. C., Tsai, C. Y. and Wang, C. C. (2006). Enhancement of thermal conductivity with Cu for nanofluids using chemical reduction method. *International Journal of Heat and Mass Transfer*, 49 (17–18), 3028-3033.
- Löbbecke, C., Hering, O., Hiegemann, L., and Tekkaya, A. E. (2016). Setting mechanical properties of high strength steels for rapid hot forming processes. *Materials*, 9(4), 229.
- Madhesh, D. and Kalaiselvam, S. (2014). Experimental study on the heat transfer and flow properties of Ag–ethylene glycol nanofluid as a coolant. *Heat and Mass Transfer*, 50 (11), 1597-1607.
- Maeno, T., Mori, K. and Nagai, T. (2014). Improvement in formability by control of temperature in hot stamping of ultra-high strength steel parts. *CIRP Annals - Manufacturing Technology*, 63(1), 301–304.
- Mahbubul, I. M., Saidur, R. and Amalina, M. A. (2012). Latest developments on the viscosity of nanofluids. *International Journal of Heat and Mass Transfer*, 55 (4), 874-885.
- Maheshwary, P. and Nemade, K. (2015). Enhancement in heat transfer performance of ZrO₂/H₂O nanofluid via ultrasonication time. *International Journal on Recent and Innovation Trends in Computing and Communication*, 3 (2), 035– 037.
- Mahian, O., Kianifar, A. and Wongwises, S. (2013). Dispersion of ZnO nanoparticles in a mixture of ethylene glycol–water, exploration of temperature-dependent density, and sensitivity analysis. *Journal of Cluster Science*, 24 (4), 1103-1114.
- Mariano, A., Pastoriza-Gallego, M. J., Lugo, L., Camacho, A., Canzonieri, S. and Piñeiro, M. M. (2013). Thermal conductivity, Rheological behaviour and density of non-Newtonian ethylene glycol based SnO₂ nanofluids. *Fluid Phase Equilibria*, 337, 119-124.
- Mariano, A., Pastoriza-Gallego, M. J., Lugo, L., Mussari, L. and Piñeiro, M. M. (2015). CO₃O₄ ethylene glycol-based nanofluids: Thermal conductivity, viscosity and high pressure density. *International Journal of Heat and Mass Transfer*, 85, 54-60.
- Melissa, B. (2012). Fluid Flow Rates. Retrieved from <http://www.education.com/science-fair/article/fluid-flow-rates/> (22 JUNE 2016)

- Merklein, M., Johannes, M., Lechner, M., and Kuppert, A. (2014). A review on tailored blanks - Production, applications and evaluation. *Journal of Materials Processing Technology*, 214(2), 151–164.
- Misumi. (2015). Misumi Press Stock Booklet 2015.
- Mojarrad, M. S., Keshavarz, A., Ziabasharhagh, M. and Raznahan, M. M. (2014). Experimental investigation on heat transfer enhancement of alumina/water and alumina/water–ethylene glycol nanofluids in thermally developing laminar flow. *Experimental Thermal and Fluid Science*, 53, 111-118.
- Mori, K., Maeno, T. and Maruo, Y. (2012). Punching of small hole of die-quenched steel sheets using local resistance heating. *CIRP Annals - Manufacturing Technology*, 61(1), 255–258.
- Mori, K., Maeno, T., Yamada, H., & Matsumoto, H. (2015). International Journal of Machine Tools & Manufacture 1-Shot hot stamping of ultra-high strength steel parts consisting of resistance heating, forming , shearing and die quenching. *International Journal of Machine Tools and Manufacture*, 89, 124–131.
- Motahar, S., Nikkam, N., Alemrajabi, A. A., Khodabandeh, R., Toprak, M. S. and Muhammed, M. (2014). A novel phase change material containing mesoporous silica nanoparticles for thermal storage: A study on thermal conductivity and viscosity. *International Communications in Heat and Mass Transfer*, 56, 114-120.
- Naderi, M. (2007). *Hot Stamping of Ultra High Strength Steels* (PhD Thesis) RWTH Aachen University, Germany.
- Naderi, M., Ketabchi, M., Abbasi, M. and Bleck, W. (2011). Analysis of microstructure and mechanical properties of different high strength carbon steels after hot stamping. *Journal of Materials Processing Technology*, 211(6), 1117–1125.
- Naganathan, A. (2010). *Hot Stamping of Manganese Boron Steel* (PhD Thesis) The Ohio State University, America.
- Naganathan, A. and Penter, L. (2012). Hot Stamping. *In Sheet Metal Forming-Processes and Applications*, pp. 133–156.

- Namburu, P. K., Kulkarni, D. P., Misra, D. and Das, D. K. (2007). Viscosity of copper oxide nanoparticles dispersed in ethylene glycol and water mixture. *Experimental Thermal and Fluid Science*, 32 (2), 397-402.
- Namklang, P. and Uthaisangasuk, V. (2016). Description of microstructures and mechanical properties of boron alloy steel in hot stamping process. *Journal of Manufacturing Processes*, 21, 87–100.
- Nikkam, N., Haghghi, E. B., Saleemi, M., Behi, M., Khodabandeh, R., Muhammed, M., Palm, B. and Toprak, M. S. (2014). Experimental study on preparation and base liquid effect on thermo-physical and heat transport characteristics of α -SiC nanofluids. *International Communications of Heat and Fluid Flow*, 55, 38-44.
- Nuraini, A. and Aqida, S. N. (2013). Optimization of quenching process in hot press forming of 22MnB5 steel for high strength properties. *ICMER International Conference on Mechanical Engineering Research*, (50), 012064
- Pak, B. C. and Cho, Y. I. (1998). Hydrodynamic and heat transfer study of dispersed fluids with submicron metallic oxide particles. *Experimental Heat Transfer*, 11 (2), 151-170.
- Pang, C., Jung, J. Y., Lee, J. W. and Kang, Y. T. (2012). Thermal conductivity measurement of methanol-based nanofluids with Al_2O_3 and SiO_2 nanoparticles. *International Journal of Heat and Mass Transfer*, 55 (21), 5597-5602.
- Parekh, K. and Lee, H. S. (2010). Magnetic field induced enhancement in thermal conductivity of magnetite nanofluid. *Journal of Applied Physics*, 107 (9), 09A310.
- Pastoriza-Gallego, M., Lugo, L., Legido, J. and Piñeiro, M. (2011). Thermal conductivity and viscosity measurements of ethylene glycol based Al_2O_3 nanofluids. *Nanoscale Research Letters*, 6 (1), 1-11.
- Peyghambarzadeh, S., Hashemabadi, S., Hoseini, S. and Seifi Jamnani, M. (2011a). Experimental study of heat transfer enhancement using water/ethylene glycol based nanofluids as a new coolant for car radiators. *International Communications in Heat and Mass Transfer*, 38 (9), 1283-1290.
- Qu, J., Wu, H. Y. and Cheng, P. (2010). Thermal performance of an oscillating heat pipe with Al_2O_3 -water nanofluids. *International Communications in Heat and Mass Transfer*, 37 (2), 111-115.

- Ravikumar, S. V., Haldar, K., Jha, J. M., Chakraborty, S., Sarkar, I., Pal, S. K. and Chakraborty, S. (2015). Heat transfer enhancement using air-atomized spray cooling with water–Al₂O₃ nanofluid. *International Journal of Thermal Sciences*, 96, 85-93.
- Reddy, M. C. S. and Rao, V. V. (2013). Experimental studies on thermal conductivity of blends of ethylene glycol-water-based TiO₂ nanofluids. *International Communications in Heat and Mass Transfer*, 46, 31-36.
- Said, Z., Sajid, M. H., Alim, M. A., Saidur, R. and Rahim, N. A. (2013). Experimental investigation of the thermophysical properties of Al₂O₃-nanofluid and its effect on a flat plate solar collector. *International Communications in Heat and Mass Transfer*, 48 (0), 99-107.
- Salman, B., Mohammed, H. and Kherbeet, A. S. (2014). Numerical and experimental investigation of heat transfer enhancement in a microtube using nanofluids. *International Communications in Heat and Mass Transfer*, 59, 88-100.
- Samira, P., Saeed, Z., Motahare, S. and Mostafa, K. (2015). Pressure drop and thermal performance of CuO/ethylene glycol (60%)-water (40%) nanofluid in car radiator. *Korean Journal of Chemical Engineering*, 32 (4), 609-616.
- Sarafraz, M., Hormozi, F. and Kamalgharibi, M. (2014). Sedimentation and convective boiling heat transfer of CuO-water/ethylene glycol nanofluids. *Heat and Mass Transfer*, 50 (9), 1237-1249.
- Sekhar, Y. R. and Sharma, K. (2015). Study of viscosity and specific heat capacity characteristics of water-based Al₂O₃ nanofluids at low particle concentrations. *Journal of Experimental Nanoscience*, 10 (2), 86-102.
- Serebryakova, M., Dimov, S., Bardakhanov, S. and Novopashin, S. (2015). Thermal conductivity, viscosity and rheology of a suspension based on Al₂O₃ nanoparticles and mixture of 90% ethylene glycol and 10% water. *International Journal of Heat and Mass Transfer*, 83, 187-191.
- Sereelakshmy, K. R., Aswathy, S. N., Vidhya, K. M., Saranya, T. R. and Sreeja, C. N. (2014). Review Article - An overview of recent nanofluids research. *International Research Journal of Pharmacy*, 5 (4), 239-234.
- Sever, N. K., Mete, O. H., Demiralp, Y., Choi, C. and Altan, T. (2012). Springback prediction in bending of AHSS-DP 780. In *NAMRI/SME*, Vol. 40.

- Sharma, K. V., Sarma, P. K., Azmi, W. H., Noor, M. M., Kadirgama, K. and Mamat, R. (2009). Validation of turbulent flow heat transfer data of water based nanofluids. *18 International Conference on Composites/Nano Engineering*, pp. 3606-3612.
- Shegokar, R. and Müller, R. H. (2010). Nanocrystals: Industrially feasible multifunctional formulation technology for poorly soluble actives. *International Journal of Pharmaceutics*, 399 (1–2), 129-139.
- Sheikhbahai, M., Nasr Esfahany, M. and Etesami, N. (2012). Experimental investigation of pool boiling of Fe₃O₄/ethylene glycol–water nanofluid in electric field. *International Journal of Thermal Sciences*, 62, 149-153.
- Sidik, N. A. C., Mohammed, H. A., Alawi, O. A. and Samion, S. (2014). A review on preparation methods and challenges of nanofluids. *International Communications in Heat and Mass Transfer*, 54, 115-125.
- Sidik, N. A. C., Yazid, M. N. A. W. M. and Mamat, R. (2015). A review on the application of nanofluids in vehicle engine cooling system. *International Communications in Heat and Mass Transfer*, 68, 85-90.
- Sigma-Aldrich 2015. (Aluminium oxide - Safety data sheet for Product No. 718475 [online]). 19 June 2015 editions.
- Skrikerud, M., Megahed, M., & Porzner, H. (2010). Simulation of Hot Stamping Process.
- So, H., Faßmann, D., Hoffmann, H., Golle, R. and Schaper, M. (2012). An investigation of the blanking process of the quenched boron alloyed steel 22MnB5 before and after hot stamping process. *Journal of Materials Processing Technology*, 212(2), 437–449.
- Sonawane, S. S., Khedkar, R. S. and Wasewar, K. L. (2015). Effect of sonication time on enhancement of effective thermal conductivity of nano TiO₂–water, ethylene glycol, and paraffin oil nanofluids and models comparisons. *Journal of Experimental Nanoscience*, 10 (4), 310-322.
- Srithananan, P., Kaewtatip, P., and Uthaisangsuk, V. (2016). Materials Science & Engineering A Micromechanics-based modeling of stress – strain and fracture behaviour of heat-treated boron steels for hot stamping process. *Materials Science & Engineering A*, 667, 61–76.

- Strandberg, R. and Das, D. K. (2010). Finned tube performance evaluation with nanofluids and conventional heat transfer fluids. *International Journal of Thermal Sciences*, 49 (3), 580-588.
- Suganthi, K. and Rajan, K. (2012a). Temperature induced changes in ZnO–water nanofluid: zeta potential, size distribution and viscosity profiles. *International Journal of Heat and Mass Transfer*, 55 (25), 7969-7980.
- Suganthi, K. and Rajan, K. (2014). A formulation strategy for preparation of ZnO–propylene glycol–water nanofluids with improved transport properties. *International Journal of Heat and Mass Transfer*, 71, 653-663.
- Suganthi, K. S. and Rajan, K. S. (2012b). Temperature induced changes in ZnO–water nanofluid: Zeta potential, size distribution and viscosity profiles. *International Journal of Heat and Mass Transfer*, 55 (25–26), 7969-7980.
- Sundar, L. S. and Singh, M. K. (2013). Convective heat transfer and friction factor correlations of nanofluid in a tube and with inserts: A review. *Renewable and Sustainable Energy Reviews*, 20, 23-35.
- Sundar, L. S., Farooky, M. H., Sarada, S. N. and Singh, M. (2013a). Experimental thermal conductivity of ethylene glycol and water mixture based low volume concentration of Al₂O₃ and CuO nanofluids. *International Communications in Heat and Mass Transfer*, 41, 41-46.
- Sundar, L. S., Sharma, K. V., Naik, M. T. and Singh, M. K. (2013b). Empirical and theoretical correlations on viscosity of nanofluids: A review. *Renewable and Sustainable Energy Reviews*, 25 (0), 670-686.
- Sundar, L. S., Singh, M. K. and Sousa, A. C. M. (2013c). Thermal conductivity of ethylene glycol and water mixture based Fe₃O₄ nanofluid. *International Communications in Heat and Mass Transfer*, 49 (0), 17-24.
- Sundar, L. S., Venkata Ramana, E., Singh, M. K. and Sousa, A. C. M. (2014). Thermal conductivity and viscosity of stabilized ethylene glycol and water mixture Al₂O₃ nanofluids for heat transfer applications: An experimental study. *International Communications in Heat and Mass Transfer*, 56, 86-95.
- Suresh, S., Chandrasekar, M., Selvakumar, P. and Page, T. (2012). Experimental studies on heat transfer and friction factor characteristics of Al₂O₃/water nanofluid under laminar flow with spiralled rod inserts. *International Journal of Nanoparticles*, 5 (1), 37-55.

- Suresh, S., Venkitaraj, K. P., Selvakumar, P. and Chandrasekar, M. (2011). Synthesis of Al₂O₃-Cu/water hybrid nanofluids using two step method and its thermo physical properties. *Colloids and Surfaces A: Physicochemical and Engineering Aspects*, 388 (1-3), 41-48.
- Taha, Z., Yusoff, A. R., Farid, M., Sharif, M., Saharudin, M. A. H., & Zamri, M. F. (2014). Comparison of Cooling Performance Between High Thermal Conductivity Steel (HTCS 150) and Hot Work Tool Steel (SKD 61) Insert for Experimental Tool Using Finite Element Analysis. *Advanced Materials Research* 903, 163-168.
- Tajik, B., Abbassi, A., Saffar-Avval, M. and Najafabadi, M. A. (2012). Ultrasonic properties of suspensions of TiO₂ and Al₂O₃ nanoparticles in water. *Powder Technology*, 217, 171-176.
- Teng, T. P. (2013). Thermal conductivity and phase-change properties of aqueous alumina nanofluid. *Energy Conversion and Management*, 67 (0), 369-375.
- Teng, T. P. and Hung, Y. H. (2012). Estimation and experimental study of the density and specific heat for alumina nanofluid. *Journal of Experimental Nanoscience*, 9 (7), 707-718.
- Teng, T. P., Hung, Y. H., Teng, T. C., Mo, H. E. and Hsu, H. G. (2010). The effect of alumina/water nanofluid particle size on thermal conductivity. *Applied Thermal Engineering*, 30 (14-15), 2213-2218.
- Thanadngarn, C., Sirivedin, K., Engineering, M., Thai-german, T. S. I., Buakaew, V., Neamsup, Y. (2013). The study of the springback effect in the UHSS by U-bending process, 6, 19-25.
- Timofeeva, E. V. (2011). Nanofluids for heat transfer-potential and engineering strategies. *Two Phase Flow, Phase Change and Numerical Modelling*, 435-450.
- Timofeeva, E. V., Moravek, M. R. and Singh, D. (2011a). Improving the heat transfer efficiency of synthetic oil with silica nanoparticles. *Journal of colloid and interface science*, 364 (1), 71-79.
- Timofeeva, E. V., Yu, W., France, D. M., Singh, D. and Routbort, J. L. (2011b). Base fluid and temperature effects on the heat transfer characteristics of SiC in ethylene glycol/H₂O and H₂O nanofluids. *Journal of Applied Physics*.

- Tondini, F., Bosetti, P. and Bruschi, S. (2011). Heat transfer in hot stamping of high-strength steel sheets. *Journal of Engineering Manufacture*, 225, 1813–1824.
- Tony John and Krishnakumar, T. S. (2013). Experimental studies of thermal conductivity, viscosity and stability of ethylene glycol nanofluids. *International Conference on Energy and Environment - 2013 (ICEE 2013)*, 2(1), pp. 611-617.
- Vajjha, R. S., Das, D. K. and Kulkarni, D. P. (2010a). Development of new correlations for convective heat transfer and friction factor in turbulent regime for nanofluids. *International Journal of Heat and Mass Transfer*, 53 (21-22), 4607-4618.
- Vajravelu, K., Prasad, K. V. and NG, C. O. (2013). The effect of variable viscosity on the flow and heat transfer of a viscous Ag-water and Cu-water nanofluids. *Journal of Hydrodynamics, Ser. B*, 25 (1), 1-9.
- Wang, S. and Lee, P. (2013). Investigation of die quench properties of hot stamping. *China Steel Technical Report*, 2(26), 22–31.
- Wei, X. and Wang, L. (2010). Synthesis and thermal conductivity of microfluidic copper nanofluids. *Particuology*, 8 (3), 262-271.
- Wong, K. V. and De Leon, O. (2010). Applications of nanofluids: current and future. *Advances in Mechanical Engineering*, 2, 519659.
- Wu, J. M. and Zhao, J. (2013). A review of nanofluid heat transfer and critical heat flux enhancement—Research gap to engineering application. *Progress in Nuclear Energy*, 66 (0), 13-24.
- Xiaoda, L., Xiangkui, Z., Ping, H. and Xianghui, Z. (2016). Thermo-mechanical coupled stamping simulation about the forming process of high-strength steel sheet. *International Journal of Control and Automation*, 9(1), 93–102.
- Xie, H., Li, Y. and Yu, W. (2010). Intriguingly high convective heat transfer enhancement of nanofluid coolants in laminar flows. *Physics Letters A*, 374 (25), 2566-2568.
- Yang, X. F. and Liu, Z. H. (2011). Pool boiling heat transfer of functionalized nanofluid under sub-atmospheric pressures. *International Journal of Thermal Sciences*, 50 (12), 2402-2412.

- Yiamsawas, T., Mahian, O., Dalkilic, A. S., Kaewnai, S. and Wongwises, S. (2013). Experimental studies on the viscosity of TiO₂ and Al₂O₃ nanoparticles suspended in a mixture of ethylene glycol and water for high temperature applications. *Applied Energy*, 111, 40-45.
- Yu, W. and Xie, H. (2012). A review on nanofluids: preparation, stability mechanisms, and applications. *Journal of Nanomaterials*, 2012, 1.
- Yu, W., Xie, H., Chen, L. and Li, Y. (2010). Investigation on the thermal transport properties of ethylene glycol-based nanofluids containing copper nanoparticles. *Powder Technology*, 197 (3), 218-221.
- Yu, W., Xie, H., Li, Y., Chen, L. and Wang, Q. (2012). Experimental investigation on the heat transfer properties of Al₂O₃ nanofluids using the mixture of ethylene glycol and water as base fluid. *Powder Technology*, 230, 14-19.
- Zakaria, I., Azmi, W. H., Mohamed, W. A. N. W., Mamat, R. and Najafi, G. (2015). Experimental investigation of thermal conductivity and electrical conductivity of Al₂O₃ nanofluid in water-ethylene glycol Mixture for proton exchange membrane fuel cell application. *International Communications in Heat and Mass Transfer*, 61, 61-68.
- Zamri, M. F. (2017) *Heuristic Optimization of Cooling Channel Design for Hot Stamping Tool Process* (MSc. Thesis) Universiti Malaysia Pahang, Malaysia.
- Zhang, Z., Li, X., Pan, L. and Wei, X. (2010). Numerical Simulation on Hot Forming of B Pillar.
- Zhang, Z., Li, X., Zhao, Y. and Li, X. (2014). Heat transfer in hot stamping of high-strength boron steel sheets. *Metallurgical and Materials Transactions B: Process Metallurgy and Materials Processing Science*, 45(4), 1192–1195.
- Zhong-De, S., Mi-Ian, Z., Chao, J., Ying, X. and Wem-Juan, R. (2010). Basic study on die cooling system of hot stamping process. *International Conference on Advanced Technology of Design and Manufacture*, 67(2), 5–8.
- Zhu, D., Li, X., Wang, N., Wang, X., Gao, J. and Li, H. (2009). Dispersion behavior and thermal conductivity characteristics of Al₂O₃–H₂O nanofluids. *Current Applied Physics*, 9 (1), 131-139.

APPENDIX A
G-CODE FOR CUTTING TENSILE TEST SPECIMEN FROM HAT-SHAPED
PART

(= ON OFF IP HRP MAO SV V SF C PIK CTRL WK WT WS WP PC SK);
C000 = 005 014 2215 000 240 +040.0 8.0 0102 0 000 0000 020 120 100 045 0000 00;
C001 = 006 014 2215 000 251 +030.0 8.0 0102 0 000 0000 020 120 100 045 0000 00;
H000 = +000000.0100 ;
H001 = +000000.1470 ;
(FIG-1 1T ALL CIRCUMFERENCE);
G54;
G90;
G92X-3.0Y1.0Z0;
G29;
T94;
T84;
C000;
G42H000G01X-1.0Y1.0;
C001X0.0;
H001;
M98P0001;
T85;
G149G249;
M02;
N0001;
G01X0.0Y30.0;
G03X2.0Y34.4721I-4.0J4.4721;
G01Y65.5279;
G03X0.0Y70.0I-6.0J0.0;
G01Y100.0;
X10.0;
Y70.0;
G03X8.0Y65.5279I4.0J-4.4721;
G01Y34.4721;
G03X10.0Y30.0I6.0J0.0;
G01Y0.0;
X0.0;
Y1.0;
G40H000X-3.0;
M99;

APPENDIX B
HEAT TRANSFER COEFFICIENT VALUES OF NANOCOOLANT

$$\begin{aligned}\text{Flow rate, } \dot{V} &= \left(\frac{l}{\text{min}}\right) = 14 \\ &= \left(\frac{14l}{60s}\right) = 0.2328 \frac{l}{s} \\ &= \left(\frac{m^3}{s}\right) = 2.328 \times 10^{-4} \frac{m^3}{s}\end{aligned}$$

$$\begin{aligned}\text{Volume flow rate, } V &= \frac{\dot{V}}{A} \\ &= \frac{2.328 \times 10^{-4}}{5.027 \times 10^{-5}} = 4.631 \frac{m}{s}\end{aligned}$$

$$\begin{aligned}\text{Reynolds number, } Re &= \frac{\rho_{nf} VD}{\mu_{nf}} \\ &= \frac{(1082.27)(4.631)(0.008)}{0.00401} = 9998.987\end{aligned}$$

$$\begin{aligned}\text{Prandtl number, } Pr &= \frac{C_p \mu}{k_{nf}} \\ &= \frac{3465.46 \times 0.004}{0.425} = 32.698\end{aligned}$$

$$\begin{aligned}\text{Nusselt number, } Nu_{nf} &= 0.025 \times Re_{nf}^{0.76} \times Pr_{nf}^{0.45} \left[(0.01 + BR)^{-0.1} \left(1 + \frac{T_b}{70} \right)^{0.14} \right] \\ &= 0.025 (9998.987)^{0.76} (32.698)^{0.45} \left[(0.01 + 0.60)^{-0.1} \left(1 + \frac{25}{70} \right)^{0.14} \right] \\ &= 189.519\end{aligned}$$

$$\begin{aligned}\text{Heat transfer coefficient, } h_{conv} &= \frac{Nu(k_{nf})}{D} \\ &= \frac{189.519(0.425)}{0.008} = 10068.181 \frac{W}{m^2 K}\end{aligned}$$

APPENDIX B1
SAMPLE OF COOLING RATE FOR HEATED SHEET METAL BLANK

Heat transfer of boron steel

$$\text{Heat transfer, } Q = \Delta U = mC_p(T_2 - T_1)$$

$$\text{Where, } m = 3.294 \times 10^{-2} \text{ kg}$$

$$C_p = 590 \text{ J} \cdot \text{kg}^{-1} \cdot \text{K}^{-1}$$

$$\text{Hence, } Q = (3.294 \times 10^{-2}) \cdot (590) \cdot (375.67 - 162.35)$$

$$= 4145.789 \text{ J}$$

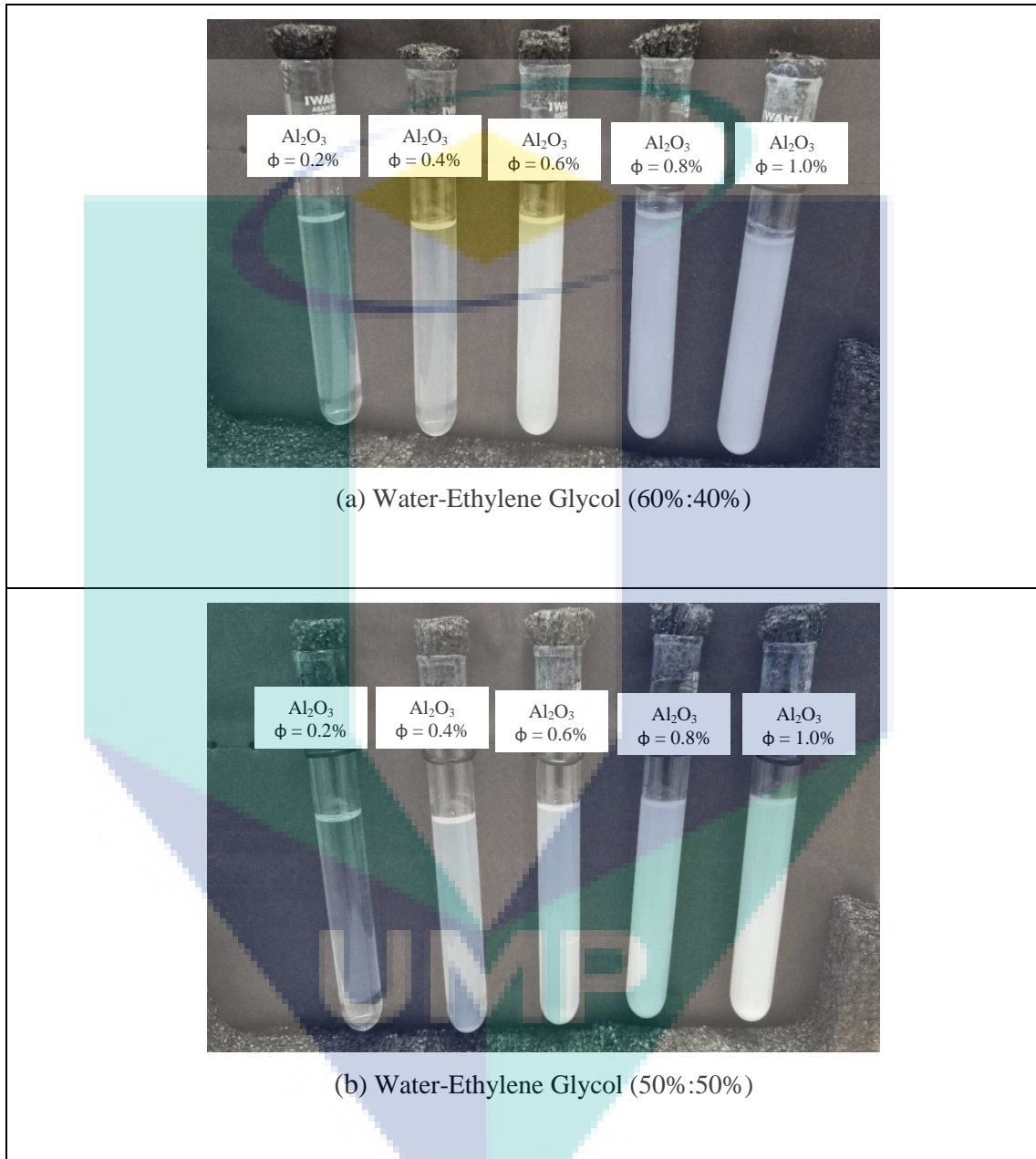
Cooling rate

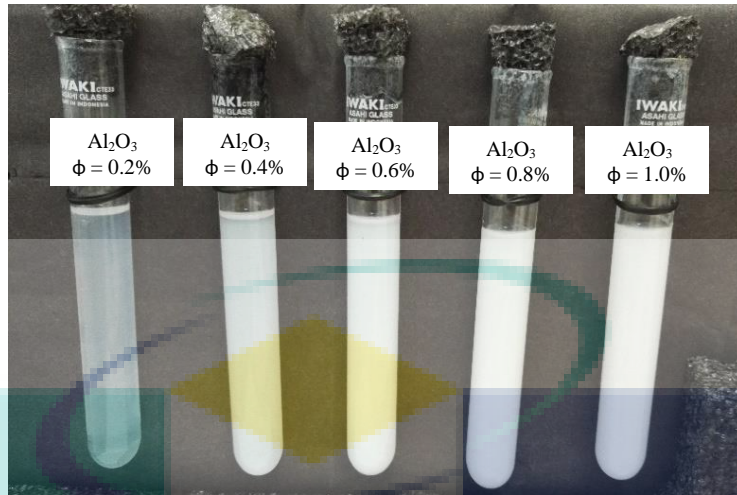
$$\text{Cooling rate, } \dot{Q} = \frac{Q}{\Delta t}$$

$$= \frac{4145.789}{7-1}$$
$$= 592.256 \text{ J} \cdot \text{s}^{-1}$$

UMP

APPENDIX C
SEDIMENTATION OBSERVATION OF ALUMINIUM OXIDE/WATER-EG
MIXTURE AFTER A MONTH OF PREPARATION





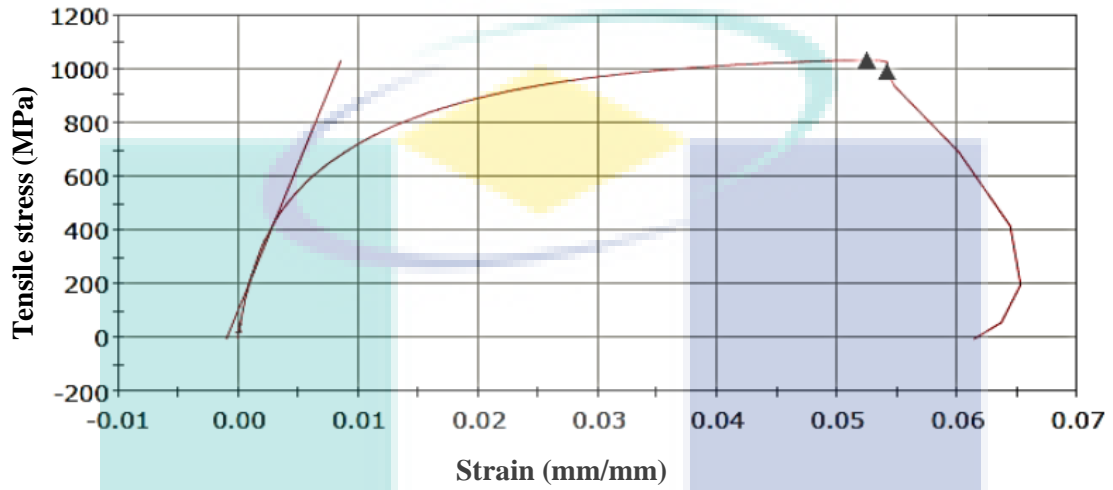
(c) Water-Ethylene Glycol (40:60%)

UMP

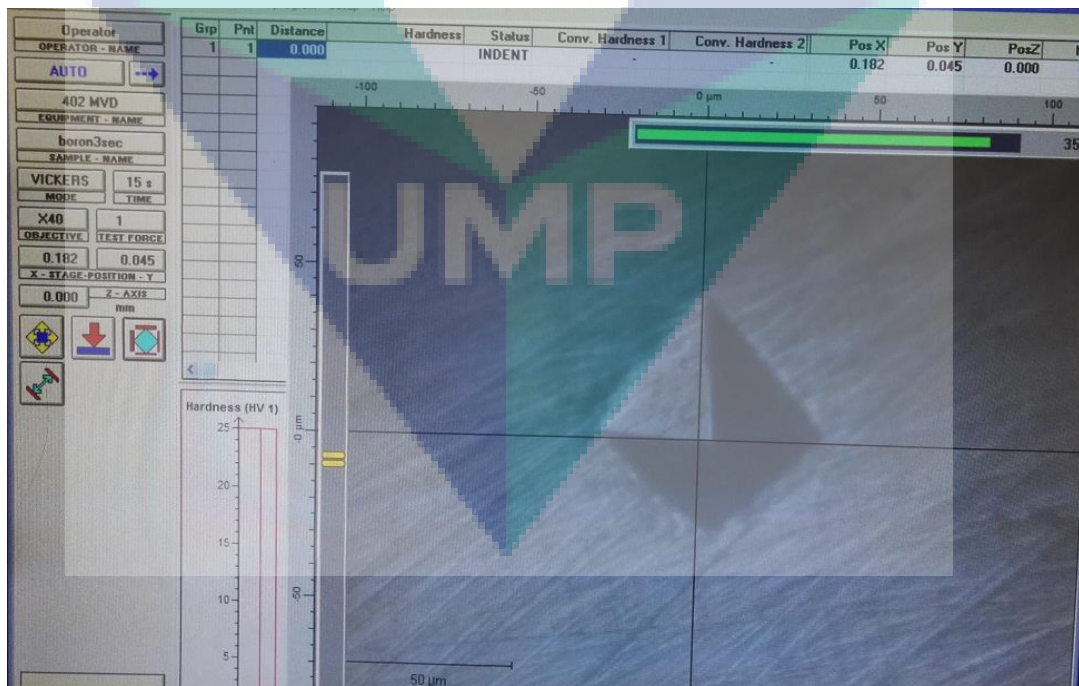
APPENDIX D

SAMPLE OF TENSILE STRENGTH AND HARDNESS MEASUREMENT

a)



b)



LIST OF PUBLICATION

ISI Indexed Journals:

Lim, S. K., Azmi, W. H. & Yusoff, A. R. (2016). Investigation of thermal conductivity and viscosity of Al₂O₃/water–ethylene glycol mixture nanocoolant for cooling channel of hot-press forming die application. *International Communications in Heat and Mass Transfer*, 78, 182–189. **Published ISI Q1 (IF 3.718)**

Scopus Journals:

Zamri, M. H., **Lim, S. K.** & Yusoff, A. R. (2016). Experimental validation for hot stamping process by using taguchi method. *IOP Conf. Series: Materials Science and Engineering*, 114, 012033. **Published**

Lim, S. K., Zamri, M. F. & Yusoff, A. R. (2017). Numerical simulation of hot press forming process for quenched boron steel between nanocoolant and chilled water. *International Conferences on Nanoscience and Nanotechnology 2018*. **Accepted**

Award:

Gold Medal Award (Manufacturing Engineering) in Creation, Innovation, Technology Research Exposition, CITREX 2017, Gambang, Pahang, Malaysia.

Yusoff, A. R., & **Lim, S. K.** (2017). Nanocoolant for improving cooling channel performance in hot press forming die.

Silver Medal Award (Manufacturing Engineering) in International Invention, Innovation and Technology Exhibition, ITEX 2017, Kuala Lumpur, Malaysia

Yusoff, A. R., & **Lim, S. K.** (2017). Nanocoolant for martensitic material transformation.